8-30-2011

Creep and fracture of self-consolidating concrete incorporating fly ash

Rick Grahn

Rick Rainier Grahn
Candidate

Civil Engineering
Department

This thesis is approved, and it is acceptable in quality and form for publication:

Approved by the Thesis Committee:

Dr. Mahmoud Reda Taha , Chairperson

Dr. Arup Maji

Dr. Walter Gerstle

Creep and Fracture of Self-Consolidating Concrete Incorporating Fly Ash

by

Rick Grahn

B.S. Civil Engineering, University of New Mexico, 2009

Thesis

Submitted in Partial Fulfillment of the
Requirements for the Degree of

Master of Science

Civil Engineering

The University of New Mexico
Albuquerque, New Mexico

July, 2011

Dedication

I dedicate this work to my family, Mom, Dad, and Sky. Thanks for all the support and inspiration over the years.

Acknowledgments

First, I would like to thank Dr. Mahmoud Reda Taha, my Master's thesis advisor and committee chair for the continued support and encouragement during my years as a graduate student at the University of New Mexico. Without your guidance and inspiration, this work would not have been possible. I would also like to thank my committee members Dr. Walter Gerstle and Dr. Arup Maji for their help throughout my graduate student studies.

I would also like to thank Jacob Hays, whom I worked with throughout this project and to Kenny Martinez for all the help in the laboratory setting up experiments and testing specimens. I want to also recognize Eslam Soliman for all the help received setting up experiments and finite element modeling. Lastly, I would like to thank the New Mexico Department of Transportation for funding my assistantship and this research.

Creep and Fracture of Self-Consolidating Concrete Incorporating Fly Ash

by

Rick Grahn

B.S. Civil Engineering, University of New Mexico, 2009

Thesis

Submitted in Partial Fulfillment of the
Requirements for the Degree of

Master of Science

Civil Engineering

The University of New Mexico
Albuquerque, New Mexico

July, 2011

Creep and Fracture of Self-Consolidating Concrete Incorporating Fly Ash

by

Rick Grahn

B.S. Civil Engineering, University of New Mexico, 2009

Abstract

Self-consolidating concrete (SCC) is a relatively new type of concrete that has the ability to flow under its own weight such that it can pass through tightly spaced reinforcement and fill corners of molds without the use of mechanical vibration. Due to the favorable plastic properties of SCC, there has been an increased interest in using SCC in precast and pre-stressed bridges. However, SCC achieves this flowability by reducing the maximum aggregate size in the concrete mix, significantly increasing the volume of the cement paste and incorporating large content of powder fillers. This mix design of SCC was hypothesized to affect two critical criteria for concrete used in bridges: creep and crack propagation. Therefore, this study is focused on investigating creep and fracture toughness of SCC. Furthermore, we compare creep and fracture toughness of SCC with that of normal vibrated concrete (NVC) typically used in bridge applications in New Mexico.

Five different SCC mixes were designed using two different New Mexico aggregate sources and varying amounts of fly ash ranging from 20-40% by weight of Portland cement. Two NVC mixes using the same local aggregate were produced for comparison.

Creep of SCC was measured experimentally and compared to commonly used code prediction models including AC1 209R-92 and CEB-FIP MC90-99. Three of the SCC mixes with varying amounts of fly ash (20%, 30%, and 40% by weight of Portland cement) were also tested to classify SCC fracture toughness as a function of fly ash content. Two fracture tests including the stiff tension fracture test and the notched beam level II test were conducted. The two tests provided good information on the significance of increasing powder content (here fly ash) on fracture toughness of SCC.

Based on the experimental observations, it was concluded that SCC with high volume fly ash exhibited higher creep strains than conventional vibrated concrete mixes. However, the aggregate source also played an important role in controlling creep of SCC. SCCs produced using Placitas aggregate showed significantly higher creep compared with that produced using Griego and Sons aggregate. A modification of the ACI code was necessary to enable the prediction of creep in SCC. On the other hand, the CEB-FIP code was able to successfully predict creep of all SCCs mixes. It was also concluded that fracture toughness of SCC decreased as the fly ash content in the mix increased. The significance of increasing the cement paste volume and eliminating the large aggregate on reducing fracture toughness of SCC is evident.

CONTENTS

LIST OF FIGURES

LIST OF TABLES

Chapter 1. Introduction

Concrete is an extremely important construction material that is used extensively all over the world for structural applications. As structural designs become more sophisticated, the materials used for construction must also be improved. In the past few decades, many researchers continue to progress the field of concrete materials by enhancing and quantifying the different mechanical and durability metrics of concrete.

Self-consolidating concrete (SCC) concrete is one advancement in the "self-compacting" concrete materials field with enhanced plastic properties that were developed by Ozawa et al [1] in Japan in the late 1980's. SCC has the ability to flow under its own weight without segregation or bleeding during casting while maintaining a constant viscosity. This characteristic of SCC is advantageous in precast and pre-stressed applications because of its ability to flow through tightly spaced reinforcement and fill corners of forms without the need for mechanical vibration. Since SCCs development, SCC mixes have grown increasingly popular for use in bridges and structures where the SCC plastic properties are desired [2-3] .

1.1 Importance of Self-Consolidating Concrete Characterization

Precast and pre-stressed structures needing the plastic properties of SCC mixes can be greatly affected by time-dependent effects. Time dependent effects, such as creep, in pre-stressed applications, will cause loss in pre-tensioning stresses. An incorrect creep prediction can cause more pre-stressed losses than originally calculated for the service loads in the pre-stressing strands making the concrete more prone to cracking. There is

therefore a need to explore the time-dependent effects of the newly developed SCC mixes; however, there isn't a clear consensus on how SCC behaves over time under constant stresses and constant humidity [4-8].

It is also important to determine the fracture properties of different SCC mixes because crack propagation can play an important part in overall structural serviceability and safety. The current design methods are based on two important criteria: ultimate and serviceability limit state design. The current method for classifying serviceability limit state safety is by visual inspection. However, by understanding the fracture toughness properties of concrete, better serviceability limit state criteria can be utilized.

SCC's constituent materials and amounts utilized in SCC mixes are very different when comparing them to their NVC counterparts. The amounts of cementitious fillers (i.e. fly ash, silica fume, etc.) and the aggregate grading/sizes used in SCCs vary greatly when compared to commonly used NVC mixes. In the current, although limited, literature, it is observed that these properties have effects on the time-dependent and fracture toughness properties of the concrete. By increasing the cementitious filler within a concrete mix, it is my hypothesis that the creep strains will increase and the fracture toughness properties will decrease due to the properties of the cement paste. It is also hypothesized that the aggregate grading present in SCCs will lead to a decrease in fracture toughness properties because no coarse aggregate is utilized to provide crack arresting properties. It is of interest to classify creep and fracture toughness properties of SCC's due to the differences in mix designs and classify these mixes because of the limited literature present within the field of SCC materials.

Due to the increase in popularity in using SCCs for precast, pre-stressed applications because of their enhanced flowabiltiy characteristics, an investigation of the hardened properties of SCCs is necessary to understand the behavior of these mixes when utilized in structural applications. Time-dependent effects and crack propagation properties are both extremely important parameters in determining the serviceability and safety of a structure that utilizes SCC mixes. By classifying time-dependent and fracture properties of these SCCs and comparing them to commonly used conventional NVCs; changes in structural design recommendations to meet serviceability and ultimate limit state requirements with SCC can be made. In this investigation, we will classify the SCCs according to the hardened properties mentioned above and compare them with conventional NVC mixes typically used in highway projects in New Mexico and determine their performance characteristics.

1.2 Outline of Thesis

The overall goal of this thesis is to characterize new SCC mix designs by their time-dependent and fracture toughness properties and to compare their characteristics to conventional NVC mix designs that are currently being used for highway bridge design by the New Mexico Department of Transportation (NMDOT). There are many advantages of SCCs and if properly characterized, they can be utilized to their full potential in pre-stressed, precast bridge applications.

The first chapter provides a literature review of the research that has already been conducted relating issues of designing SCCs and their time-dependent and fracture toughness properties. The aggregate grading, mix designs for all the different concrete

mixes using two local aggregate sources are presented along with basic plastic and hardened characteristics of the different concrete mixes in Chapter 2. The test methods for the different time-dependent tests and fracture toughness tests are presented in Chapter 3 followed by results of creep and fracture tests of SCCs in Chapter 4. Conclusions and recommendations are presented in Chapter 5 along with possible future work to further understand SCC characteristics and potential uses.

Chapter 2. Literature Review

2.1 Introduction

Self-consolidating concrete (SCC) is a relatively new type of concrete developed in the late 1980's that has the ability to flow under its own weight. The first mix was designed by Ozawa et al. [1] in Japan in 1988 and has become increasingly popular in precast and pre-stressed structural applications. There have already been numerous examples of SCC being implemented in structural applications and being very successful, including being used to construct the World's tallest building in Dubai [2-3, 9-10]. SCC mixes are characterized by their ability to flow under their own weight, without bleeding or segregation of the aggregate, all while maintaining a constant viscosity. This characteristic allows SCC to flow through tightly spaced reinforcement and fill corners and voids in the formwork without the aid of mechanical vibration.

2.2 Methods for Producing Self-Consolidating Concrete

Two different methods of producing SCC currently exist in the literature. The first being the powder type SCC and the second being the viscosity modifying admixture (VMA) type SCC. Both mix types have certain advantages and disadvantages, and are both used equally in the concrete industry [11-15].

The first type is the powder type SCC, which uses well-graded aggregate, superplasticizers, limited aggregate content, and reduced water to cement ratio. A low water-cement ratio creates the viscosity needed to limit the local internal stresses when aggregate comes into contact with the reinforcement. However, to keep the water-cement

ratio low, superplacticizers are needed to maintain the flowability characteristics of an SCC mix [16]. The reason this type of mix is referred to as the powder type is the large amount of cementitious fillers that are needed to compensate for the low aggregate content and to keep cost low. The cementitious fillers that are commonly used are silica fume, fly ash, and limestone powders. A reduced aggregate content is also required to reduce collisions with coarse aggregate particles. These collisions result in higher internal stresses and frictional forces that create blockages when the flowable concrete comes into contact with different obstacles in the plastic phase. Since flowability is desired and an important criterion of SCC, coarse aggregate needs to be limited and compensated for with the different cement fillers mentioned above. The disadvantage of this type is its relatively high heat of hydration and shrinkage due to the high cement content. Careful curing is also necessary with powder-type SCCs.

The second type is the VMA-type SCC. By using VMAs, SCC mixes can be produced with a desired viscosity, thus eliminating the need to keep the water/cement ratio low. The increased viscosity reduces the kinetic energy while maintaining the flowability characteristics that are desired. VMAs are typically water-soluble polysaccharides that help the cement paste phase retain water [13]. VMAs change the cohesion properties in concrete while maintaining the fluidity desired [17-18]. SCCs are very sensitive to minor changes in water content, and a small amount of water can create a very fluid mix with an exponentially reduced viscosity. When the viscosity is high, it is advantageous to add VMAs to control the overall segregation of the mix.

Early work by Khayat [13] showed the optimal combination of superplacticizers and VMAs to produce an SCC mix with the desired flowability characteristics with

resistance to segregation. In more recent studies, VMA type SCCs also show an increased filling capacity while maintaining resistance to aggregate segregation and bleeding [19-20]. Khayat [13] also provided evidence that VMAs increase stability in highly flowable SCC mixes. It was shown that increasing the VMA content from .025% to .075% (by weight) results in a large reduction of settlement and segregation in mixes incorporating fly ash, while maintaining similar flow characteristics. Several other researchers have also concluded that SCCs with a higher percentage of VMA produce enhanced filling characteristics; up to a 60% increase in filling capacity [13, 21-22]. This characteristic will be discussed later.

Additional research conducted by the National Cooperative Highway Research Program (NCHRP) concluded that SCC mixes with at least a 40% water/cement ratio and limited superplasticizers exhibited enhanced stability when VMAs were added. NCHRP also recommended that VMAs only be used in mixes with a 40% water/cement ratio; however, lower ratios can be used to create an extremely stable SCC mix, but with reduced flowability characteristics.

The main difference between SCC mixes and the conventional NVC mixes is the way they perform during their plastic phase. The plastic properties of SCC's are what make these mixes so popular in different structural applications. The main characteristics that differentiate an SCC mix are the flowability, viscosity, passing ability, and the mix's overall resistance to segregation. The flowability characteristic determines how well the mix can flow under its own weight. The viscosity is defined as how well the mix resists flow once fluidity has been initiated. Overall passing ability of a mix is defined as to how well the mix is able to flow and pass through obstacles without segregation or blocking,

and finally, the mix's resistance to segregation is defined by the ability of the mix to sustain homogeneous composition during the plastic state. There are several methods to test these characteristics and appropriately classify different SCC mixes.

Overall flowability of a mix can be tested using a very similar test to the slump of normally vibrated concrete[23]. However, instead of measuring the slump of the concrete, you measure how far the mix flows across the slump table. Like the slump test for NVC, a slump cone is filled to the top, however, one layer is used and no rodding is to be performed while filling the slump cone. Once filled, the cone is lifted slowly and the fresh concrete is allowed to flow freely across the slump table. Once the concrete stops flowing, measurements are taken to classify the SCC mix. Instead of measuring how far the concrete slumps, you measure the largest diameter of the flow and the diameter of the flow ninety degrees in relation to the first measurement. These diameters are averaged and the flowability of the mix is classified by how large the mean diameter is. A more flowable mix will produce a larger mean diameter. In Figure 2.1, a schematic is presented on how one is to take measurements for the slump flow of a given SCC mix [2, 24-27].

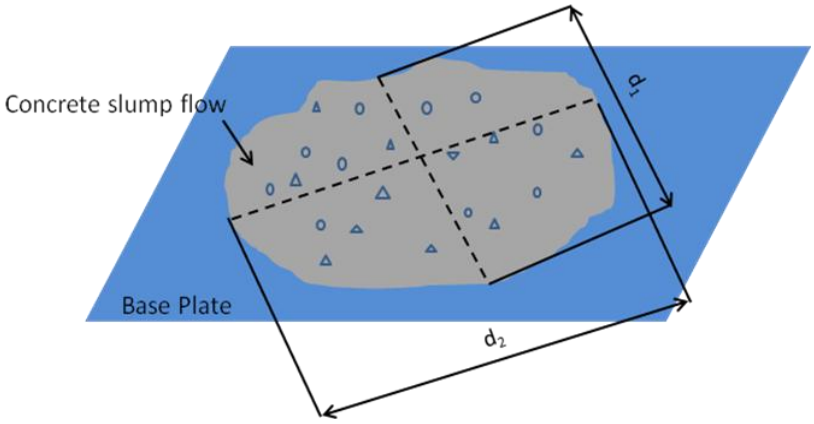

Figure 2.1 – Schematic of slump flow test

According to the European Guidelines for classification of self-consolidating concretes [24], there are three different classes of SCC mixes. The three classifications are shown in Table 2.1.

Table 2.1 – European slump flow classifications for SCC's [24]

Class	Flow Range (mm)	Application
SF1	550-650 (22-26in)	Small sections with large reinforcement spacing
SF2	650-750 (26-30in)	Columns and walls
SF3	750-850 (30-34in)	Tightly spaced reinforcement and complex form shapes

SCC's with larger flow diameters than 850mm (34in) can be produced, however, segregation starts to become a major issue and needs to be monitored very closely [28-31].

The next characteristic that classifies different SCCs is the viscosity of the mix in its fluid state. The mix needs to be a certain viscosity to prohibit the internal stresses that result in low-viscosity mixes that create blockages at obstacles. The test typically used to classify the mix's viscosity is the T_{500} test. Before the start of the slump flow test, the slump table is marked with a circle that has a diameter of 500mm. The slump cone is placed at the center of the marked circle and is then filled with the wet concrete. Once the slump cone is lifted, a stopwatch is started, and the time it takes for the concrete flow to hit the diameter of 500mm is recorded. Since viscosity is defined as resistance to flow once fluidity has been initiated, the different times recorded for the concrete to reach the given diameter allows for a viscous classification based on flow rates. The time recorded

for this test is considered the mix's T_{500} time. There are currently two different classifications for viscosity classifications of an SCC mix. The criteria can be observed in Table 2.2.

Table 2.2 – Viscosity classifications for SCC mixes [24,32]

Class	T_{500} time (sec)	Applications	Disadvantages
VS1	> 2	Highly congested formwork	Segregation problems due to low viscosity
VS2	< 2	Less congested formwork	Better overall stability and increased resistance to segregation

The next important rheological property when classifying an SCC mix is its ability to pass through obstacles or reinforcement. There are several tests constructed for this classification, however, the most common test to classify passing ability is the L-box test. The L-box test has two different setups that can be run to further classify the passing ability of a mix. The first test setup is with two reinforcing bars where the gate is what separates the two compartments. The second test setup is with three reinforcing bars to simulate a highly congested area. The test is run the same as the U-box, in that the vertical compartment of the test setup is filled with the fresh concrete. The gate is lifted allowing the concrete to flow freely through the obstacles. Once the flow ceases, the difference in height from the two compartments is recorded. The schematic can be seen in the Figure 2.2.

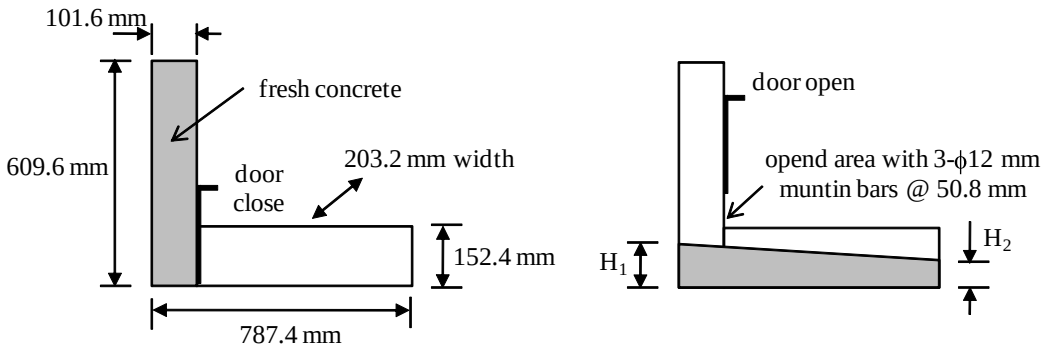

Figure 2.2 – Test setup of the L-box test to classify passing ability of an SCC mix

Three measurements are taken to obtain an average of both H_1 and H_2 seen above. The mean values are used to determine the ratio of H_2/H_1 and the passing ability is classified by this ratio. There are currently two different passing ability classifications that are given to an SCC mix. The first is the PA1, which is assigned to a mix that has a H_2/H_1 ratio of 0.8 when two rebar obstacles are present in the L-box test setup. The second classification is the PA2, which is given to a mix with this same ratio of 0.8, but the test setup contains three rebar obstacles instead of two. The PA2 classification characterizes a highly fluid mix that is typically used when highly congested reinforcement is present in the structural design [20, 25, 28-37]. Table 2.3 summarizes the passing ability classifications.

Table 2.3 – Passing ability classifications for SCC mixes [24]

Class	# of rebars	Applications
PA1	2	Less congested formwork
PA2	3	Highly congested formwork

The last plastic property that needs to be tested to classify SCC is the ability of the mix to resist segregation. It is important for the concrete to remain homogenous during its plastic phase to achieve the performance characteristics needed for a given application. There are a few tests used to assign a classification for the SCC mix that can be conducted during the casting phase. One test that is commonly used is the sieve segregation test. To conduct this test, one must place a 5mm (3/16") sieve over a container. The fluid concrete is poured upon the sieve. The initial concrete weight is known, and after two minutes of letting the concrete stand on the sieve, another weight measurement is taken. The percentage of the concrete mix that flows through the sieve are then calculated [24, 28, 38-40]. There are currently two classifications for a given mix's resistance to segregation. The first is the SR1 classification that is assigned to a mix with 20% or less (by weight) that flows completely through the sieve. This type of mix is used when a flow distance of over 80mm is needed. The second classification is the SR2, which is given to a mix the 15% or less (by weight) that flows through the sieve. SR2 mixes are typically used when the flow distance is less than 80mm.

It has also been discovered by many researchers that the air content of SCC mixes is much harder to control. The flowability of SCCs can cause air-bubbles to form and conventional practices using air-entraining admixture is not accurate [41-44]. The new generation superplasticizers that are needed to produce SCCs are shown to cause inconsistent results in designing a mix for a certain air-content [44]. Because of this problem, anti-foaming admixtures are recommended to help control the air content in SCC mixes.

Another important component incorporated in many different concrete mixes (both NVC and SCC mixes) is coal fly ash. Fly ash is a byproduct of coal power plants and is a pozzolan that chemically reacts with calcium hydroxide (CH) to produce strong calcium silica hydrate (C-S-H). When fly ash is added to concrete mixes it produces a pozzolanic reaction that converts the calcium hydroxide, which doesn't contribute to overall strength of the concrete, to C-S-H gels that are major contributors to the concrete strength [45]. This pozzolanic reaction also increases many of the durability properties of the concrete. Research has showed improvements in resistance to sulfate attacks as compared to mixes without fly ash. The absorption characteristics also increase, which results in better freeze-thaw resistance due to the entrained air that helps relieve internal pressures that occur when the water inside the concrete expands and contracts. Chloride Ion penetration was reported to be typically lower in concretes incorporating fly ash also [46]. Many mechanical and durability properties have shown improvement when a concrete mix incorporates fly ash. Another important topic that has arisen in the last decade is the sustainability of construction materials. By replacing a percentage of the "fossil fuel hungry" cement with recycled coal fly ash, which doesn't need any processing, we can create a more sustainable construction material. Many researchers are starting to study how to incorporate more fly ash in all concrete mix designs for this sustainability issue [47].

In addition to improved mechanical and durability properties, fly ash has shown the ability to help the plastic properties in SCC mixes as well. Research has shown that an increased fly ash content could also increase the slump of the mix and also reduce cement/fine filler use that is needed to produce SCCs [46]. It has also been shown that

fly ash helps maintain a constant optimum viscosity for SCCs to control segregation, thus reducing the need for VMAs; resulting in a reduced cost [46].

There are also micro-structural differences between conventional NVC and SCC mixes. The differences arise because the components of the different types of concrete are much different. SCC mixes have an increased amount of cementitious fillers, superplasticizers, and admixtures which react differently during the plastic phase than a normal vibrated concrete mix. Another contributing factor is that SCC mixes do not need any mechanical vibration [48]. Several micro-structural differences result, but the most prominent differences are the structural differences in the interfacial transition zone (ITZ). The interfacial transition zone is the area located along the aggregate face and the surrounding cement paste. The cause of failure for many normal strength concretes occur due to structural deficiencies in this region. Researchers have shown that the ITZ of NVC's have a more porous micro-structure when compared to SCCs, when analyzed using scanning electron microscopes (SEM) [49]. This relatively high porosity in NVC results in reduced failure strength of the concrete mix. The conclusion drawn from this high porosity in the ITZ of a NVC mix was explained by the accumulation of pore fluid as a result of mechanical vibration. Such pore fluid is not present in SCC because it doesn't require any vibration [49]. Moreover, vibration can result in internal and microbleeding in concrete producing micro-water pockets that increases the porosity at the ITZ. The absence of vibration in a SCC reduces the possibility of internal and micro-bleeding, thus creating a less-porous ITZ [49-52].

The cementitious fillers or pozzolans that are typically used more in SCCs than NVCs alter the hydration process, which results in micro-structural differences between

mixes. Some pozzolans increase the rate of hydration, like limestone fillers that are used in the powder-type SCCs, which results in different micro-structural properties [48]. Fly ash is cementitious filler that is used in SCC mixes that actually slows the hydration phase causing a delay in strength gain [53-54]. Research conducted by El-Dieb [56] actually shows the change of microstructure when looking at the ITZ of a high-strength powder type SCC. The figure below shows the dense microstructure in the ITZ of the SCC mix [55]. Altering the chemical processes during concrete curing produces micro-structural changes between mixes.

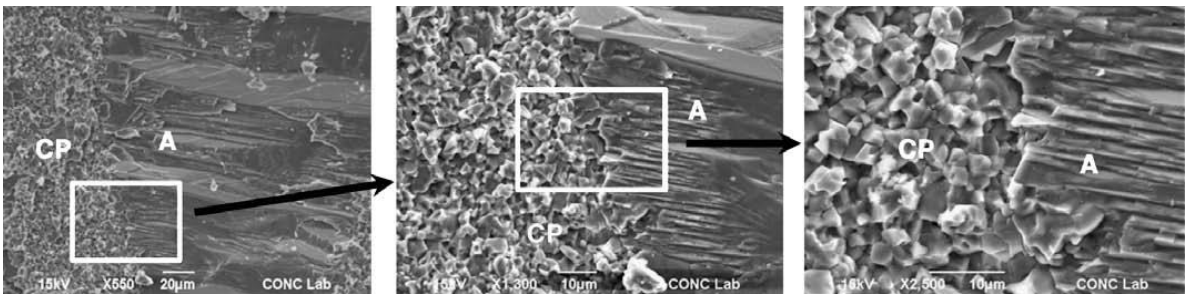

Figure 2.3 – Interface between aggregate particle and cement paste [55]

Because SCCs and NVCs contain very different constituent materials and have different fresh state properties, hardened properties are expected to also differ. When comparing hardened properties of SCCs and NVCs, different SCC mixes tend to exhibit higher variations in hardened properties because of the many different classifications of SCC mixes and the varied materials that can be used to create a SCC [56]. The micro-structural differences for SCCs and the less-porous ITZ enhance the overall strength and durability characteristics as opposed to NVC mixes with similar water/cement ratios.

Researchers have also shown that powder-type SCCs containing limestone had significant strength gains at early age compared to a similar NVC mix [55-56].

Many researchers are now experimenting with different cementitious fillers and amounts used in a given concrete to try and study the effects of these fillers on the hardened properties of concrete. Research has shown that using a high volume of fly ash (50% by weight of cement) with some replacement actually reduces compressive strength in fiber reinforced SCCs [43]. Another important finding by Golaszewski [57] was that VMAs can affect a mix's overall compressive strength. Golaszewski [58] shows that when VMAs interact with superplacizers in a mortar mix, compressive strength can be affected.

It is expected that since SCCs have a reduced coarse aggregate content, that the Young's Modulus will also be reduced when compared to conventional NVC mixes. Comparisons of Young's Modulus of elasticity of different SCC and NVC mixes have also been reported and at low-strengths, the elastic modulus was shown to be up to 40% lower in a SCC mix when compared to a similar NVC [56]. However, at higher compressive strengths, the difference was reduced to 5% [56]. In more recent research by Schindler et al. [58], it was concluded that there is no significant difference in stiffness when comparing SCC and NVC mixes.

2.3 Creep

Viscoelastic materials exhibit both viscous and elastic properties when subjected to stress. Viscoelastic materials, like concrete, are materials that show time dependent strain increase when subjected to sustained stresses. Creep and stress relaxation are

phenomena of viscoelasticity. Creep is a property that is observed in concrete. Another example of viscoelasticity is stress-relaxation. Commonly seen in steel, stress relaxation is the reduction in stress seen if the material is subjected to constant deformation. These time dependent properties are extremely important to consider in structural design due to the fact that typical creep in concrete can result in observed deformation 2-3 times the instantaneous deformation observed at load application [59].

When concrete is subjected to constant stress, large deformations occur which can lead to catastrophic failure of structures. For instance, constant stress is observed by the concrete in pre-stressed applications. Creep will result in pre-stressing losses and stress redistributions that need to be considered during design. Extensive research tried to predict creep strains to design safer concrete structures. Much of this research has looked into how to model creep strains and predict its effect on structural systems [60-62]. It has also been shown that concrete is a material that exhibits very high creep strains over time due to its microstructure [63-66]. The type of creep that we will focus on when examining time-dependent deformations is primary creep occurring at relatively low stresses. We also limit our discussion to viscoelasticity and its implications of that creep on concrete serviceability since most of the constant stresses seen in structural concrete applications are well below the compressive elastic limit of concrete materials.

Generally, there are three stages of creep deformations. First, there is elastic strain that occurs at the instant a load is applied. This is a deformation that is directly related to the stiffness of concrete. The first stage of creep is called the primary creep. Concrete will exhibit deformations that decrease with time within this range. The second

stage of creep is referred to as the secondary creep which can also be referred to as stationary creep. This range designates the stage where steady state creep is observed and if the material possesses a minimum creep rate, it will occur within this range. Finally, the last stage is called the tertiary creep. This range may or may not occur depending on the kind of stress. However, in this range, the creep rate increases again until structural failure. For typical concrete, no distinction can be made between the first two stages of concrete and the third stage. However, tertiary creep, is rarely observed because the sustained loads typically seen in a concrete structure are in the ranges 25-40% of the ultimate resistance of the structure. Tertiary creep takes place at stress levels close to 60-70% of ultimate strength of concrete [60]. In Figure 2.4, a graphical representation of the different stages of creep [59] is shown.

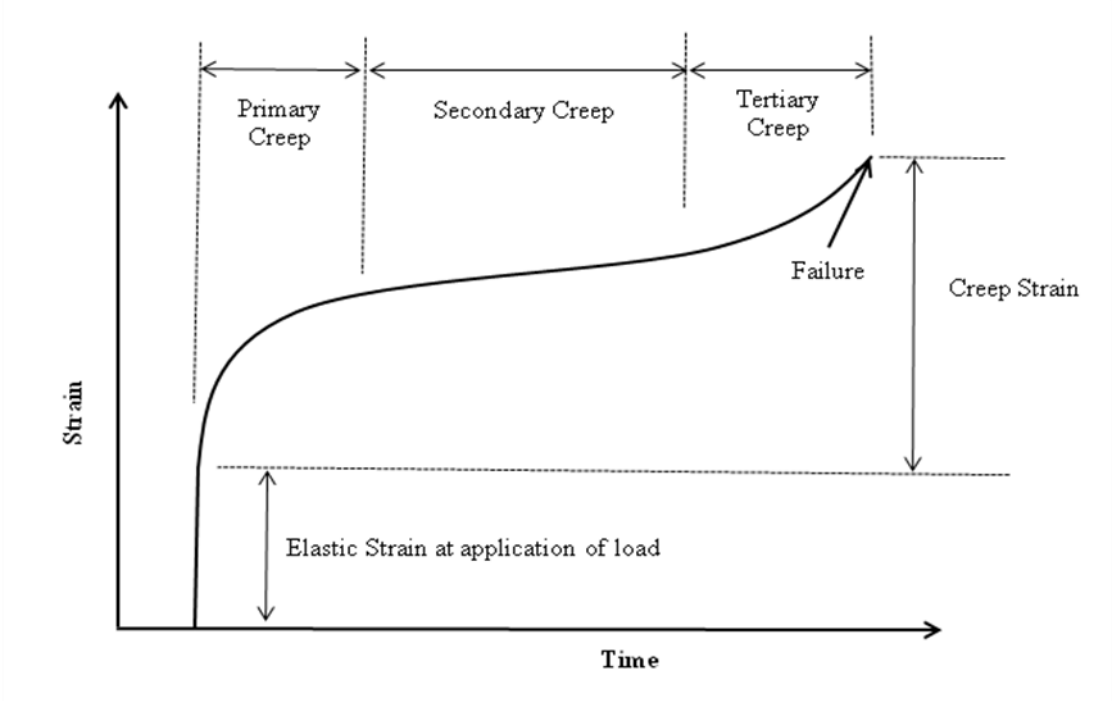

Figure 2.4 –Creep behavior showing all possible creep stages [60]

Recoveries in creep deformations can also be observed once the load is removed from the structure. However, load removal does not typically happen in service because most sustained loads that result in the sustained stresses (self-weight, dead loads, etc.) causing creep are usually not removed from an in-service structure. Once the load is removed, an instantaneous recovery is observed, and this recovery is where most of the deformation is recovered. However, there is also a creep recover stage, in which strains are recovered over time [59, 65]. In Figure 2.5, a graphical representation of the creep recovery process is presented.

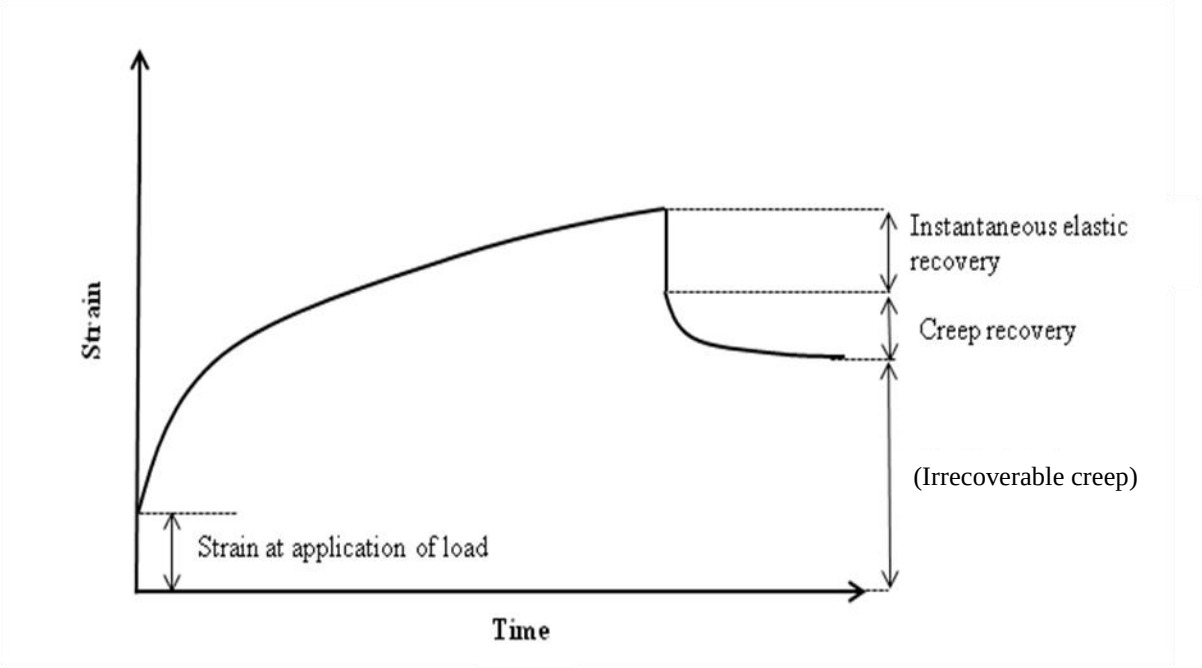

Figure 2.5 – Creep and creep strain recovery upon constant stress removal [60]

To understand creep and appropriately model creep characteristics, different rheological models have been developed. There are many different models for creep phenomena; however, the most popular models include the Kelvin, Maxwell, and Burgers

models [60]. These models use spring elements to represent the Hookean solid, the Newtonian liquid modeled by a dashpot, and the friction element is modeled by the St. Venant body. The differences between the mentioned models is to how they model instant, delayed, and total deformations of the material under loads [59, 65]. The Kelvin, Maxwell, and Burgers models are described below in equations (2.1), (2.2), and (2.3) and are shown in Figure 2.6.

$$\varepsilon(t) = \sigma\left(\frac{1}{k} + \frac{t}{\eta}\right) \tag{2.1}$$

$$\varepsilon(t) = \frac{\sigma}{k}\left(1 - e^{\frac{-tk}{\eta}}\right) \tag{2.2}$$

$$\varepsilon(t) = \frac{\sigma}{k_1}\left(1 - \frac{-tk_2}{\eta_1}\right) + \sigma\left(\frac{1}{k_2} + \frac{t}{\eta_2}\right) \tag{2.3}$$

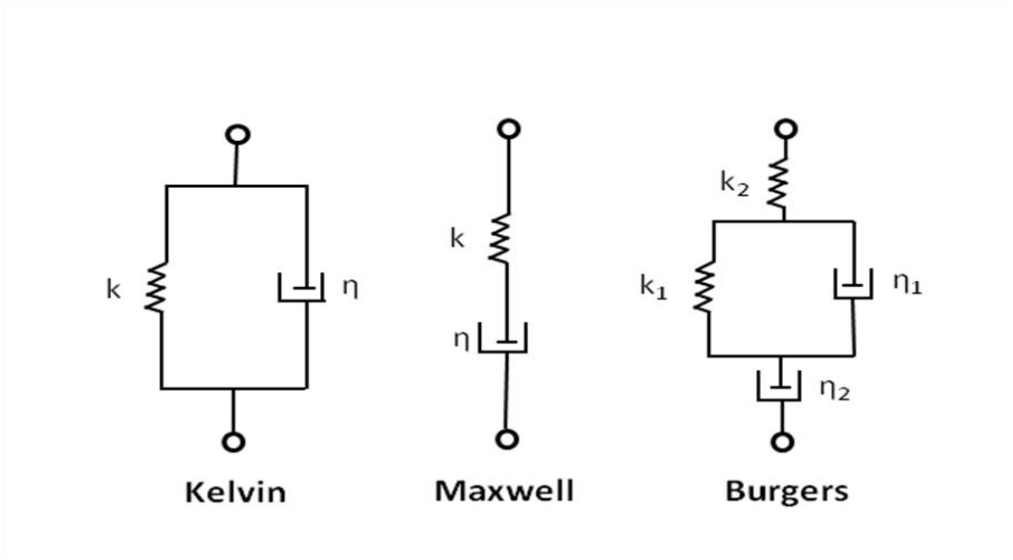

Figure 2.6 – Schematic representation of rheological models [60]

In each of the above equations, $\varepsilon(t)$ is the strain of the material at a given time (t). k represents the stiffness of the spring and σ is the applied stress. The η_{1-2} represents the damping coefficient used for the dashpot.

To adequately model creep, one must understand the mechanisms of creep and how different mechanics affect total creep within a material. There are many theories that exist for the mechanics of creep behavior in concrete. Some of the theories include mechanical deformation theory, plasticity theory, viscous and visco-elastic flow theories, solid solution theory and seepage theory [59, 65]. However, due to the brittle nature of concrete, micro-cracking might also be used to explain part of concrete creep.

When concrete is subjected to sustained stresses, the interfacial transition zone (ITZ) between the aggregate and the cement paste shows non-linearities that are not seen in neat cement paste. The interface provides a discontinuity in the concrete that is known as a bond crack. This bond cracking in the ITZ is the underlying idea behind micro-cracking theory. At certain stress levels, this is the region where bond cracks begin to increase and the strains within this region increase creep at a higher rate than other creep mechanisms. The density of micro-cracks within the ITZ region is a major factor influencing the fraction of creep attributed to micro-cracking. These micro-cracks can be formed at application of load, under certain sustained loads depending on the ratio of the sustained load compared to the ultimate load, and any shrinkage micro-cracks that form before load application. It is estimated that micro-cracking is responsible for up to 25% of the total creep deformation when concrete sustains compressive stresses [59]. It is also important to note that the creep deformations that occur due to micro-cracking are irreversible strains and cannot be recovered [59].

The cement paste properties are also very important in creep calculations. It is believed that the cement paste is the major contributing factor in concrete creep. Micro-cracking theory, as presented above, is a major factor in creep calculations, however, other creep theories help explain different creep mechanisms within the cement paste. During the hydration process of the cement paste, calcium silica hydrate (C-S-H) forms, and when the concrete is subjected to a humidity of less than 100%, physically absorbed water is lost, and shrinkage strains are observed. This same phenomenon can be observed when a wrapped specimen is subjected to a constant stress. The water within the C-S-H layers is physically forced from these layers which directly causes creep strains. This idea is attributed to the seepage theory. This process is another contributing factor to the overall creep of concrete [59, 65].

Aggregate type can also affect creep mechanisms in concrete. The type of aggregate used and how the aggregate is graded is a major factor influencing the modulus of elasticity [65]. The best explanation as to how aggregate affects the creep is how well the aggregate restrains creep of the cement paste. A concrete mix with aggregate that produces a higher modulus of elasticity will offer a great restraint to creep. Light-weight aggregate concretes were often observed to have higher creep values than that of normal weight aggregate concretes. However, in recent research, it has been shown that these high creep values were attributed to the low modulus of elasticity of light-weight aggregates. A concrete mix using light weight aggregate was shown to have similar creep values when compared to normal weight concrete when the modulus of elasticity's were comparable [59].

There are currently two different types of creep that have been realized in concrete. The first is classified as drying creep, which is caused by the loss of water in hardened concrete that results in strains. Drying creep is classified as the creep that occurs when the concrete specimen is exposed to humidity conditions that are less than optimum, or conditions when the concrete is not completely saturated by water. These strains that result in the drying process tend to be higher than basic creep strains because of the micro-cracking that takes place as a result. This micro-cracking will lead to higher deformations when the specimen is subjected to a constant stress. The other creep is referred to as basic creep. Basic creep is classified as the deformations that take place when a specimen is saturated but still under a constant stress. We try to differentiate and observe the two types of creep in experiments by wrapping a specimen subjected to sustained stress such that no drying strains will occur. The deformations from the wrapped specimen will be the basic creep strains, while a specimen under the same stress but unwrapped will observe both drying and basic creep strains. The unwrapped specimen, therefore will creep more, and the difference between the two specimen strains is drying creep strain [59] . In Figure 2.7, a graphical representation of the different creep strains in concrete can be observed. It is important to note that it is extremely difficult to accurately separate the different creep deformations into their respective classifications because there are many creep mechanisms that are hard to classify into a given category. For instance, how to differentiate drying shrinkage and drying creep has been a major point of argument and debate among researchers [67].

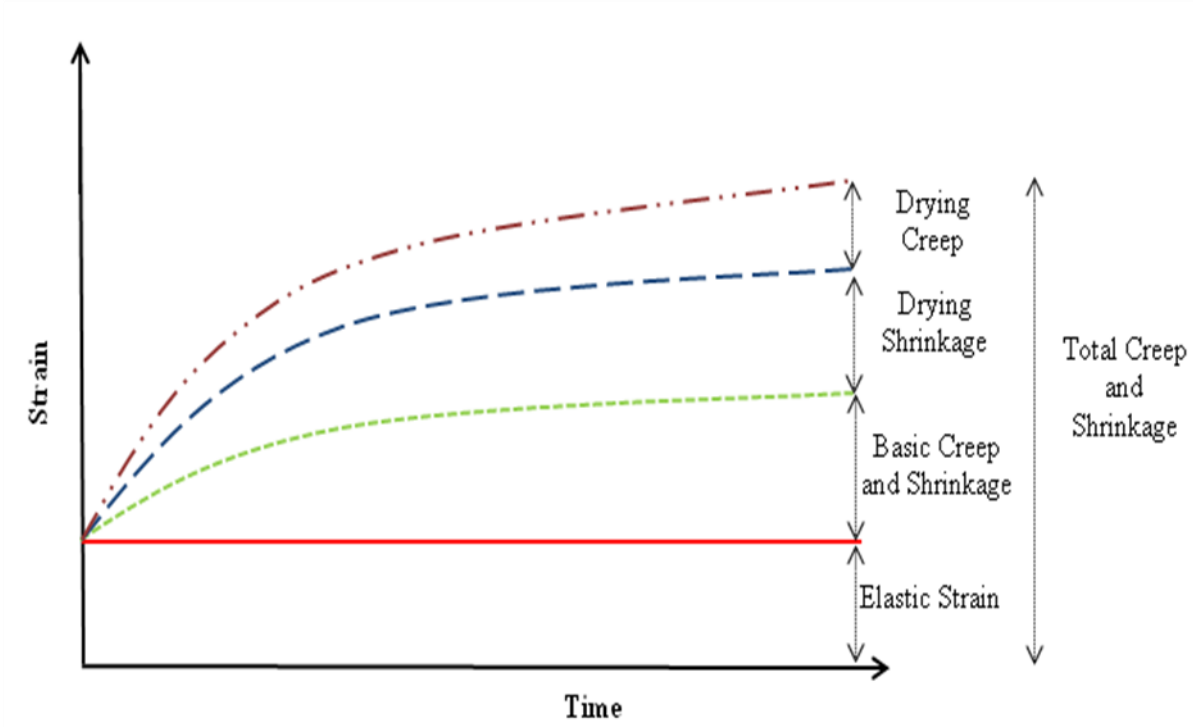

Figure 2.7 – Different creep mechanisms (components) in concrete [60]

2.3.1 Factors affecting creep of concrete

There are many factors that occur simultaneously that affect the overall creep of a given concrete mix. One of the major influencing factors is the total volume ratio of the cement paste. Extensive research has tried to correlate the volume of cement paste to long-term creep deformations. However, many other factors also contribute to the creep characteristics of different concrete mixes. The size, shape, texture, and amount of aggregate present in a concrete mix are all contributing factors to overall creep characteristics. These different aggregate properties affect the volume of the cement paste and modulus of elasticity of concrete. The initial creep strain is altered with varying modulus of elasticity. The overall time a concrete is subjected to constant stress and

changing relative humidity also affects creep strains. When the relative humidity is low, an increased amount of micro-cracking results from drying strains and more water will be lost from the CSH layers, thus the overall creep attributed to drying creep is increased. Some other factors are the volume to surface area ratio, curing history, compressive strength, constant stress to ultimate strength ratio, and ambient temperature. All these factors contribute to creep deformations in concrete [59, 68].

Due to the many advantages of SCC being used in pre-stressed applications, the time-dependent properties must be understood to ensure safe designs of these structures. Many researchers have tried to compare creep deformations of SCC and NVC mixes, but much of the literature is contradicting [5-8, 42-43, 51, 69-71]. With no clear conclusion of creep behavior in SCCs, it is very hard for a designer to consider time dependent creep deformations and ensure that the structure is safe without understanding the creep and shrinkage characteristics of SCC. Research has shown SCCs that used certain types of VMAs actually exhibited drying shrinkage strains 50% greater than that of an NVC mix will similar volumes of cement paste [72]. These conclusions showed the necessity for good field curing to prevent these drying strains. Further research by Turcry and Loukili [73] showed the tendency for early shrinkage cracks and careful field curing is needed to prevent these cracks. Much of the research related the higher creep deformations of SCC to an increased volume of cement paste. Research has also shown that SCCs incorporating fly ash results in higher shrinkage values than comparable NVC mixes. The shrinkage was also shown to increase as the fly ash content increased [7].

Other researchers have also investigated shrinkage strains of SCC mixes as compared to NVC mixes with constant water/cement ratios that were all within the range

of 0.35 to 0.45. Class F fly ash was used to partially replace cement content. The percentages of fly ash were 40%, 50%, and 60%. The samples were cured for 7-days in a lime-saturated bath and drying shrinkage strains after 224 days were comparable to similar NVC control mixes with no fly ash [74]. Additional research by Sahmaran [34] showed that SCC mixes incorporating high-volumes of fly ash exhibited less shrinkage strains after 1 year when compared to control mixes containing no fly ash. It was concluded that when fly ash is used, the cementitious matrix became denser due to the fly ash addition and helped prevent internal moisture losses [34].

Research has also been conducted to evaluate creep of SCCs and compared them with conventional NVC mixes. Work done by Persson [4] compared SCC creep values with NVCs and concluded that creep strains were comparable in both types of concretes. Four mixes of NVCs and SCCs with different water/cement ratios were designed ranging from 0.24 all the way up to 0.80. Different constant stresses were also applied to the different specimens at values of 0.20, 0.40, 0.55, and 0.70, all percentages of the ultimate compressive strengths of the given mixes. In addition, Persson [4] also loaded the different specimens at varying curing histories ranging from 2 days up to 90 days. From all of these specimens, Persson [4] concluded that SCC and NVC mixes performed similar when comparing in total creep deformations. It was also noted that by loading the specimens at a young age (reduced curing time), much higher creep deformations were observed as opposed to loading the specimens that have had ample time to cure and hydrate. In addition, Persson [5] compared high-performance SCC mixes with NVCs in terms of creep strains and concluded that there was no observable difference between the SCCs and the control NVCs.

Other factors in SCC mixes, like the use of admixtures, might also contribute to creep deformations in different ways than commonly seen in NVC mix designs. Sukumar [41] noticed that SCCs incorporating VMAs and fly ash as the cementitious filler actually creeped less than a control NVC mix. Lowke [75] also investigated effects of VMAs and varying powder contents of SCC to try to understand how creep properties might be effected. His first conclusion was that the VMAs used had no effect on total creep deformations. It was also shown that increasing the air-entrainment resulted in an increase in the air voids. These additional air voids increased the creep and shrinkage strains of the SCC considerably. In the same investigation, Lowke [75] varied the limestone powder content in the different SCC mixes and it was determined that mixes with lower limestone powder contents showed less creep deformations when compared with similar mixes with high limestone powder contents. It was observed that the mixes with a reduction in limestone powder content had a courser pore structure which might be a reason as to why these mixes exhibited higher creep strains [76].

When comparing different cementitious fillers and their overall effects on creep, research has shown that SCCs using limestone powders deform less than similar mixes that used fly ash [77]. However, this can be attributed to the fly ash within the mix not being fully reacted when the constant stress was applied. The un-reacted fly ash showed deformations at time of loading and this can be the major reason as to why the SCC mix that utilized fly ash, as opposed to limestone powders, showed higher creep deformations [77].

Mazzotti and Ceccoli [78] analyzed shrinkage values of four different SCCs by varying the cement content within the mix. All admixtures, superplasticizer and VMAs,

were held constant and cement content was the only changing variable. It was noticed that by increasing the cement content, much higher shrinkage strains were observed.

Further research has been conducted focusing on the effects of varying cement paste volumes and how they contribute to creep and shrinkage strains in SCC mixes [79]. The different SCC mixes all used Portland cement, limestone filler, superplasticizer, coarse and fine siliceous sand, and coarse crushed stone granite. The different mixes were moist cured and loaded at 24 hours, 3 days, and 7 days. It was observed that all mixes loaded at 3 and seven days exhibited similar total creep strains. However, when loaded at 24 hours, the mix with the smallest volume of cement paste actually resulted in the highest creep deformations. It was also shown that shrinkage strains can be correlated directly to the volume of cement paste [79].

Research conducted by Reinhardt et al. [7] investigated total and basic creep deformations using the VMA-type SCC mixes and by varying fly ash contents by partial replacement of cement. The moist cured SCC specimens were loaded at 35% of the ultimate compressive strength at 10 days. The results showed that SCC mixes with increased amounts of fly ash replacement resulted in an increase in creep compliance. It was also observed that the SCC mixes had higher creep compliance when compared to a conventional NVC mix with no fly ash present [7].

2.4 Fracture Mechanics of SCC

The fracture toughness of the material can be defined as the materials ability to resist crack growth. Different materials undergo different mechanisms to resist crack propagation, whether it is plastic deformation or having different crack "arresters" present, and the overall amount of "resistance" can be determined to represent the fracture toughness of the material.

The current design codes for structural applications require the designer to consider both strength and serviceability limit states during the design process. The difference between the two criteria is that the ultimate limit state is based on the strength criteria and the serviceability limit state is based on the cracking criteria. Currently, the serviceability limit state is based on modulus of rupture models that proved to contain significant uncertainty in the overall structural design [80]. In addition, reinforced concrete members are designed to behave in a ductile fashion, however, problems can arise due to possible quasi-brittle failure of the concrete [81]. For instance, the debonding or slipping of the steel reinforcement at crack locations can drastically affect a structures overall safety. A similar problem can arise in estimating the shear or tensile strength of concrete in a large structure when the size effect of the structure is neglected [82].

Pioneering work in the world of fracture mechanics was done by Griffith in 1921 [83] when he determined that there is an energy requirement to propagate a crack by an incremental length when the stress condition is met (tensile stress). Since this early work, many researchers have determined more complexities in fracture mechanics since materials do not all behave in a perfectly brittle fashion. Three different subsets of fracture mechanics models have arisen due to this research; linear elastic fracture

mechanics (LEFM), elastic plastic fracture mechanics (EPFM), and quasi-brittle fracture mechanics (QBFM). The most accurate model to utilize is determined by the ductility behavior of the material and the fracture resistance mechanisms present within the material.

The first paper looking at fracture mechanisms in concrete was in 1923 when Richart et al [84] determined that the failure mechanisms of concrete under compression were due to tensile stresses forming at the internal voids in the concrete. It wasn't until 1961 when Kaplan showed experimentally that a certain strain-energy density release rate is needed to propagate the crack which will consequently lead to compression failure [85]. This work by Kaplan led to a paper produced by Glucklich in 1963 [87], who proposed a new fracture criterion related to the energy criteria first formulated by Griffith. However, this elastic energy release rate, denoted G_{IC}, that was proposed by Glucklich [87] can be directly applied to concrete as a fracture criterion [86]. Although proven later to be incorrect or incomplete, the work by Glucklich [87] was some of the early work to address concrete heterogeneity.

In the past several decades, more research has been conducted, and it has been reported that there is a major difference between theoretical and experimental results when applying LEFM to concrete materials. The complexities of a heterogeneous material like concrete contain many mechanisms that cannot be theoretically accounted for in LEFM modeling. The fracture process zone (FPZ) that can be observed in concrete violates LEFM because the main assumption of LEFM is that the creation of surface energy is the main source of energy consumption. The fracture process zone was first observed by Patterson and Chan in 1975 by observance of microcracks being present

ahead of the crack tip [87]. Other forms of non-linearities have been discovered; examples being crack branching, crack deflection, crack bridging, crack tip blunting, etc. that create even more problems with a simple LEFM analysis. The discovery of this fracture process zone has led to different models (EPFM and QBFM) to appropriately characterize fracture toughness properties in concrete.

The elastic plastic fracture mechanics (EPFM) approach to concrete was then investigated due to the limitations of LEFM analysis that are mentioned above. The first work trying to apply EPFM to concrete was done by Lamkin and Paschenko [88] by applying EPFM ideas to determine a critical stress intensity, which they denoted N_C. However, it wasn't until 1980 that Velazco et al. [89] applied the ideas from Rice [90] by using the J-integral and crack tip opening displacement parameters (CTOD) to try to apply EPFM to normal strength concretes. However, it is important to note that EPFM is typically used for highly non-linear concretes, which are typically fiber reinforced concretes (FRC) and polymer concretes (PC). The fracture toughness parameter J_{IC} has been shown to be most sensitive to change in fiber length [82]. It was concluded that both Gc–Δa and Jc–Δa R-curve criteria can be applied to concrete when determining the fracture resistance curves [91].

The final model used to determine fracture toughness properties in concrete is the quasi-brittle fracture mechanics (QBFM) approach. This approach provides a way to account for the different toughening mechanisms present in the fracture process zone (FPZ). It was first shown by Shah [81] that many toughening mechanisms exist in the FPZ of concrete. Shah was able to show three separate mechanisms that contribute to the fracture toughness of concrete that are all present in the FPZ; microcracking, crack

branching, and crack deflection. A schematic of the fracture process zone in concrete can be observed in Figure 2.8.

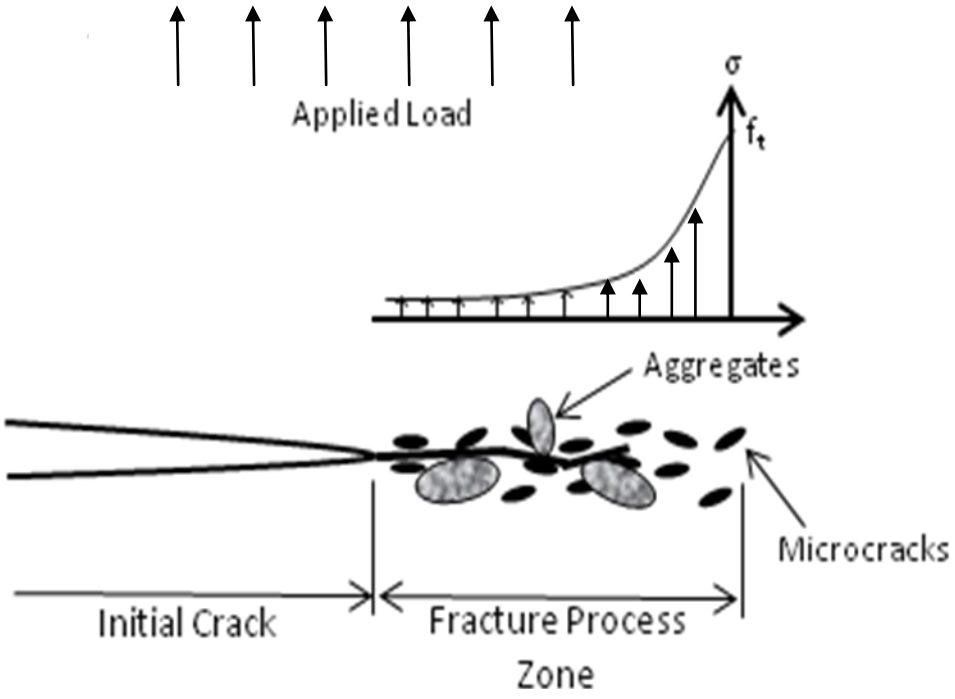

Figure 2.8 – Schematic of Fracture Process Zone in concrete

The large FPZ that is present in concrete provides many difficulties and causes very different fracture behavior when compared to perfectly brittle and fully plastic materials. The first work to try to determine an accurate modeling method of the FPZ was established by Hillerborg et al. [92]. The way he modeled the FPZ was by using an equivalent cohesive pressure that is acting on the FPZ to account for the different toughening mechanisms. This equivalent cohesive pressure provides a closing stress to the crack and is assumed to be a function of the crack opening displacement (COD). By accounting for the cohesive pressure, an equation can be determined to calculate the equivalent energy release rate in concrete, G_I. The equation first takes into account the

energy that is needed to fracture the two material surfaces, G_{IC}, and the second part takes into account the different toughening mechanisms by integrating the cohesive strength curve across the FPZ. This formulation is presented in Equation 2.4.

$$G_I = G_{IC} + \int_0^{w=CTOD} \sigma(w)d(w) \tag{2.4}$$

From the equation above, two different methods were developed by researchers to understand the fracture toughness properties of concrete. The first model was the fictitious crack model [92-95] which assumes concrete not to follow LEFT, thus G_{IC} to be zero because the surface energy in a quasi-brittle material is very small when compared to the energy required to overcome the toughening mechanisms that are present in the FPZ. The second model is the effective elastic crack model that was introduced by Jenq and Shah [96] that is able to characterize concrete by using two fracture parameters, K_{IC} and $CTOD_C$. The effective elastic crack model assumes all energy consumed by the fracture process zone to be zero by creating an effective equivalent, elastic, traction-free crack so LEFM principals can be applied to the model. The idea behind this model is to determine the critical crack length so that other fracture toughness parameters can be determined and compared. However, this procedure is not very applicable to very high strength concrete due to the fact that several load cycles need to be conducted and the specimen is expected not to fail on the first cycle.

The testing methods used to determine the fracture toughness properties for the different concrete mixes presented in this research are the Notched Beam Level II test that is a testing standard developed by ACI committee 446 and the Stiff Tension Fracture Test developed by researchers at the University of New Mexico [97]. Both the tests

mentioned are ways to determine fracture toughness properties using the cohesive crack model. The cohesive crack model is a model that utilizes the fictitious crack model to determine the area under the curve of the cohesive pressure-COD relationship, G_F, first discussed by Hillerborg [92].

Very little research in the literature examined the fracture toughness properties of SCC mixes. The author believes that the concrete mixes necessary to produce SCC might have a significant effect on their creep and fracture toughness. This is related to the fact that SCC mixes reduce aggregate size and significantly increase powder size, increased fly ash in this research. The change in the aggregate structure and size will affect the energy needed to propagate cracks and the nature of the FPZ. Due to the fact that SCC mixes contain a larger mortar matrix than conventional concrete mix designs due to their lack of coarse aggregate particles to serve as "crack arresters"; it is expected that SCC mixes might behave in a more brittle fashion and have lower fracture toughness values [56]. Research conducted by Roziere et al. [71] analyzed the fracture toughness, G_F , of different SCC concrete mix designs by varying the cement paste content using the 3-point bending fracture test. Typical superplasticizer, VMA, and varying limestone filler content were used. It was concluded that as the volume of cement paste increases, the fracture toughness decreases. In Figure 2.9, a graphical representation is shown from Roziere's research.

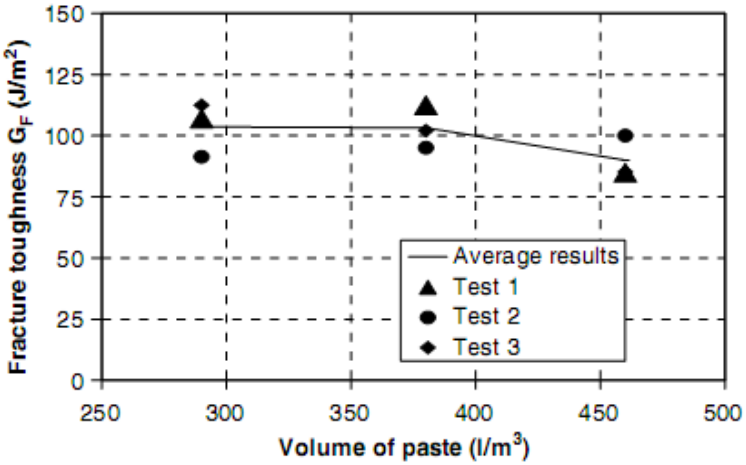

Figure 2.9 – Fracture toughness vs. volume of cement paste [71]

Research was also conducted by Zhao et al. [98] to analyze the fracture toughness of SCC mixes with varying strengths by utilizing the splitting wedge test. The tests were conducted on four different SCC mixes and concluded that the overall fracture toughness values obtained from the SCC mixes was lower than the typical values obtained with the same test using conventional NVC. Nevertheless, contrasting research results were published by Fava et al. [99] comparing fracture toughness and fracture processes in SCC and NVC mixes of similar strengths by using the three point bending test. Fava et al [100] work concluded that both SCC's and NVC's have similar fracture toughness properties.

An important parameter when comparing fracture toughness values of different concrete mixes is the strength of the concrete at time of test. Concrete becomes more brittle at higher strengths, due to microstructure differences in the ITZ, resulting in lower fracture toughness values. SCC incorporating fly ash will grow strength with time and thus fracture toughness values might be reduced with time. In the research conducted by Roziere [72], the intention of the research was to determine how different volumes of cement paste affect the concretes fracture toughness. The strengths reported by Roziere

[72] for all the mixes tested were between 42-47 MPa. Zhao [99] reported two different strength groups for the tests that were performed; 46-48 MPa and 61-63 MPa respectively. However, the research conducted by Fava et al. [100] comparing SCC and NVC fracture toughness values reported higher strengths for all SCC mixes when compared to NVC. The three SCC mixes had strength values of 59, 58, and 51 MPa, while the three NVC mixes for comparison reported strength values of 41, 45, 38 MPa. The contrasting results obtained by Fava et al. [100] might be a result of the variation in concrete strength as opposed to the micro-structural differences between SCC and NVC concretes.

Chapter 3. Concrete Mix Designs and Testing Methods

3.1 Introduction

The purpose of this research is to first compare SCC mix designs with NVC mix designs that the New Mexico Department of Transportation (NMDOT) currently uses in precast and pre-stressed bridge applications. Time-dependent and fracture characteristics of the hardened concrete are important in bridge applications for serviceability and limit state design. SCC results need to be compared to a baseline NVC mix that currently works well under these conditions to determine if SCCs can be utilized in NMDOT projects. Moreover, two different aggregate sources are used and varying fly ash contents within the different SCC mixes are compared to identify the optimal SCC mix that will maximize the performance in NMDOT bridge projects.

The first aggregate source that was to be used was the Placitas source located in Placitas, New Mexico, fifteen miles north of Albuquerque. This source is widely used in construction and infrastructure projects in the Albuquerque and Santa Fe regions due to its close proximity. From this source, three mixes were created. The first mix was an NVC baseline mix provided by the NMDOT which contained 25% fly ash and three different nominal maximum sized aggregates. The next two mixes were both SCC mixes designed by the University of New Mexico using two nominal maximum sized aggregates and two different fly ash contents (25% and 40%). The three mixes were batched and compared to determine the time-dependent properties.

The second aggregate source utilized was from the Griego and Sons pit located in Fort Sumner, New Mexico (three hours east of Albuquerque). From this source, four

mixes were designed and batched. The first mix was a NVC baseline mix provided by the NMDOT for the Griego and Sons pit that has shown good performance characteristics in NMDOT projects. The next three mixes were SCC mixes designed and created by the University of New Mexico with varying fly ash contents (20%, 30%, and 40%). These mixes were compared with one-another and also to the Placitas mixes to determine which mix performed the best in terms of time-dependent properties. Fracture properties from the three Griego and Sons SCC mixes were also determined with varying fly ash percentages.

In total, seven mixes were batched, two commonly used NVC mixes and five SCC mixes and were compared to identify an SCC mix that can be used for pre-stressed, precast bridge applications. An SCC mix with similar or improved performance when compared to the baseline NVC mix would be preferable due to its plastic characteristics and ability to flow through the highly congested reinforcement that is present in bridge applications.

3.2 Mix Designs and Aggregate Grading

The first source that was used in this project was the Placitas pit that is located fifteen miles north of Albuquerque, New Mexico. The first mix produced was the commonly used NVC mix provided by the NMDOT. The nominal maximum size for the coarse, intermediate, and fine aggregate used was 3/4, 3/8, and 3/16 inch respectively. Class F fly ash obtained from Salt River Materials Group located in Farmington, New Mexico and Type I-II ordinary Portland cement (OPC) provided by the Rio Grande Cement factory located in Tijeras, New Mexico was used for all the mixes.

Polycarboxylate-based superplasticizer (Glenium 3030 NS by BASF®) was also used for the High Range Water Reducer. Grace Daravair AT-60 Resin-based air-entrainment admixture was used to ensure the target air-content in the concrete was obtained (6-9%). To ensure that each mix can be recreated with excellent quality control, aggregate tests need to be performed to determine the different aggregate's ability to absorb water and the different specific gravities. ASTM standards to determine specific gravities and absorption percentages of the different aggregates were used and presented in Table 3.1 [100]. In Table 3.2, the mix design for the NVC1 control batch is presented.

Table 3.1 – Properties of Placitas Source Aggregate

Material Description	Bulk Specific Gravity	Absorption
S.G. Rio Grande Type 1/2 Cement	3.150	
S.G. SRMG Class F - Fly Ash	1.990	
S.G. Placitas C33 Fine Aggregate	2.593	1.5
S.G. Placitas C33 Intermediate Agg	2.564	1.7
S.G. Placitas C33 Coarse Aggregate	2.597	1.1

The first step in conducting and classifying the different aggregate sizes and properties is to adequately review the methods in obtaining, storing, and randomly sampling the aggregate to ensure proper statistical results for the aggregate properties in which we are testing. The aggregate was obtained from the source and stored in air-tight barrels in the concrete materials lab at the University of New Mexico. To properly classify the aggregate, a random sample of aggregate must be used in all the aggregate tests so the properties of the aggregate can be properly used for the duration of the research project. To accomplish this, before any test was conducted, aggregate was sampled from every barrel used in storing the aggregate and was randomly sampled according to the ASTM splitting practices [101]. Once a random sample was determined,

the aggregate testing began. Three separate specific gravity and absorption tests were conducted to ensure accurate statistical results. The means recorded from these tests were recorded and used for the duration of the NMDOT research project.

The same sampling techniques were used for the sieve testing to determine the aggregate grading curves for the different concrete mixes. Individual sieve tests were conducted on the different nominal maximum sized aggregates and from these results, combined aggregate sieve testing was conducted to determine the combined aggregate grading curves. These individual sieve tests proved to be important to optimize the grading curves to match known NMDOT mixes that is discussed in the next section.

The other materials used in the mix designs mentioned above (fly ash, Portland cement, and admixtures) were all obtained at the beginning of the project and were utilized throughout the project.

Table 3.2 – NVC 1– Placitas Source

Component	Batch Weight (lbs/yd^3)	Absolute Volume (ft^3)	Batch Weight (kg/m^3)	Absolute Volume (m^3)
Cement Type 1-2	569	2.90	338	0.107
Fly Ash - Class F	169	1.36	100	0.050
Water	271	4.35	161	0.161
Fine Aggregate (X3)	965	5.97	573	0.221
Intermediate Agg. (X2)	1073	6.70	636	0.248
Coarse Aggregate (X1)	644	3.97	382	0.147
Air entrainment (6.5%) Grace AT60	18 oz	1.75	725 mL	0.065
HRWR BASF Glenium 3030	44 oz		1709 mL	
VMA BASF Rheomac	---	---	---	---
Total Aggregate	3691		2190	
Total Volume		27.00		1.000
Sand/Total Aggregate	0.36			
Water/Cementitious Ratio	0.368			

To recreate the mix design for the NVC control batch provided by the NMDOT, optimization techniques were performed to create similar aggregate grading curves.

Table 3.4 presents the results of the different percentages used for the different aggregate sizes. A combined grading curve is produced to compare the University of New Mexico mix and the NMDOT mix to ensure that the two mixes are similar. The different percentages of aggregate were determined by optimization techniques and were used to produce the combined grading curve that was created from actual laboratory testing. The ASTM standard for sieve analysis was used for all aggregate grading curves [102].

Table 3.3 – NVC 1 aggregate proportions from optimization

Aggregate Type	ASTM Designation	% of Total Aggregate
Coarse	%C33 #6	24%
Intermediate	% C33 #8	40%
Fine	% 8515 Blended	36%

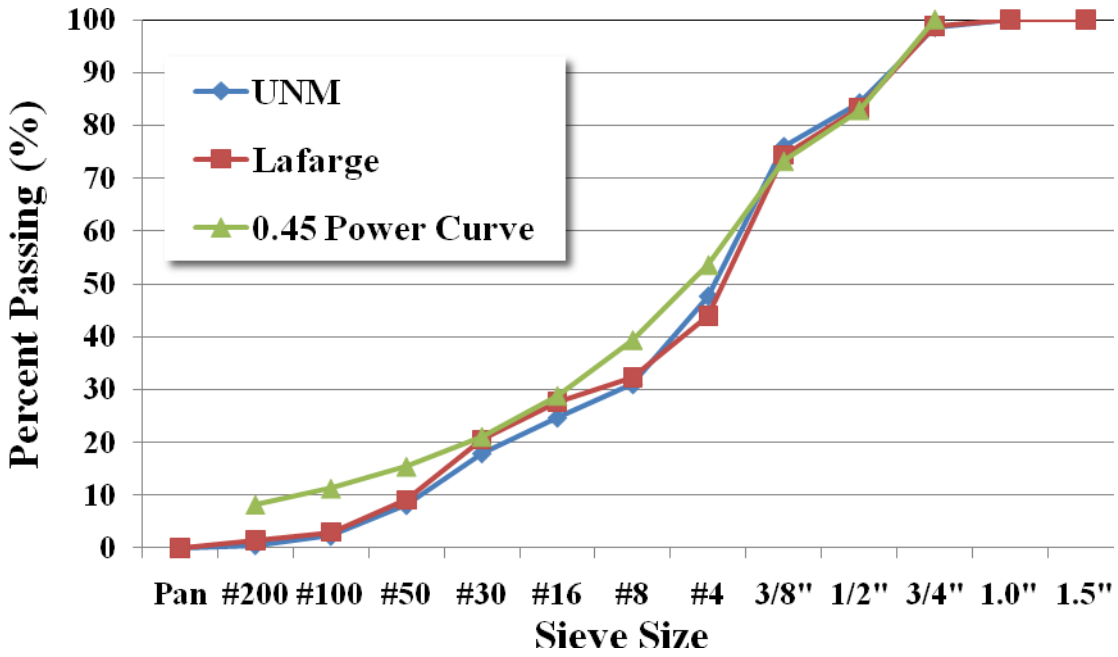

Figure 3.1 – NVC aggregate grading curve

Residuals were calculated at each sieve size and a total root mean square error (RMSE) was computed to be 1.92, which differed a small amount from our optimization results which produced an RMSE of 1.75. The grading results ensured that the grading of

the two mixes was very similar and the NVC mix can be reproduced in the University of New Mexico lab.

The mix designs for the two SCCs used the same super-plasticizers, cement, and fly ash as the above NVC mix. However, viscosity modifying admixture (VMA) was added to achieve SCC characteristics (Rheomac VMA 362 by BASF®). The mix designs for both SCC's can be seen in Tables 3.4 and 3.5.

Table 3.4 – SCC 1 (25% Fly Ash) mix – Placitas Source

Component	Batch Weight (lbs/yd^3)	Absolute Volume (yd^3)	Batch Weight (kg/m^3)	Absolute Volume (m^3)
Cement Type 1-2	520.0	2.646	308.5	0.098
Fly Ash - Class F	130.0	1.047	77.1	0.039
Water	267.0	4.279	158.4	0.158
Fine Aggregate (X3)	1531.1	9.463	908.3	0.350
Intermediate Agg. (X2)	1249.8	7.811	741.4	0.289
Coarse Aggregate (X1)	0.0	0	0	0
Air entrainment (6.5%) Grace AT-60	0.44 oz	1.75	17 mL	0.065
HRWR BASF Glenium 3030	197 oz		7650 mL	
VMA BASF Rheomac	106 oz	---	4140 mL	---
Total Batch Weight	3697.9		2194	
Total Volume		27.00		1.000
Sand/Total Aggregate	0.55			
Water/Cementitious Ratio	0.411			

Table 3.5 – SCC 2 (40% Fly Ash) mix – Placitas Source

Component	Batch Weight (lbs/yd^3)	Absolute Volume (ft^3)	Batch Weight (kg/m^3)	Absolute Volume (m^3)
Cement Type 1-2	499.7	2.542	296.5	0.094
Fly Ash - Class F	199.9	1.610	118.6	0.060
Water	280.4	4.494	166.4	0.166
Fine Aggregate (X3)	1471.4	9.094	872.9	0.337
Intermediate Agg. (X2)	1201.1	7.507	712.6	0.278
Coarse Aggregate (X1)	0.0	0.000	0	0
Air entrainment (6.5%) Grace AT-60	0.44 oz	1.75	17 mL	0.065
HRWR BASF Glenium 3030	197 oz		7650 mL	
VMA BASF Rheomac	106oz	---	4140 mL	---
Total Batch Weight	3652.5		2167	
Total Volume		27.00		1.000
Sand/Total Aggregate	0.55			
Water/Cementitious Ratio	0.401			

The two SCC mixes that were designed by UNM had the same aggregate grading, however, differed on the amount of fly ash used. Since the SCC mix design was created by UNM, no optimization was needed to reproduce a given mix design. In Figure 3.2, the grading curve is presented for the two different SCC mixes. The grading was plotted with a .45 power curve to provide a comparison.

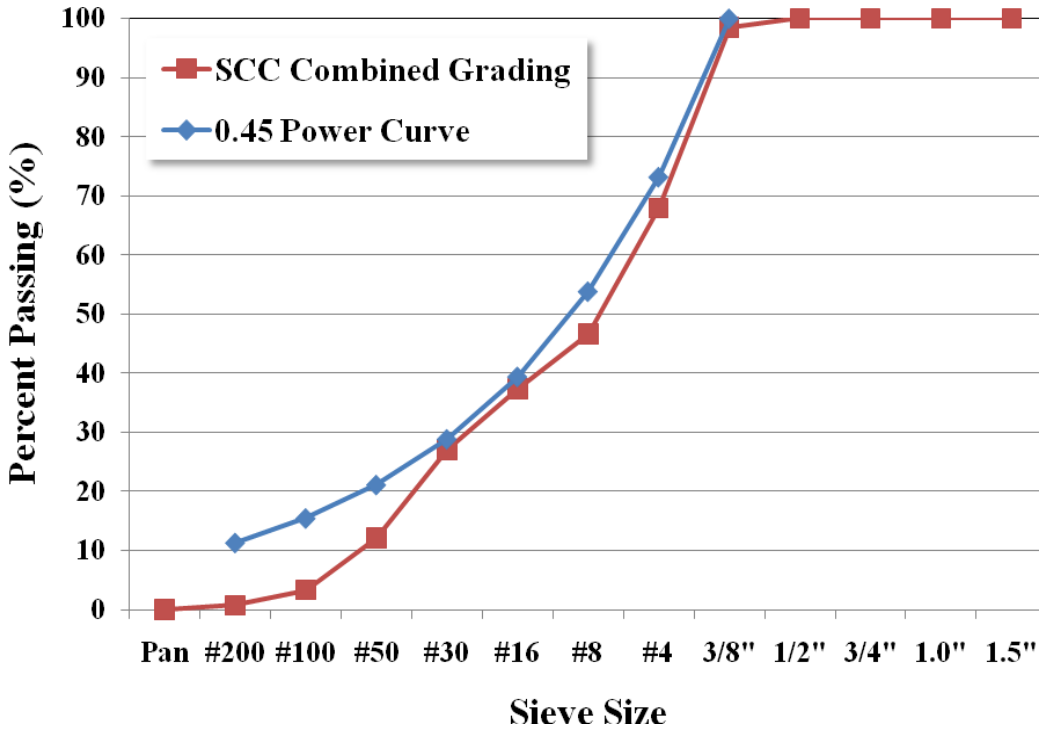

Figure 3.2 – SCC combing aggregate grading curve

The second aggregate source used was the Griego and Sons pit located in Fort Sumner, New Mexico. Four mixes were produced using the Griego and Sons source and compared. The first mix was the NVC 1 control batch that was provided by the NMDOT. The nominal maximum size for the coarse, intermediate, and fine aggregate used was 3/4, 3/8, and 3/16 inch respectively. The same admixtures, Portland cement, and fly ash that were used in the Placitas mixes were also used in the Greigo and Sons mixes. Three SCC

mixes were produced in addition to the NVC 2 control batch for the Griego pit. The three SCCs only varied by the percentage of fly ash that was utilized (20%, 30%, and 40%). To ensure quality control and be able to recreate the different mixes, aggregate tests were performed (same tests that were performed on the Placitas aggregate) and the data is presented in Table 3.6. The NVC 2 mix design provided by the NMDOT is presented in Table 3.7.

Table 3.6 – Griego and Sons Aggregate Properties for mix design

Material Description	Bulk Specific Gravity	Absorption
S.G. Rio Grande Type 1/2 Cement	3.150	
S.G. SRMG Class F - Fly Ash	1.990	
S.G. Placitas C33 Fine Aggregate	2.634	1.05
S.G. Placitas C33 Intermediate Agg	2.661	1.36
S.G. Placitas C33 Coarse Aggregate	2.673	0.95

Table 3.7 – NVC 2 Mix Design – Griego and Sons Source

Component	Batch Weight (lbs/yd^3)	Absolute Volume (ft^3)	Batch Weight (kg/m^3)	Absolute Volume (m^3)
Cement Type 1-2	466	2.37	276	0.088
Fly Ash - Class F	116	0.93	69	0.035
Water	241	3.85	143	0.143
Fine Aggregate (X3)	1497	9.11	888	0.337
Intermediate Agg. (X2)	299	1.80	177	0.067
Coarse Aggregate (X1)	1197	7.18	710	0.266
Air entrainment (6.5%) Grace AT-60	12 oz	1.75	490 mL	0.065
HRWR BASF Glenium 3030	56 oz		2176 mL	
VMA BASF Rheomac	---	---	---	---
Total Batch Weight	2993		2263	
Total Volume		26.99		0.999
Sand/Total Aggregate	0.50			
Water/Cementitious Ratio	0.414			

To recreate the mix design for the NVC control batch provided by the NMDOT, optimization techniques were performed to create similar aggregate grading curves. The same optimization techniques that were conducted for the Placitas mix were conducted

for the Griego and Sons mixes. The different aggregate percentages were determined by these optimization techniques and can be viewed in Table 3.8.

Table 3.8 – NVC 2 aggregate proportioning used for mix design

Aggregate Type	ASTM Designation	% of Total Aggregate
Coarse	% C33 #6	40%
Intermediate	% C33 #8	10%
Fine	% 8515 Blended	50%

Once the percentages of the different aggregates were determined theoretically, a combined grading was performed using the above percentages. The combined grading curve can is presented in Figure 3.3.

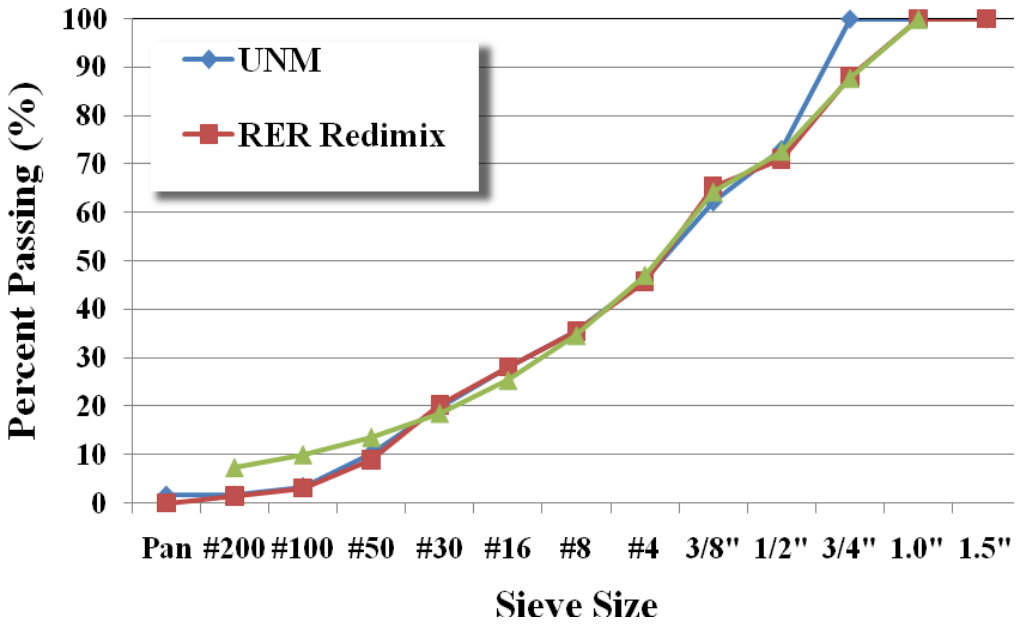

Figure 3.3 – Combined Grading – NVC (Griego Source)

The RMSE for the combined grading was 3.75 which was a fraction higher than the predicted RMSE value from optimization techniques of 3.67. The higher RMSE for the Greigo and Sons aggregate as opposed to the Placitas source shows that the aggregates being produced by Griego at the time of retrieval were slightly different from

the aggregate values used by the NMDOT when the mix was created by using Sam Sanders pit source (also located in Fort Sumner, New Mexico), which was the source that was used when the NVC mix design was created.

Three separate SCC mix designs were created using the Griego and Sons source. The only parameter that varied from one mix design to the next was the percentage of fly ash that was used. By holding all other parameters constant, the different performance characteristics can be directly related to the different fly ash percentages. However, to try to keep the cement paste volumes similar, a small amount of cement replacement by fly ash was needed, and as the fly ash percentages increased, the amount of cement decreased a small amount. In Tables 3.9, 3.10, and 3.11, the different mix designs can be viewed for the different SCC mixes that were produced for comparisons.

Table 3.9 – SCC 3 mix (20% fly ash) – Griego and Sons Source

Component	Batch Weight (lbs/yd^3)	Absolute Volume (ft^3)	Batch Weight (kg/m^3)	Absolute Volume (m^3)
Cement Type 1-2	563.7	2.868	334	0.106
Fly Ash - Class F	113.5	0.914	67	0.034
Water	241.1	3.864	143	0.143
Fine Aggregate (X3)	1935.6	11.776	1148	0.436
Intermediate Agg. (X2)	968.3	5.831	574	0.216
Coarse Aggregate (X1)	0.0	0	0	0.000
Air entrainment (6.5%) Grace AT-60	0.44 oz	1.75	17 mL	0.065
HRWR BASF Glenium 3030	197 oz		7650 mL	
VMA BASF Rheomac	106 oz	---	4140 mL	---
Total Batch Weight	3822.2		2267	
Total Volume		27.00		1.000
Sand/Total Aggregate	0.67			
Water/Cementitious Ratio	0.36			

Table 3.10 – SCC 4 mix (30% fly ash) – Griego and Sons Source

Component	Batch Weight (lbs/yd^3)	Absolute Volume (ft^3)	Batch Weight (kg/m^3)	Absolute Volume (m^3)
Cement Type 1-2	526.7	2.680	312	0.099
Fly Ash - Class F	158.0	1.273	94	0.047
Water	244.2	3.913	145	0.145
Fine Aggregate (X3)	1912.2	11.634	1134	0.431
Intermediate Agg. (X2)	955.6	5.755	567	0.213
Coarse Aggregate (X1)	0.0	0	0	0.000
Air entrainment (6.5%) Grace AT-60	0.44 oz	1.75	17 mL	0.065
HRWR BASF Glenium 3030	197 oz		7650 mL	
VMA BASF Rheomac	106 oz	---	4140 mL	---
Total Batch Weight	3796.8		2252	
Total Volume		27.00		1.000
Sand/Total Aggregate	0.67			
Water/Cementitious Ratio	0.357			

Table 3.11 – SCC 5 mix (40% fly ash) – Griego and Sons Source

Component	Batch Weight (lbs/yd^3)	Absolute Volume (ft^3)	Batch Weight (kg/m^3)	Absolute Volume (m^3)
Cement Type 1-2	509	2.590	302.0	0.096
Fly Ash - Class F	204	1.640	120.8	0.061
Water	240	3.838	142.1	0.142
Fine Aggregate (X3)	1887	11.482	1119.4	0.425
Intermediate Agg. (X2)	943	5.680	559.4	0.210
Coarse Aggregate (X1)	0.0	0	0	0
Air entrainment (6.5%) Grace AT-60	0.44 oz	1.75	17 mL	0.065
HRWR BASF Glenium 3030	197 oz		7650 mL	
VMA BASF Rheomac	106 oz	---	4140 mL	---
Total Batch Weight	3782.5		2244	
Total Volume		27.0		1.00
Sand/Total Aggregate	0.67			
Water/Cementitious Ratio	0.336			

The three SCC mixes that were designed and produced for this research all had the same aggregate grading curves. All parameters were held as constant as possible to try to analyze the effects of different fly ash percentages on the performance characteristics of the different SCC mix designs. No optimization was performed on the SCC mixes due to the fact that the mix designs were designed and produced by the University of New Mexico and there were no SCC mix designs that needed to be created

to match NMDOT mix designs. Like above in the Placitas Source case, the SCC combined aggregate grading curves are plotted vs. the SCC curves generated from the Placitas aggregate source for comparison purposes. In Figure 3.4, the SCC combined aggregate grading curves can be viewed.

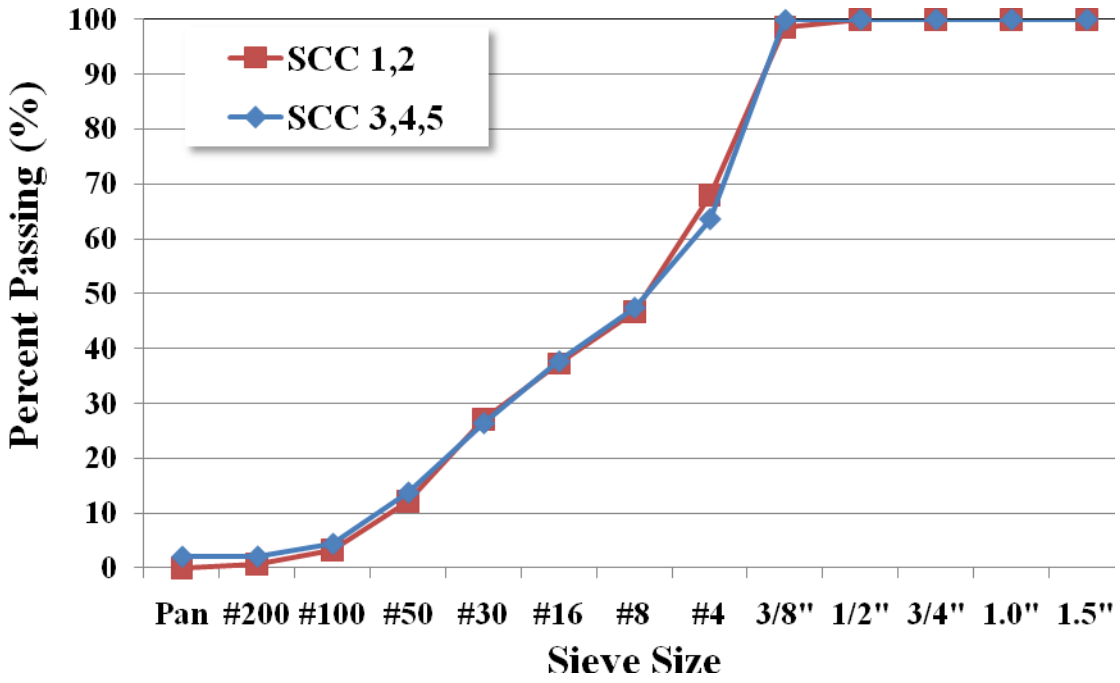

Figure 3.4 – Combined Grading SCC – Griego Source

Now that the aggregate grading curves have been produced and the different mix designs presented, the next step is the batch the different mix designs and determine the plastic and hardened properties of each mix.

3.3 Batching Procedure and Plastic Properties

The overall batching procedure of the different concrete mixes is crucial to maintaining a high level of quality control throughout the research project. Since so many batches were being cast; the batching procedure must be held constant throughout

the entire research project to ensure the quality control needed. The day before every mix was cast; three separate random moisture contents were sampled for each aggregate and dried in the oven over night at 110 degrees Celcius. This ensured the high quality control needed to batch all seven batches of concrete and appropriately to create a valid concrete mix design.

The batching procedure that was used for this research is similar to the ASTM for batching concrete [103]. The step-by-step process went as follows:

1. Wet concrete mixer and add aggregate from largest to smallest and mix aggregate.
2. Turn on the mixer and mix the aggregate for two minutes to ensure proper dispersion of the different sized aggregates.
3. Incrementally add cement and fly ash and mix additional one minute.
4. Add half of the water to the mix with all of the admixtures and continue mixing for an additional one minute.
5. Add the rest of the water and mix for an additional two minutes.

After the mixing process that was outlined above, concrete was poured from the mixer into wetted wheel barrels and brought into the lab to perform plastic tests and fill molds that were needed for future hardened testing. It is important to note that all plastic tests were performed before filling of the molds. This process was used throughout the entire project so that accurate comparisons of plastic test results can be analyzed.

There are certain plastic performance characteristics that need to be achieved before a mix can be tested for its hardened properties. First, NMDOT expects all mixes to have a total entrained plus entrapped air percentage to be between 6-9% for freeze

thaw durability in the state of New Mexico because of the climate. The slump of the NVC control mixes need to be under five inches and greater that three inches to ensure workability standards desired by the NMDOT. Also, plastic tests to determine if a mix qualifies as an SCC mix need to be performed to correctly classify the different SCC mixes. The plastic tests that were performed for the NVC control mixes were all ASTM tests for slump, volumetric and gravimetric air contents, unit weights, and yields [23, 104-105]. The plastic tests for the SCC mixes were the same as the ASTM tests mentioned above, however, a slump flow test was performed according to ASTM [26] instead of the conventional slump test, and an L-Box test was performed on all SCC mixes to determine the concretes passing ability through tightly spaced rebar [European code]. There were no requirements from the New Mexico Department of Transportation for the SCC mixes during to meet during plastic testing because the overall purpose of the project was to develop an SCC mix design for the NMDOT to use for pre-cast, pre-stressed bridge applications. However, basic ASTM requirements were needed to be met to properly classify a concrete mix as SCC or NVC.

The first plastic test to be performed was the slump test for the NVC 1 control mixes or a slump flow test for the SCC mixes. According to ACI standards, an SCC mix must have a slump flow greater than 600 mm (23.6in) to be classified as an SCC mix. The T_{500} test was also performed in conjunction with the slump flow tests for the SCC mixes. This test determines the overall viscosity of the concrete mix by timing how long the plastic concrete takes to flow to a diameter of 500mm. In Figure 3.5, a picture of the slump flow test of the concrete can be seen after the concrete has ceased to flow.

Figure 3.5 – Slump flow test

The next plastic test that was performed on all mixes (both NVC and SCC) was the unit weights of each mix. To determine the unit weight, a container of known volume was filled with concrete and weighed. To determine the unit weight, the equation below was used.

$$\gamma_{concrete} = W_{concrete} / V_{measure} \quad (3.1)$$

The amount of air present in a given concrete mix is very important for different reasons. However, the freeze-thaw durability of a concrete mix can be directly related to the air content. Since the NMDOT mixes need to meet a certain air criteria (6-9%) for concretes used in transportation projects in New Mexico due to the climate, volumetric air content tests were performed to determine the air contents of each concrete mix. The process to determine the air content of a given concrete is relatively simple. A container of a known volume is filled with concrete in its plastic state first. A pressure is applied to the concrete to compact the plastic concrete until no air voids are present. The pressure is then released and the difference in volume of the concrete can be assumed to be the air content of the concrete. In Figure 3.6, the volumetric air meter can be seen.

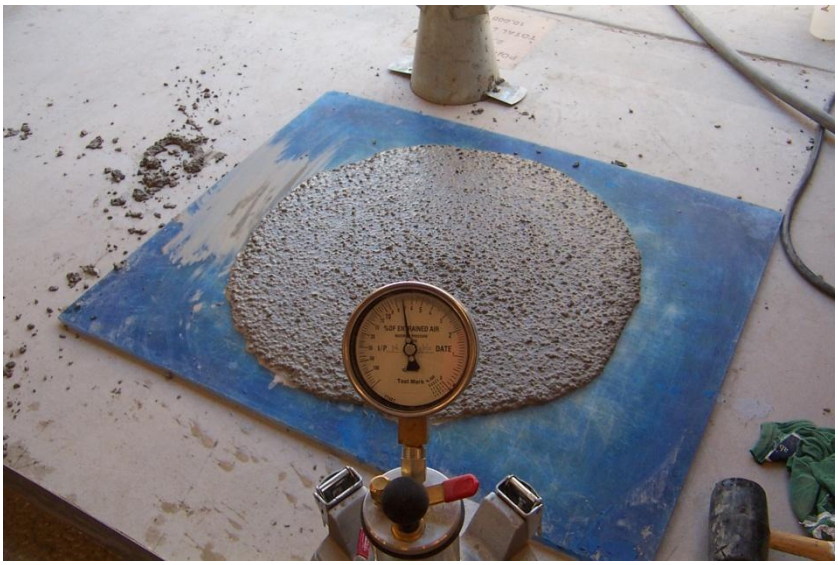

Figure 3.6 – Volumetric air meter

The gage seen the Figure 3.6 is located at the top of the pressure compartment and can be used to determine the volumetric air content in a given concrete mix.

The last plastic test performed was the L-Box test. This test is only performed on SCC mixes and is used to determine the passing ability of an SCC mix. The L-Box test is not a specification in the American Concrete Institute (ACI), however, is used in Europe to determine an SCC's ability to pass through tight obstacles. Although not required by ACI to classify SCC mixes, the L-Box test is important to determine passing ability in pre-stressed, precast bridge applications and provides an easy way to compare many different SCC mixes according to their passing ability.

Figure 3.7 – L-Box test to determine SCC passing ability

To summarize all of the plastic testing, all results can be viewed in Table 3.13.

Table 3.12 – Summary of Plastic Characteristics of SCC mixes

	Mix Design	**w/cm***	**V_{cp} (%)**	**Slump/ Slump Flow (in)**	**Visual Stability Index (VSI)**	**Passability L_{box} (%)**	**T_{500} (sec)**	**Pressure Method Air Content (%)**
Placitas Source	SCC1 (25% F.A.)	0.411	36.1	31.75	1	94	1.8	8.2
	SCC2 (40% F.A.)	0.401	38.5	30.75	1	93	2.6	7.8
	NVC1	0.368	38.4	3.2	N/A	N/A	N/A	6.5
Greigo Source	SCC3 (20% F.A.)	0.356	34.8	26.5	0	81	4.5	7.4
	SCC4 (30% F.A.)	0.357	35.6	27.75	1	86	3.6	7.6
	SCC5 (40% F.A.)	0.336	36.5	27.25	0	83	4.2	6.6
	NVC2	0.414	33.1	3	N/A	N/A	N/A	7.6

w/cm* is the water/total cementitious materials (including Portland cement and fly ash)

Table 3.12 presented above summarizes the plastic tests that were performed on the different mixes. It is important to note that the slump flow for the SCC mixes are completely different tests than the slump tests performed on the NVC mixes, hence the drastic difference in values. The visual stability index (VSI) is a way to determine the how much the different SCC mixes bleed. This test cannot be performed on NVC mixes because it is a visual index taken from the slump flow test. The different ratings that can be awarded to the different SCC mixes are 0, 1, and 2. Zero being no water ring at the outer circumference of the slump flow and two being a noticeable water ring (over 1mm) at the outer circumference of the slump flow. Table 3.13 also lists the water/cement ratios of the different mixes by mass as well as the volume of cement paste. These values are of interest when comparing the plastic and hardened properties of different concrete mixes. The passing ability numbers are also listed for the SCC mixes, which are simply the H_1 to H_2 ratio that was discussed in the previous section.

3.4 Hardened Properties

When trying to compare time-dependent and fracture toughness properties, certain hardened characteristics are very important to be able to compare and contrast and design tests to accurately access the different characteristics mentioned above. The 28-day compression test is the most common test and helps determine the compressive strength of the given concrete. This test is also important when analyzing time-dependent, compressive creep characteristics. All mixes have different 28-day compressive strengths and to accurately determine a mixes creep properties, this compressive strength is needed

to design the creep test to be able to compare creep characteristics across the different mixes.

Not only is the 28-day compressive strength important in classifying different mixes in terms of strength, but it is also used to determine the compressive load that needs to be constantly applied to the creep specimens. Since the creep specimens are loaded at 28 days, the 28-day compressive strength is the only hardened property needed to adequately design the creep test. The 28-day static modulus of elasticity is also important for comparison reasons and to determine the initial elastic deformations when the constant load is applied to the creep specimens.

A summary of the results of the different 28-day tests that were performed on all the mix designs can be viewed in Table 3.13. All the tests were performed according to ASTM testing protocol [106-107]. The equations used in determining the different concrete mixes compressive strength, modulus of elasticity, and Poisson's ratio can be seen below in Equations 3.2-3.5.

$$\sigma = \frac{P}{A} \tag{3.2}$$

σ is the compressive strength of the concrete, *P* is the load at failure of the concrete cylinder, and *A* is the cross-sectional area of the concrete cylinder.

$$\varepsilon = \frac{\Delta L}{L_0} \tag{3.3}$$

ε is the longitudinal strain, ΔL is the change in length and L_0 is the original length of the concrete cylinder. The units for strain are length divided by length.

$$E = \frac{\sigma_2 - \sigma_1}{\varepsilon - 0.00005} \tag{3.4}$$

E is the modulus of elasticity of the concrete. σ_2 and σ_1 are the stress corresponding to 40% of the ultimate load and to the stress when the strain equals 0.00005 in/in. ε is the final strain when the stress equals 40% of the ultimate load.

$$\nu = -\frac{d\varepsilon_y}{d\varepsilon_x} \tag{3.5}$$

ν is the Poisson's ratio that is defined by the change in strain in the longitudinal direction ($d\varepsilon_y$) divided by the change in strain in the lateral direction ($d\varepsilon_x$).

Table 3.13 – Summary of Hardened Properties for Seven SCC and NVC mixes

	Placitas Source			**Griego and Sons Source**			
	NVC1	SCC1	SCC2	NVC2	SCC3	SCC4	SCC5
Unit Weight (lb/ft^3)	138.9	138.1	135.0	141.0	145.0	141.0	143.0
28-day Comp. Strength (psi)	4467	4795	4340	4084	7576	6681	7047
Modulus of Elasticity (ksi)	4153	4175	4184	4460	4849	4549	4402
Poisson's Ratio	0.17	0.18	0.20	0.16	0.18	0.18	0.19

The 28-day compression test to determine the compressive strength is the only hardened property needed to design a creep test because the constant load used in the creep test percentage of the overall concrete strength. The constant load used in the creep test performed in this research was 35% of the ultimate concrete strength.

In this research, modulus of rupture (MOR) tests were performed to classify and compare tensile characteristics of the different concrete mix designs. The MOR test is a simple 3-point bending test where a load is applied until the concrete beam fractures. The maximum tensile stress is determined by the stress at the outer most fiber of the concrete

beam in the tension region. The equation to determine the MOR of a given concrete beam is shown below in Equation 3.6 and the test setup can be seen in Figure 3.8.

$$MOR = \frac{PL}{wh^2} \tag{3.6}$$

P is defined as the load recorded when the beam fails. *L* is the span length of the beam and *w* and *h* are the width and height of the beam respectively.

Figure 3.8 – Modulus of rupture testing

The modulus of rupture test was performed in accordance with ASTM standards [108]. In Table 3.14, a summary of MOR results can be seen for the different mix designs produced.

Table 3.14 – Modulus of Rupture Results

Aggregate Pit	Batch Title	Modulus of Rupture psi (MPa)
Placitas Source	NVC 1	706 (4.9)
	SCC 1	606 (4.2)
	SCC 2	645 (4.5)
Griego and Sons Source	NVC 2	598 (4.2)
	SCC 3	842 (5.9)
	SCC 4	769 (5.4)
	SCC 5	1012 (7.1)

Now that the different mix designs are presented with the different aggregate grading curves and the desired hardened properties are presented, the fracture and time-dependent tests to be performed on the different concrete mix designs can be designed.

3.5 Creep Methods

Creep is defined as the deformation that takes place over time when a material is subject to a constant load. Creep occurs in visco-elastic materials, like concrete, and can be an extremely important design characteristic in pre-stressed or precast bridges. For instance, creep and shrinkage properties of a concrete mix are important when calculating the amount of pre-stressing losses that occur over time in a pre-stressed bridge. Without taking creep deformations into account, the overall safety of the bridge can be sacrificed.

In this research we are interested in determining the total and basic creep compliance of the different concrete mix designs. Compliance is defined as how a material strains over time and is the inverse of stiffness. The equation used to calculate creep compliance can be seen below in Equation 3.7:

$$J(t, t_o) = \frac{1}{E(t_o)} + \frac{\varepsilon_{cr}(t_o)}{\sigma} \tag{3.7}$$

$E(t_o)$ is the modulus of elasticity of the concrete at the time of loading. ε_{cr} is the time-dependent creep strain and σ is the stress that is applied to the concrete cylinder. The calculations to determine the strain at time of loading and creep coefficient can be observed in Equations (3.8) and (3.9).

$$\varepsilon(t_0) = \frac{\sigma(t_0)}{E(t_0)} \tag{3.8}$$

$$\phi(t, t_0) = \frac{\varepsilon_{cr}(t)}{\varepsilon(t_0)} \tag{3.9}$$

The creep testing that was performed using a constant compressive stress and applying it to one unwrapped and one wrapped specimen. The wrapped specimen was completely covered with duct tape to prevent any loss of moisture during the test. The reason that both an unwrapped and a wrapped specimen were tested was to try to determine the different types of creep that were present in the different concrete mix designs. By wrapping a specimen and prohibiting moisture loss during the testing period, one can determine basic creep compliance by eliminating creep mechanisms dealing with drying. The constant compressive stress that was utilized was 35% of the ultimate 28-day compressive strength. By using a percentage of the ultimate load for the compressive creep testing allowed us to normalize the data, in a sense, and compare the data across different mix designs with different ultimate strengths. All creep specimens were cured in water baths according to ASTM standard curing procedures [103]. At 28 days of age, the creep specimens were ground on both top and bottom of the cylinder to try to create a perfectly flat surface. A flat surface is desired so that the compressive stress being applied to the specimens was distributed evenly across the entire cylinder. After the grinding was completed, the specimens were taken to the constant humidity room to be loaded at 28 days of age. A schematic of the compression creep test setup can be seen in the Figure 3.9 and the creep test in progress can be seen in Figure 3.10.

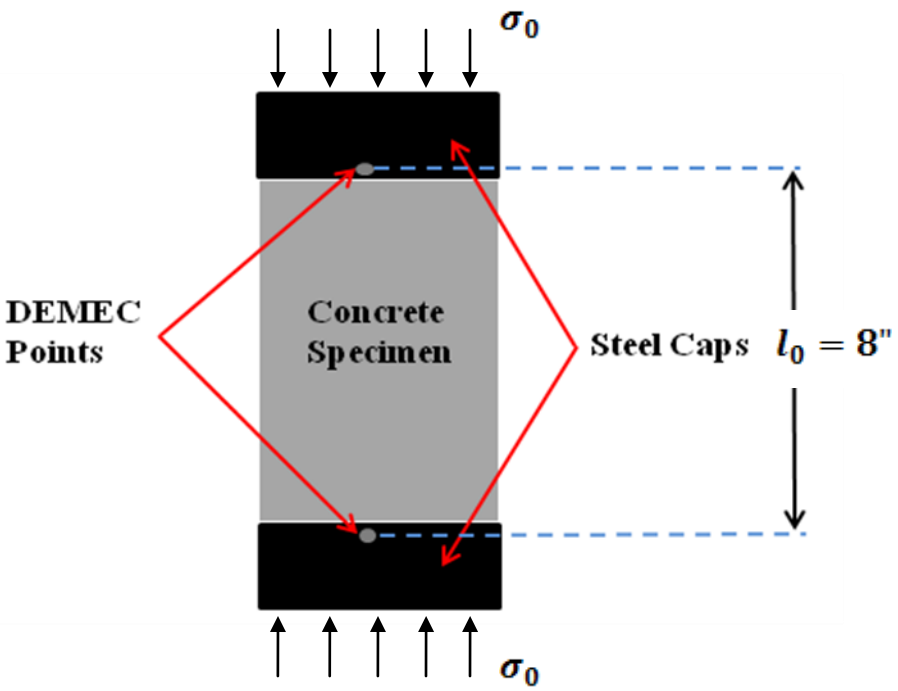

Figure 3.9 – Schematic of creep test

An eight inch gage length (l_0) mechanical caliper manufactured by Mayes Instruments, Co. was used to determine displacements of the concrete specimen with a resolution of 0.002mm. The caliper range was 1.62 mm which provides the range needed for the creep experiments. Because the gage length of the caliper was 8 in, steel caps were used at the top and bottom of the creep specimen to obtain accurate displacements from the caliper. Since the elastic strain at the time of loading was not considered, no corrections for the small amount of steel strain needed to be deducted to obtain correct displacement values. From the displacements obtained from the test, creep strains can be calculated using Equation 3.10.

$$\varepsilon_{creep} = \frac{\Delta l}{l_o} \tag{3.10}$$

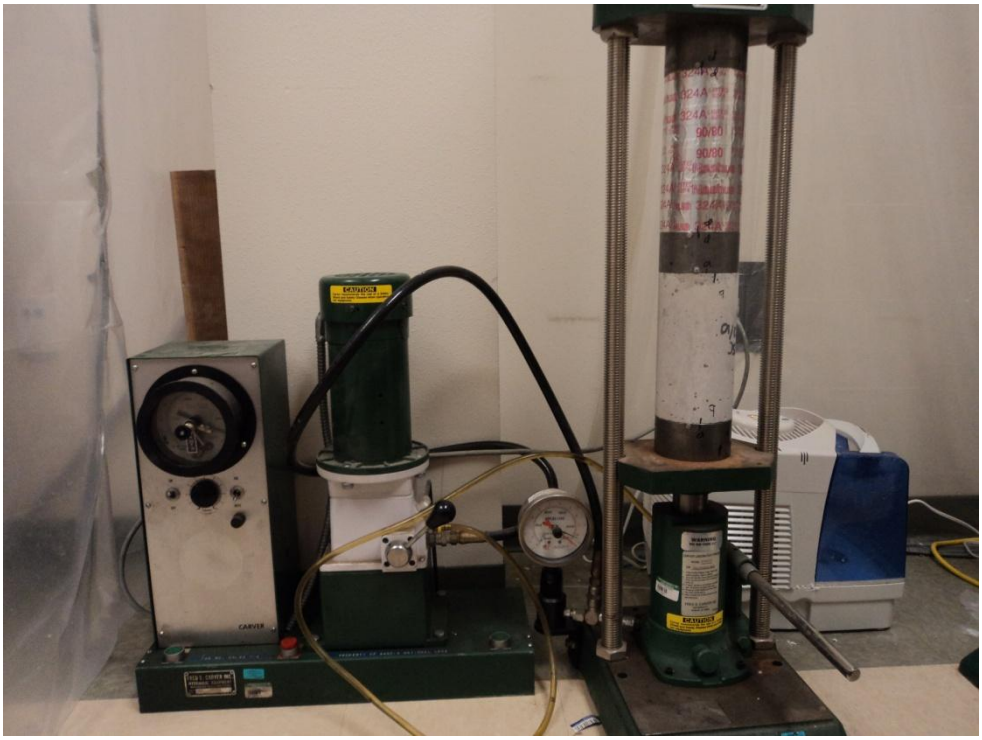

Figure 3.10 – Creep test in progress utilizing creep frame

The creep frame that is observed in Figure 3.11 was the method used to apply constant stress, and maintain that stress as the specimen strained. A constant force is applied to the creep frame observed on the right with the two specimens (one wrapped and one unwrapped). Once the force starts to drop due to creep strains in the concrete, the hydraulic pump on the left recognizes this and applied more displacement to the bottom platen of the frame until the initial force is re-obtained.

Shrinkage values were also measured to determine the total and basic creep compliance of the concrete mixes. To determine the shrinkage values, two specimens similar to the creep specimens were used, one unwrapped and one wrapped. The specimens were not subjected to any stress but were stored in the same room as the compressive creep specimens to ensure that the humidity was constant when comparing the shrinkage and creep specimens. To eliminate fluctuation in humidity, a constant

humidity room was constructed. Humidifiers were used to control the humidity and the relative humidity that was recorded in the room during the test never dropped below 45% and never climbed above 55%. By controlling the humidity, we were able to analyze the creep characteristics of the different concrete mixes. The constant humidity room can be observed in Figure 3.11.

Figure 3.11 – Constant humidity room

To set up the concrete creep test, a series of steps were followed to minimize variability and ensure the testing conditions could produce accurate and repeatable results. The steps include:

1. The concrete creep specimens were 4 in (101.6mm) diameter by 8 in (303.2mm) length cylinders, similar to the specimens commonly used for compression strength testing.
2. The ends of the concrete cylinder were then ground to create a flat surface to ensure that the stress was being applied constantly across the entire specimen.

3. Steel caps were placed on the top and bottom of both the unwrapped and wrapped specimens with demic points so accurate micro-strain measurements could be conducted. Demic points were attached on both sides of the steel plates so two measurements of each specimen could be conducted to create and average reading for analysis. This also corrects if the specimen ends were not completely flat and one side of the cylinder was seeing slightly more load than the other. The creep specimens are shown in Figure 3.12.

Figure 3.12 – Creep specimen preparation

4. Compression strengths were determined for the mix at 28 days of age.
5. At 28 days, the cylinders were loaded at 35% of their ultimate compressive strengths.
6. Micro-strain measurements were conducted every six hours for the first day after loading then continued once per day for the first week. Measurements were then taken every three days until day 21. Weekly measurements were taken until 56 days of age.

It is important to note that the creep frames were able to test up to two specimens at a time and two creep frames were used. The lack of more creep frames was why the testing was cut off at 56 days. The measurements of interest were to determine the total and basic creep compliance's for the seven different NVC and SCC mixes. The total creep values were determined from the unwrapped specimens to allow for drying creep mechanisms. The basic creep measurements were taken from the unwrapped specimens to prevent drying creep strains. From these two separate tests, drying creep was determined for each mix.

3.6 Compression Creep Modeling

There are currently two design codes that are most commonly used in the structural engineering design community to predict creep compliance values to be used during the design process. The first model, ACI 209R – 92 [110], is a popular model that was developed by the American Concrete Institute (ACI). The second design model, CEB-FIP model MC-90-99 [115], is a model utilized in the European Code. It is important to compare the experimental compression creep results with common design codes to understand if these models can correctly predict creep of SCC mixes. The above models were selected based on their common use in structural design.

3.6.1 ACI 209R – 92 Model

The idea of the ACI 209R – 92 [110] model is to determine a creep coefficient, which is a ratio of the creep stain at a given time over the initial creep strain, based on

empirical formulas and different hardened and plastic properties to predict how the material will comply over time. The compliance equations are described below.

$$J(t,t_o) = \frac{1}{E_{cmto}} + \frac{\varepsilon_{cr}(t,t_o)}{\sigma(t_o)} \tag{3.11}$$

$\varepsilon_{cr}(t,t_o)$ is the time dependent creep strain, $\sigma(t_0)$ is the initial stress applied to the specimen and E_{cmto} is the modulus of elasticity of the concrete at the time of loading.

$$\varepsilon_{cr}(t,t_0) = \varepsilon_e(t_0)\emptyset(t,t_o) \tag{3.12}$$

To determine the time dependent creep strain; the elastic strain at time of loading is multiplied by a time dependent creep coefficient. By substituting this relationship into the compliance equation, you obtain Equation 3.13.

$$J(t,t_0) = \frac{1}{E_{cmto}} + \frac{\emptyset(t,t_0)}{E_{cmto}} \tag{3.13}$$

Where E_{cmto} is the modulus of elasticity of the concrete at the time of loading and the creep coefficient denoted $\emptyset(t,t_0)$, can be determined by empirical formulas by determining coefficients based on different hardened and plastic properties of the given concrete mix.

The determination of the creep coefficient as a function of time is calculated using Equation 3.14.

$$\emptyset(t,t_0) = \frac{(t-t_0)^{\psi}}{d+(t-t_0)^{\psi}}\,\phi_u \tag{3.14}$$

Where t is the concrete age (days) and t_0 represents the time (days) in which the creep specimen was loaded. d is a constant that is determined to take into account different geometries of creep specimens (volume-to-surface area relation) and ϕ_u is the

ultimate creep coefficient that can be determined by empirical formulas that account for testing environment conditions, hardened concrete characteristics and plastic properties of the concrete mix design. The determination of both d and ϕ_u can be seen in the following equations; equations (3.15) and (3.16) respectively.

$$d = 26.0e^{\{1.42*10^{-2}\left(\frac{V}{S}\right)\}} \tag{3.15}$$

$$\phi_u = 2.35\gamma_C \tag{3.16}$$

γ_C is a cumulative product of many different correction factors. The calculation to determine this value can be seen in Equation (3.17).

$$\gamma_C = \gamma_{c,to}\gamma_{c,RH}\gamma_{c,vs}\gamma_{c,s}\gamma_{c,\psi}\gamma_{sh,\alpha} \tag{3.17}$$

$\gamma_{c,to}$ is a correction factor that accounts for the type of curing that took place up until the day of use and is determined by an empirical formula based on moist curing conditions and is represented in Equation (3.18).

$$\gamma_{c,to} = 1.25{t_0}^{-0.118} \tag{3.18}$$

Where t_0 is the age of loading of the concrete in days. The next correction factor denoted $\gamma_{c,RH}$, is the ambient relative humidity factor and can be determined from Equation (3.19).

$$\gamma_{c,RH} = 1.27 - 0.67h \quad for\ h > 0.40 \tag{3.19}$$

h represents the relative humidity in decimal form. The relative humidity must be greater than 40% to use this equation.

The next constant to be determined is $\gamma_{c,vs}$, which is a constant that takes into account different geometries of the creep specimens to be compared. This constant

adjusts according to the volume-surface area relationship and the calculation can be seen in Equation (3.20).

$$\gamma_{c,vs} = \frac{2}{3}(1 + 1.13e^{\left\{-0.0213\left(\frac{V}{S}\right)\right\}}) \tag{3.20}$$

V and S are the volume and the surface area of the compression creep specimen.

$\gamma_{c,s}$ is the correction constant determined by the slump of the concrete. However, when dealing with SCC's, there is no slump value that can be used as input. The ACI 209R – 92 model [reference] is built around conventional concretes. However, since SCC mixes slump cannot be measured, the ACI equations need to be modified to incorporate SCC plastic properties to predict creep. The calculation for the slump correction factor is described by Equation (3.21).

$$\gamma_{c,s} = 0.82 + 0.00264s \tag{3.21}$$

Where s is the slump in millimeters when the slump can be appropriately measured.

The last correction constant needed to predict concrete creep compliance is a factor that takes into account the ratio of fine aggregate to coarse aggregate in a concrete mix design. The calculation can be viewed in Equation (3.22).

$$\gamma_{c,\psi} = 0.88 + 0.0024\psi \tag{3.22}$$

ψ is the ratio of fine to coarse aggregate in the concrete mix.

The determination of the creep coefficient with respect to time allows for the prediction of creep compliance without performing compression creep tests. However, it is important to note that the ACI 209R – 92 model is built around conventional NVC's,

and a correction constant that relates slump flow as opposed to slump needs to be determined to utilize this model with SCC mix designs.

3.6.2 CEB-FIP MC90-99 Model

The CEB-FIP MC90-99 [115] model is another model that is currently used in structural design and is able to predict creep compliance of different mix designs by determining a creep coefficient that is a function of time. This model has been recently adopted by the Canadian Highway Bridge Design Code (2010). CEB-FIP MC90-99 is widely used and has been endorsed by many researchers as the best current model to predict compression creep values of many different strength concrete mixes.

The compliance equation used by the CEB model is described by Equation (3.23). This compliance function represents the total stress dependent strain by a unit stress.

$$J(t,t_0) = \frac{1}{E_{cmto}} + \frac{\phi_{28}(t,t_0)}{E_{cm28}} \tag{3.23}$$

Where E_{cmto} is the modulus of elasticity at the time of loading and E_{cm28} is the modulus of elasticity of the concrete at 28 days. $\phi_{28}(t,t_0)$ is the creep coefficient that varies with time and is used to calculate the compliance of the given concrete mix. The determination of the creep coefficient can be seen in Equation (3.24).

$$\phi_{28}(t,t_0) = \phi_0 \beta_c (t - t_0) \tag{3.24}$$

Where ϕ_0 is the notational creep constant and $\beta_c(t - t_0)$ is coefficient that helps determine the development of creep as a function of time after initial loading. The notational creep constant can be calculated using Equation (3.25).

$$\phi_0 = \phi_{RH}(h)\beta(f_{cm28})\beta(t_0) \tag{3.25}$$

ϕ_{RH} is a correction constant that considers the relative humidity of the testing environment. $\beta(f_{cm28})$ and $\beta(t_0)$ are constants that consider the concretes strength and the how the concrete complies with respect to time. The calculation for $\phi_{RH}(h)$ can be seen in Equation (3.26).

$$\phi_{RH}(h) = [1 + \frac{1-\frac{h}{h_0}}{\sqrt[3]{0.1\left[\frac{\left(\frac{V}{S}\right)}{\left(\frac{V}{S}\right)_0}\right]}}\alpha_1]\alpha_2 \tag{3.26}$$

Where h is the relative humidity with h_0 = 1. $\left(\frac{V}{S}\right)$ is the volume-surface are ratio of the concrete specimen and $\left(\frac{V}{S}\right)_0$ = 50mm. α_1 and α_2 are constants that are determined based on the overall concrete strength. α_1 and α_2 are presented in the following equations.

$$\alpha_1 = [\frac{3.5 f_{cmo}}{f_{cm28}}]^{0.7} \tag{3.27}$$

$$\alpha_2 = [\frac{3.5 f_{cmo}}{f_{cm28}}]^{0.2} \tag{3.28}$$

Where f_{cmo} = 10 MPa and f_{cm28} is the mean compressive strength of the concrete at 28 days of age. Since the f_{cm28} was determined by breaking cylindrical specimens, a correction was used to obtain the value according to the calculation below.

$$f_{cm28} = f_c' + 8 \tag{3.29}$$

The last correction coefficient needed to determine the 28-day creep coefficient is $\beta_c(t - t_0)$ which can be calculated using Equation (3.30).

$$\beta_c(t-t_0) = \left[\frac{(t-t_0)/t_1}{\beta_H + (t-t_0)/t_1}\right]^{0.3} \quad (3.30)$$

with

$$\beta_H = 150\left[1 + \left(1.2\frac{h}{h_0}\right)^{18}\right] * \frac{\left(\frac{V}{S}\right)}{\left(\frac{V}{S}\right)_0} + 250 < 1500 \quad (3.31)$$

Where t_1=1 day, h_0=1, $\left(\frac{V}{S}\right)_0$=50mm. Now that all the correctional constants are determined, creep compliance can be predicted using the CEB model.

3.7 Fracture Methods

Fracture toughness properties are desired to determine the amount of fracture energy that can be absorbed by the different concrete mix designs. The stress and energy conditions are the two criteria that need to be satisfied to propagate a crack [83]. To satisfy the stress criterion, a tensile stress must be applied to the specimens to propagate the crack. Because both fracture tests (Notched beam Level II and Stiff Tension Fracture Test) require tensile stresses to initiate and grow the crack, tensile properties of the different concrete mix designs are desired. Modulus of rupture results can be seen in Table 3.15.

Over the years, different models to properly characterize concrete fracture toughness properties have been accepted in the literature. However, the model used in this research for both fracture toughness tests that will be conducted is the cohesive crack model. By obtaining the stress-COD (crack opening displacement) relationship, one can determine the different fracture toughness properties of the different concrete mix

designs. As mentioned above, two separate fracture tests were conducted in this research to analyze the different fracture toughness properties of SCC concrete. The first test conducted was the notched beam level II test outlined by ACI committee 446 [109]. The notched beam level II test is a 3-point beam bending test that is the most common way to determine the fracture toughness properties of a certain concrete mix design by estimating a bilinear curve of the stress vs. crack opening displacement (COD) curve. The methods are presented in ACI 446 [114].

The notched beam level II test is a three-point bending test that is feedback controlled by the crack opening displacement (COD) that allows for a controlled loading rate and accurate recording of the descending part of the load versus displacement curve. A schematic of the test is shown in Figure 3.13.

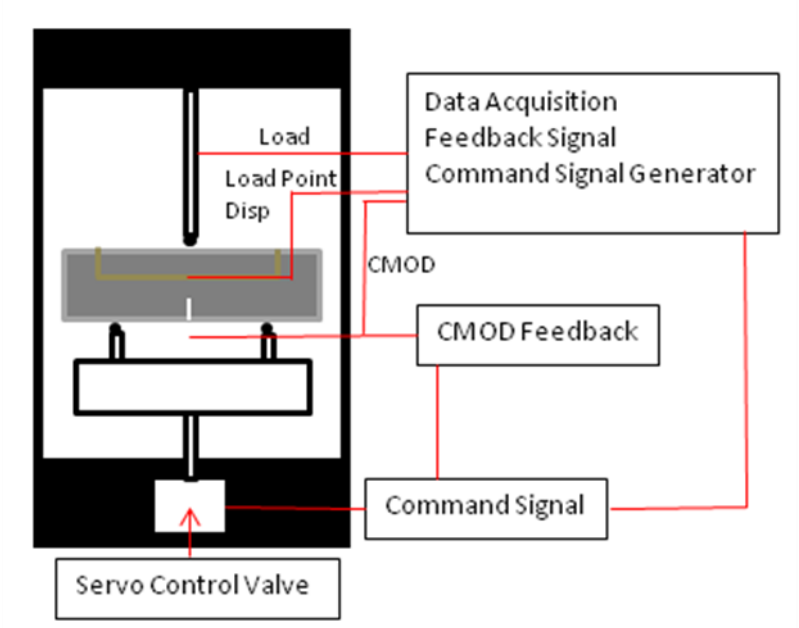

Figure 3.13 – Schematic of testing device for Notched Beam Level II test

The test was conducted on three beam specimens. All fracture specimens were tested at 42 days of age. The test setup is shown in Figure 3.14 and 3.15.

Figure 3.14 - Transporting beam to not allow drying

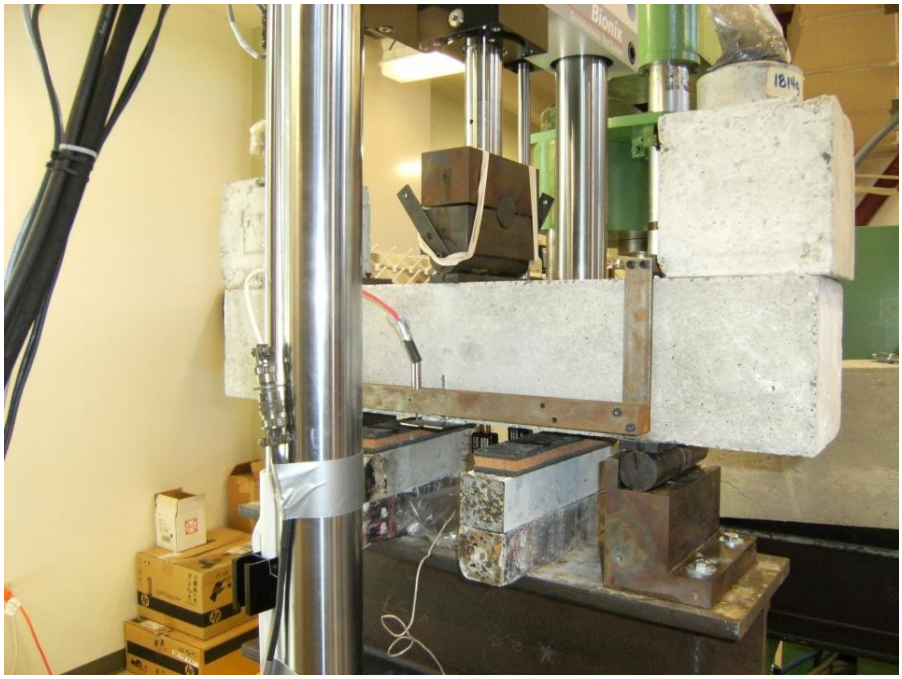

Figure 3.15 – Test setup with counterweights

Figure 3.16 – Installation of clip gages

The objective here is to compare SCC mixes with varying amounts of fly ash that were produced using local aggregate sources. Therefore, the ACI test method was used without developing critique to this method. Such critique, while necessary, can be the focus of another study.

By following ACI 446, the initial compliance can be calculated by using Equation (3.32):

$$C_i = \frac{\Delta(CMOD)}{\Delta P'} \tag{3.32}$$

Once the initial compliance is calculated, the modulus of elasticity can then be calculated using Equation (3.33) following three point bending setup:

$$E = \frac{6Sa_0}{C_i B D^2} V_1(\alpha_0') \ \ where\ \alpha_0' = \frac{a_0 + h}{D + h} \tag{3.33}$$

E is the modulus of elasticity, *S* is the span of the beam, *B* is the beam thickness, *D* represents the beam depth, a_0 is the notch length, *h* is the distance from the knife edges and finally the geometrical function $V_1(\alpha)$:

$$V_1(\alpha) = 0.8 - 1.7\alpha + 2.4\alpha^2 + \frac{0.66}{(1-\alpha)^2} + \frac{4D}{S}(-0.04 - 0.58\alpha + 1.47\alpha^2 - 2.04\alpha^3)$$

(3.34)

After determining the Young's modulus of elasticity, the next step is to determine the far end tail constant. Equation (3.35) describes that constant.

$$P_1 = P' - P'_R \tag{3.35}$$

In the Equation (3.33), P_1 represents the far end tail constant, while P' is the recorded load and P'_R is the residual load that was recorded when the crack mouth opening displacement (CMOD) was two millimeters; this value is denoted w_{MR}

To determine the far end tail constant "A", a quadratic equation must be used that is obtained by a least-square fitting of the curve of the load P_1 plotted against X, which is determined from the points that have been recorded during the test when the corrected load has less than a 5% difference from the corrected peak load. Equation (3.34) was used to determine X.

$$X = \left(\frac{4D}{S}\right)^2\left[\frac{1}{(w_M - w_{MA})^2} - \frac{1}{(w_{MR} - w_{MA})^2}\right] \tag{3.36}$$

The intersection of the rising part of the curve when plotting P_1 versus the CMOD with the CMOD axis is the value of w_{MA} that is used in Equation (3.37). The effective peak load P_{max} can then be determined as:

$$P_{max} = P_{1max} + \frac{A}{(w_{MR} - w_{MA})^2} \tag{3.37}$$

A is the far end tail constant and P_{1max} is the corrected peak load. After obtaining P_{max}, the plastic flexural strength of the beam can be calculated in Equation (3.38).

$$f_P = \frac{P_{max}S}{2tb^2} \tag{3.38}$$

To define variables, *t* is the thickness of the beam, *b* is the ligament length that is equal to the value $D - a_0$ and *S* is the test span of the beam. The brittleness length denoted l_1 can then be calculated as the ratio of tensile strength to plastic flexural strength. The tensile strength of the beam is obtained from a splitting tension test in Equation (3.39).

$$f'_{st} = \frac{2P}{\pi ld} \tag{3.39}$$

P is the failure load, *l* is the specimen length, and *d* is the specimen diameter. Once the splitting tensile strength (f'_{st}) is determined, a ratio of tensile strength to plastic flexural strength can be determined and is denoted as "x". From this ratio, the brittleness length denoted l_1 can be calculated as:

$$l_1 = \kappa D\left[\frac{11.2}{(x^2-1)^2} + \frac{2.365}{x^2}\right] \tag{3.40}$$

Where $\kappa = 1 - \alpha_0^{1.7}$ and α_0 is equal to the notch-depth to beam-depth ratio. The importance of the brittleness length is that it is used to determine the horizontal intercept of the softening curve which is denoted as w_1. This value can be determined using Equation (3.41).

$$w_1 = 1000\left(\frac{f_t}{E}\right) * l_1 \tag{3.41}$$

The next step is determining the total work of fracture that can be denoted w_F. The calculation for the total fracture work can be seen in Equation (3.42).

$$w_F = w_{FM} + \frac{2A}{\delta_R - \delta_A} \tag{3.42}$$

The variables in Equation (17) can be defined as: w_{FM} is determined from the actual measured work that is calculated from the area under the load versus displacement curve, *A* is the far end tail constant determined earlier, δ_R is the load-point displacement upon finalization of the test, and δ_A is determined from the load-point displacement at zero corrected load. From this, the fracture energy of the concrete beam (G_F) can be calculated by using Equation (3.43).

$$G_F = \frac{1000 w_F}{tb} \tag{3.43}$$

t is the beam thickness, *b* is the ligament length that was determined earlier by the equation $(D - a_0)$. Once the fracture energy is determined (G_F), the Mode I fracture toughness (K_{IC}) can be calculated by using the equation seen below. *E* is the modulus of elasticity of the concrete, and υ is the Poisson's ratio.

$$K_{IC} = \sqrt{\frac{E\, G_F}{(1-\upsilon^2)}} \tag{3.44}$$

After obtaining the fracture energy of the specimen, we can now determine the center of gravity for the softening curve that we can denote w_F. By using the far end tail constant *A* that was earlier, we can now calculate the center of gravity of the softening curve. The calculation can be seen in Equation (3.45).

$$w_G = \frac{4A}{BSG_F} * 10^6 \tag{3.45}$$

The bilinear approximation of the softening curve can now be calculated by using Equations (3.39), (3.40), and (3.42) which correspond to the brittleness length l_1 the mean value of the fracture energy G_F, and the horizontal intercept of the softening curve w_1. The mean values for the above calculated variables are all averaged values from a minimum of three fracture toughness specimens. From these values, we can now calculate the characteristic crack opening denoted as w_{ch} in the Equation (3.46).

$$w_{ch} = \frac{G_{Fm}}{f_t} \tag{3.46}$$

G_{Fm} is the mean fracture energy obtained from the three different specimens and f_t is the mean tensile strength determined from splitting tensile tests. Once the characteristic crack opening is determined, it can now be used to determine the critical crack opening denoted w_c for the bilinear approximation curve. The equation used to calculate the critical crack opening can be seen below.

$$w_c = w_{ch} \frac{3w_{Gm} - w_{1m}}{2w_{ch} - w_{1m}} * \left[1 + \sqrt{1 - \frac{2w_{Gm}(3w_{Gm} - 2w_{ch})(2w_{ch} - w_{1m})}{w_{ch}(2w_{Gm} - w_{1m})^2}}\right] \tag{3.47}$$

The stress at the kink point (σ_k) of the bilinear approximation can now be calculated in the following equation.

$$\sigma_k = f_t \frac{2w_{ch} - w_{1m}}{w_c - w_{1m}} \tag{3.48}$$

We are also interested in the crack opening at the kink point calculated above. The kink point is denoted as w_k. The equation to determine the crack opening at the kink point can be seen in Equation (3.49).

$$w_k = w_{1m} \frac{w_c - 2w_{ch}}{w_c - w_{1m}} \tag{3.49}$$

By using the testing criteria outlined above, a bilinear approximation curve can be generated to determine the mean fracture energy G_{Fm}. The area under the bilinear approximation curve is equal to the mean fracture energy. By developing this bilinear curve using three points (the mean horizontal intercept of the softening curve denoted w_{1m}, the kink point stress (σ_k) and the kink point crack opening (w_k)) and the average tensile strength of concrete obtained from splitting tension testing, the mean fracture energy can be calculated for a given concrete mix design with a minimum of three fracture toughness specimens.

The second fracture toughness test to be conducted is the Stiff Tension Fracture Test (STFT) that was developed by researchers at the University of New Mexico [97]. The test is designed as a tension test of concrete to directly obtain the stress-COD relationship. The stiff tension fracture test consists of two steel end-caps and three 1.25in (37mm) diameter steel loading rods. The concrete specimen, which is 6 inches (150mm) in diameter and 12 inches (300mm) in length is fixed to the end-caps by using steel pipe sleeves and epoxy. The three load rods are fixed the both end-caps but don't come into contact with the concrete specimen. A schematic of the test setup can be seen in Figure 3.17.

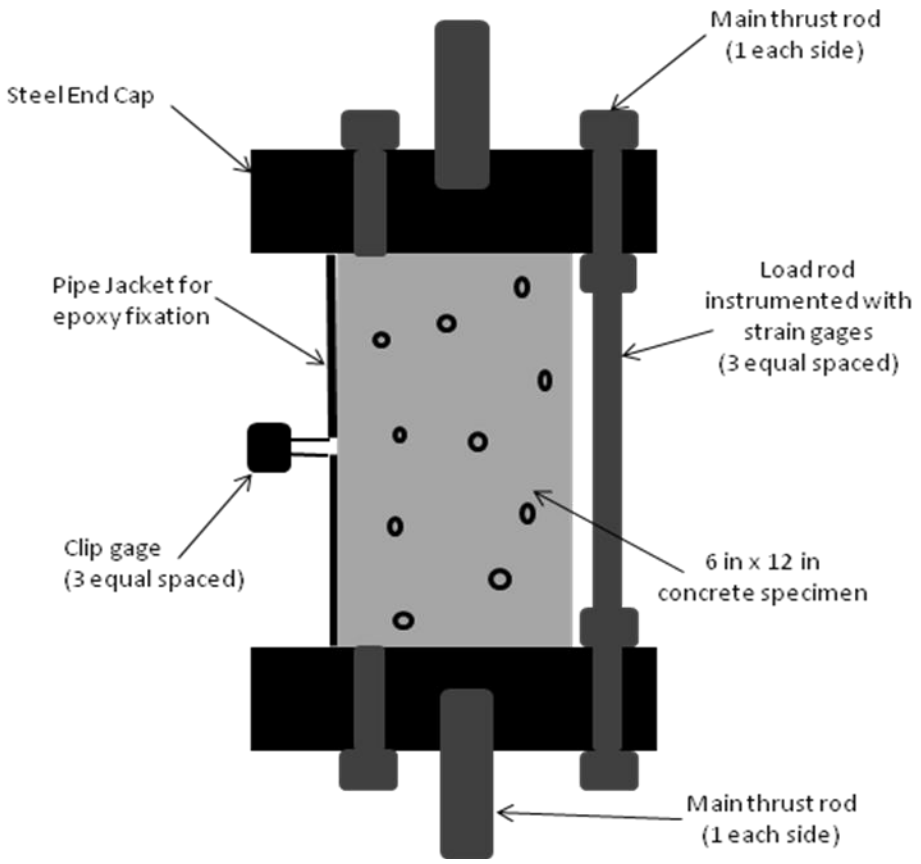

Figure 3.17 – Schematic of STFT

Each load rod is instrumented with two different strain gages on opposite sides of the load rod. They are oriented at 90 degrees in a full bridge configuration so bending stresses can be cancelled out appropriately. Once the epoxy is cured (24hrs after pouring) the test can be conducted. Tensile load is applied to the main thrust rods that are threaded into the end-caps. Once the concrete begins to crack, the three separate load rods begin to support progressively more of the load being applied as a tensile stress to the concrete specimen. By the load rods "absorbing" more of the tensile load, the crack propagation in concrete will slow and prevent any snap back of the concrete specimen being tested.

The test setup also contains three separate clip gages to monitor the crack opening displacement (COD) as the tensile load is applied. The strain gages are fixed every 120

degrees around the test specimen. As the crack begins to open, an average value of the three clip gages will allow us to monitor the COD of the specimen versus the applied load. The test setup is presented in Figure 3.18.

Figure 3.18 – STFT setup

Once the ultimate tensile strength of the concrete is reached and the applied stress is transferred from the concrete to the steel load rods; a critical crack opening displacement can be determined. With continued loading of the test specimen, an increased amount of load will be consumed by the loading rods and an appropriate concrete stress can be calculated. By appropriately monitoring the COD, the forces absorbed by the three separate load rods by knowing the strains of each rod and the associated modulus of elasticity's, and the tensile load recorded by the Universal Testing Machine; the stress versus COD relation can be determined directly. By integrating the area under this relationship, a value of fracture energy G_F can be directly calculated.

The specimens used for the Notched Beam Level II test, outlined by ACI committee 446 [114], were 6 inches in height and width and 30 inches in length. The overall preparation for the test prisms is straight-forward and is outlined below:

1) Concrete beams were first cast and cured for 42 days according to ASTM standards for standard curing of concrete in water bath at 23^0 C.
2) At 42 days of age, the concrete beams were weighed and the initial notch was cut using a thin saw.
3) Once cut, the beams were transported under wet cloths to prohibit any moisture loss during the setup period and the actual testing period.
4) The beam was then setup on the Notched Beam Level II fracture test with special frame and the test was conducted.
5) Immediately following the failure of the concrete beam, dimensions of the beam were measured and final weight of the beam was recorded.

A minimum of three beams were tested for each of the different concrete mixes of interest. Fracture toughness properties were then calculated based on the equations determined by ACI committee 446 [114]

3.8 Statistical Analysis

Due to the inherent variability between the fracture toughness values obtained between the three specimens used in the notched beam level II test, a one tailed student t-test was performed to determine if the fracture toughness values obtained were significantly different between batches. To determine if the means were significantly different, a confidence interval of 90% utilized. The student t-test was chosen due to the small populations of specimens that were tested.

Different mixes were statistically compared to determine if the fracture toughness values were significantly different. The t-score can be calculated using Equation 3.50.

$$t = \frac{\overline{X_1} - \overline{X_2}}{S_{12} * \sqrt{\frac{2}{n}}} \tag{3.50}$$

Where:

$$S_{12} = \sqrt{0.5 * S_1^2 + S_2^2} \tag{3.51}$$

S_1 and $S_2$are the two standard deviations for the two sets of data. n is the sample size and $\overline{x_1}$ and $\overline{x_2}$ are the mean values of the two different data sets. The degrees of freedom (df) is equal to (2n-2).

3.9 Finite Element Model

A finite element model was constructed for the STFT method to predict fracture toughness of concrete mixes. SOLID 95 elements were used for the steel bars, the steel end caps, and the notched concrete specimen. To obtain an accurate stress versus CMOD curve, contact elements were used at the one of the notch discontinuities of the concrete

specimen due to stress concentrations. CONTA173 and TARGE170 are three dimensional interface elements possessing 4-nodes. Each node has three degrees of freedom; translations in the x, y, and z-directions.

We define the cohesive zone material (CZM) using a bilinear relationship between stress and contact distance to model the notch of the concrete specimen. The relationship between stress and contact distance can be observed in Equation (3.52).

$$\sigma = Ku(1-d) \tag{3.52}$$

Where σ is the normal stress, K is the bonding stiffness, u is the contact gap and d is the debonding parameter that can be calculated using Equation 3.53.

$$d = \left(\frac{u-u_p}{u}\right)\left(\frac{u_f}{u_f-u_p}\right) \tag{3.53}$$

Where u_p and u_f are the contact gap distances at the peak stress and at the completion of debonding. Once the stress and the contact distance are defined, the critical fracture energy can be calculated by Equation 3.54.

$$G_F = \frac{1}{2}\sigma_{max}u_f \tag{3.54}$$

In Figure 3.19, a graphical representation can be observed for the bilinear relationship used to define the cohesive zone material (CMZ).

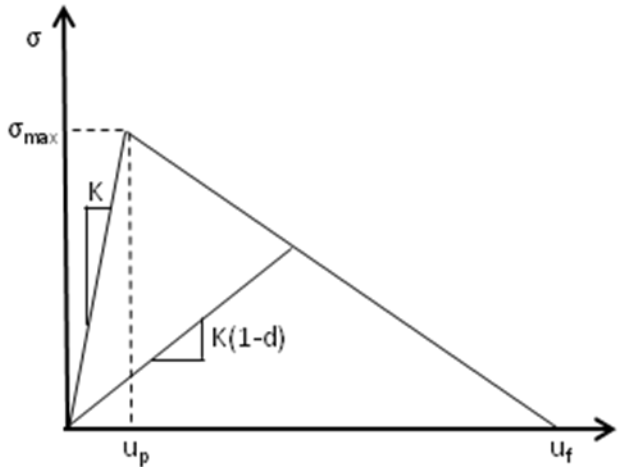

Figure 3.19 – Bilinear relationship between gap distances and contact normal stress

Two variables are needed to define the cohesive zone material (CMZ) and the third can be calculated using Equation 3.54. In the finite element model presented, the CMZ was defined by the maximum normal stress (σ_{max}) and the average fracture toughness (G_F) that was recorded from the notched beam level II test from laboratory. The fracture toughness, according to this model, is the area under the bilinear curve. It is assumed that the area under the ascending part of the curve is very small compared to the descending part, thus an approximation for the fracture toughness can be made.

The modulus of elasticity and the Poisson's ratio of the concrete elements were determined from laboratory testing and were inputs for the FE model. The modulus of elasticity for the steel load rods was assigned at 400GPa and the Poisson's ratio was 0.3.

4. Results and Discussion

4.1 Creep

The total and basic creep tests were conducted for a total of 63 days for each mix. Once the values were obtained, using the methods mentioned in the creep methods section, total and basic creep compliance figures were constructed for each of the concrete mixes. The results presented in the first two figures are the basic and total creep compliances for the Placitas source concrete mix designs (NVC1, SCC1, and SCC2). The next two figures are the basic and total creep compliances for the Griego and Sons source (NVC2, SCC3, SCC4, and SCC5). A comparison between the creep values obtained across the different mixes is not possible because of the different concrete mixes. The purpose of this research was to compare SCC mix designs with well-known conventional concrete designs for each of the different sources. In Figures 4.1 and 4.2, a comparison between the two proposed SCC mixes with the NVC1 design currently used for highway projects in New Mexico. Figures 4.3 and 4.4 present the comparison between creep compliance of the three proposed SCC mixes with the NVC2 mix.

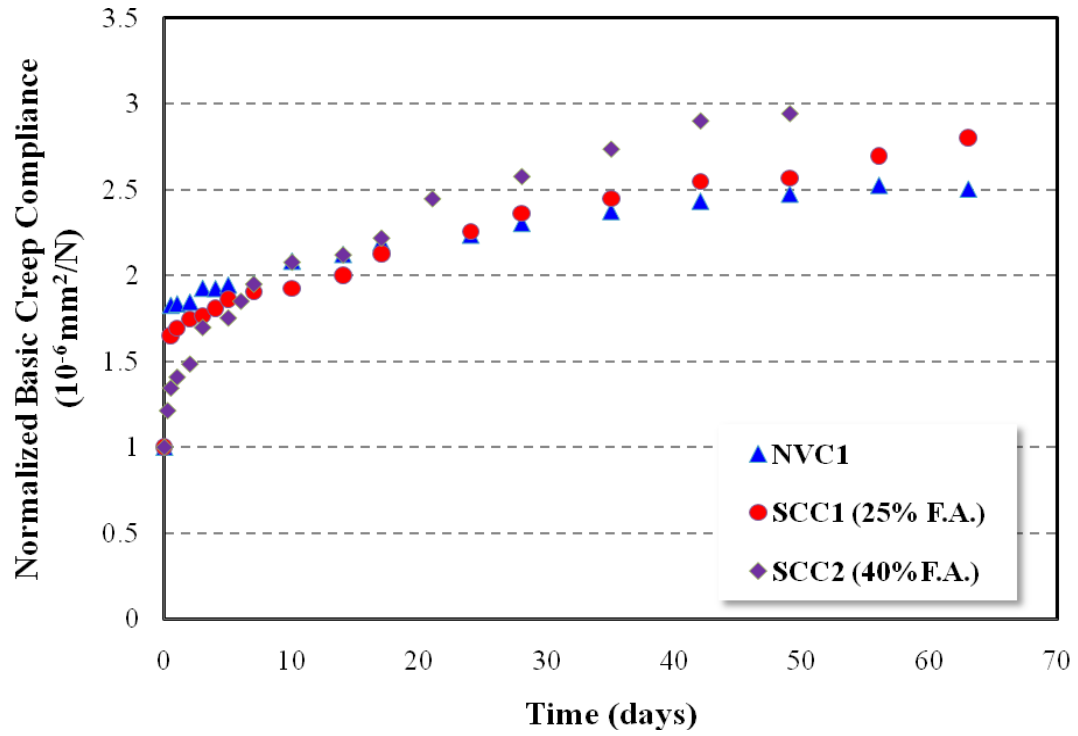

Figure 4.1 - Basic creep compliance for Placitas aggregate source

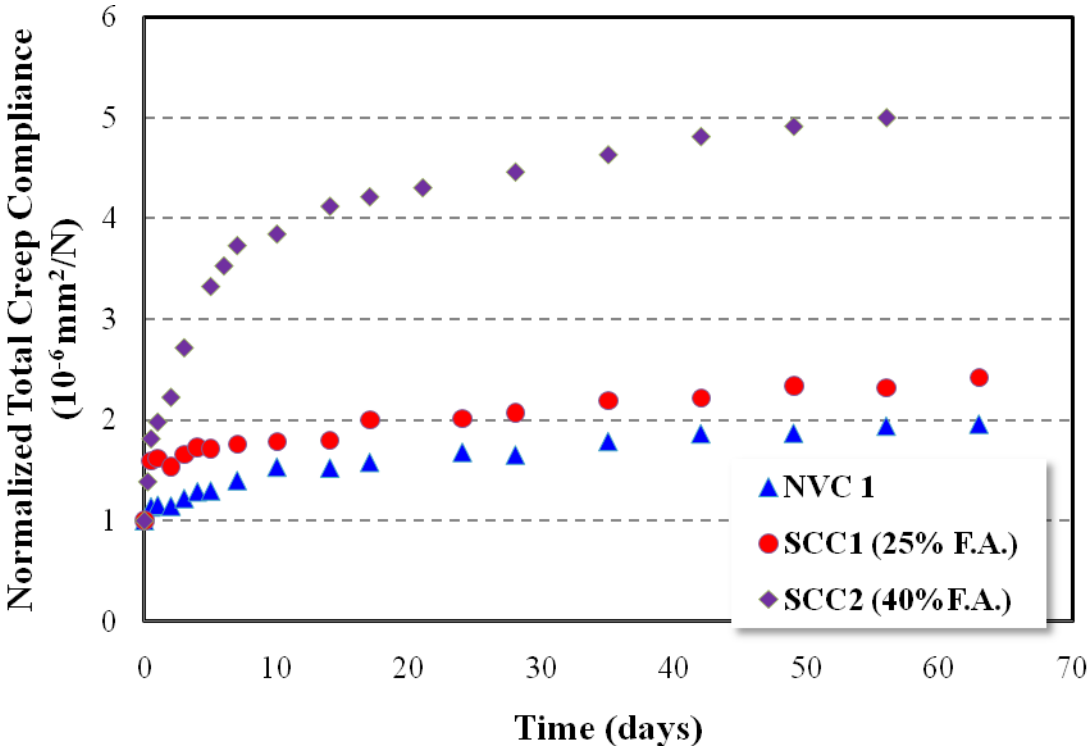

Figure 4.2 - Total creep compliance for Placitas aggregate source

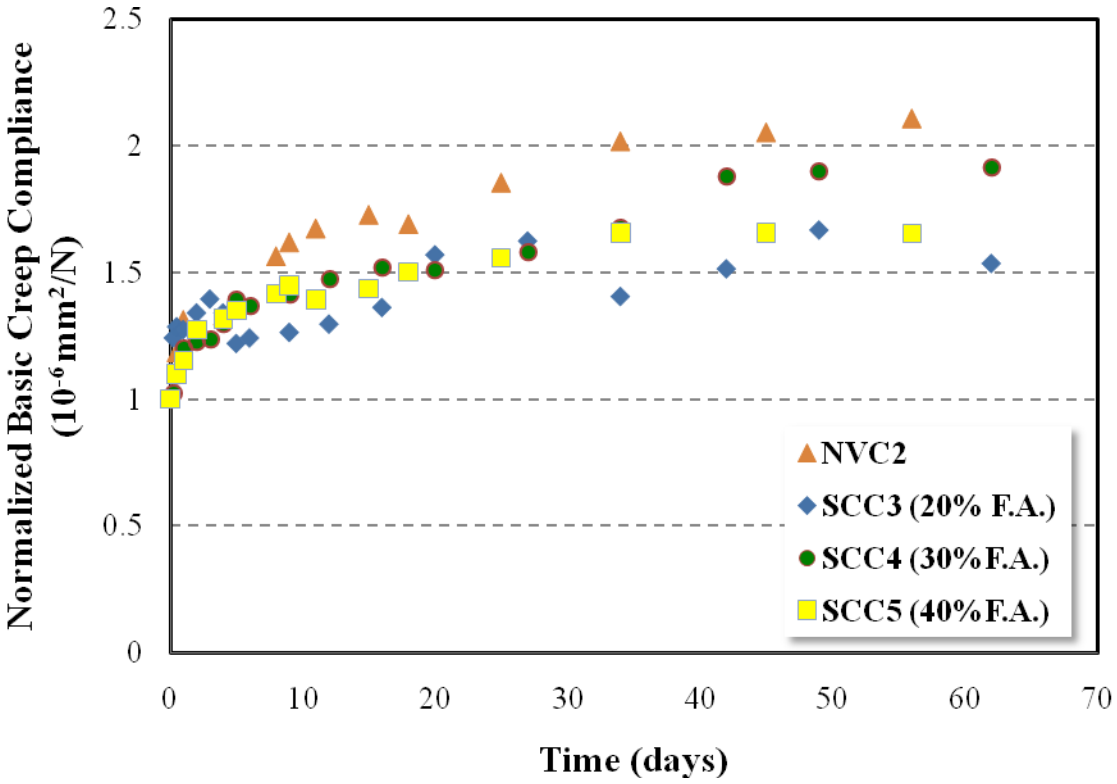

Figure 4.3 - Basic creep compliance for Griego and Sons aggregate source

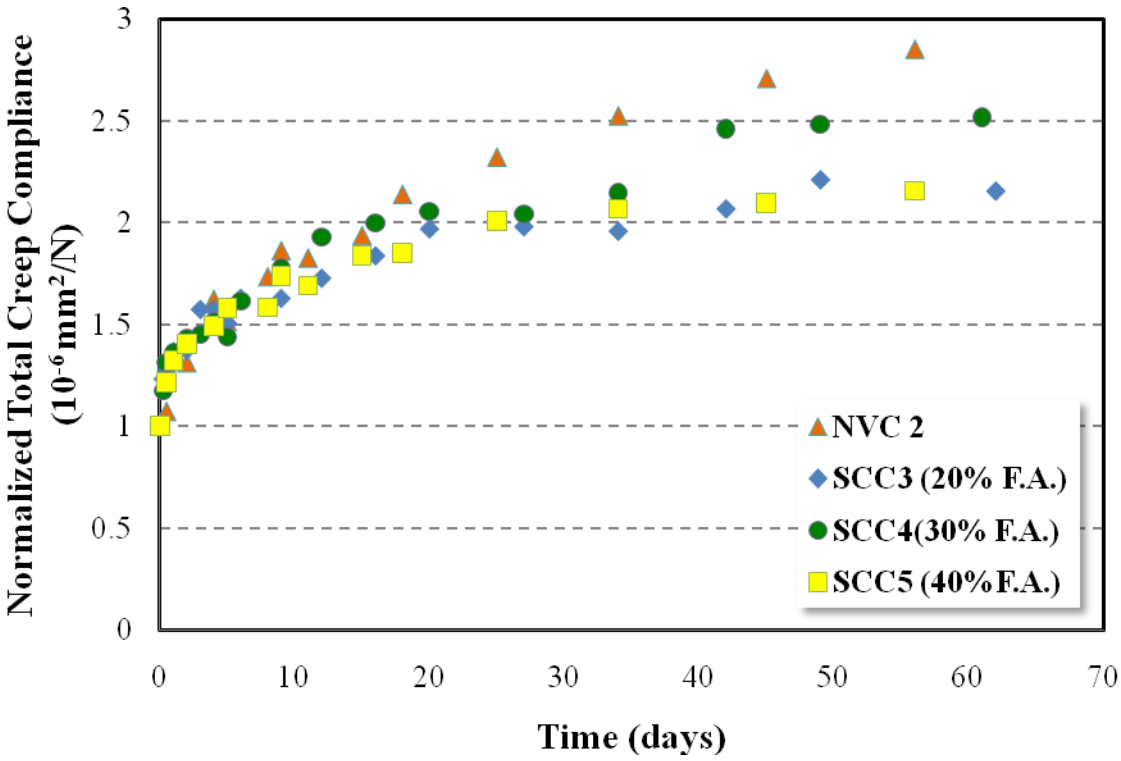

Figure 4.4 - Total creep compliance for Griego and Sons aggregate source

In comparing the proposed SCC mix designs for the Placitas aggregate source, there is no significant difference in basic creep compliance, however, the SCC mixes have total creep compliance higher than the NVC control mix and as fly ash content increases, total creep compliance increases. Since many factors affect creep strains in concrete, many explanations can be offered. The most accurate explanation might be due to the increased hydration due to increased cement paste volume. Moreover, as fly ash increased, there is an increase in the total CSH content in the hardened concrete due to chemical reactions with the silicates in fly ash converting more CH to CSH, which consumes the intercapilary water and thus increases creep. Furthermore, when subjected to constant stress, more seepage creep strains are observed because of the increased water being forced from the CSH layers. This might explain the increased creep strains observed with high fly ash content concrete mixes. However, utilization of fly ash contributes to later strength gains, which might produce lower total creep strains. The 40% fly ash mix (SCC2) was also the least stable mix produced and showed signs of minor bleeding and segregation during its plastic state. This phenomenon causes microcracks to form in the ITZ before even being subject to constant stress. An increase in initial microcracking leads to increased creep strains. This might also explain the high creep strain values recorded for SCC2.

There was no pattern observed in the Greigo and Sons aggregate source in basic and total creep compliance as a function of fly ash. However, when comparing the SCC mixes with the NVC mixes, according to the work done by Reinhardt el al. [7], it was concluded that SCC mixes of the same characteristic compressive strengths as the NVC mixes exhibited higher creep strains. This phenomenon is observed in the Placitas source

mix, the aggregate source used for Reinhardt's work, however, is not observed in the Griego and Sons concrete mixes. It is hard to compare the SCC mixes with the NVC mix in this research because of the different concrete strengths. Since many performance characteristics needed to be met with the SCC mixes and the NVC mix is a commonly used mix produced by the NMDOT that had to be replicated and compared to, the strengths of the SCC concretes were twice that of the NVC mix. It is hard to compare directly the NVC mix and the SCC mixes in terms of creep due to their different compressive strengths. Also, aggregate content and grading plays a role in creep strains because of the aggregates ability to resist creep strains. All the SCC mixes can be directly compared because the aggregate and grading was identical between SCC mixes. However, it can be concluded that the proposed SCC mixes contain similar creep characteristics when compared to the NMDOT mix currently used for precast, prestressed bridge applications. Research conducted by Kim el al. [110] concluded that high-strength SCC mixes exhibit smaller, but similar creep strains when compared to their NVC counterparts of similar strengths. Kim et al. [110] concluded that the lower creep strains in SCC's was due to increased cement used in the mix allowing the SCC to gain more strength over time when compared to the NVC mixes. However, in this research, the cement content was higher, but not as significant as the mixes tested in Kim's research. Research conducted by Leeman et al. [111] also concluded similar creep strain values when testing SCC's with three different types of cement, when compared to NVC mixes with the same water/cement ratios. However, the SCC batch using Type I cement exhibited the highest total creep strains. Both Leeman et al. [111] and Wang et al. [112] showed that when utilizing fly ash in a concrete mix (albeit at lower percentages than the

fly ash percentages used in this research), the total concrete creep strains decreased because the strength gains over time that are observed in concrete mixes utilizing fly ash. These recent findings in the literature compare with the results obtained in this thesis in terms of showing that SCC's do not necessarily exhibit higher total creep strains when compared to NVC's of similar strengths. However, SCC2 (40%) fly ash showed higher creep strains when compared to NVC1 and SCC1. This might be due to the high volume of fly ash present and the instability of SCC2 during its plastic state.

The two most commonly used models to predict creep, mentioned in the creep modeling section, are the ACI 209R-92 Model [110] (used in the United States) and the CEB-FIP MC90-99 Model [115] (used in Europe and Canada). An interest of how these two creep prediction models simulate creep strains in SCC mixes to determine if these models can be used for SCC mixes. However, in the model produced by ACI, there is factor relating the slump of the concrete mix to help predict the total creep compliance. Since there is no slump value in SCC mixes and only a slump flow value, the ACI model needs to be modified to eliminate its reliance on slump measurement. A comparison of the experimental creep compliance and the predicted ACI creep compliance was conducted. By reducing the root mean square errors (RMSE) of the predicted versus experimental values, a coefficient can be determined to fit the creep data with the predicted values by using a different parameter and eliminating its dependence on slump. Two separate equations were determined, one for the Placitas source mix and the Griego and Sons source mix predict creep as a function of fly ash content in SCC. Equations (4.1) and (4.2) represent the equations determined to calculate the fly ash constant suggested replacing the slump constant in the ACI 209 model.

$$\Upsilon_{c,s} = 0.0012\alpha^2 - 0.0095\alpha + 0.4492 \quad (4.1)$$

$$\Upsilon_{c,s} = -0.003\alpha^2 + 0.1798\alpha - 1.5288 \quad (4.2)$$

α (%) is the weight of fly ash to weight of Portland cement

Once this constant was determined, the experimental total creep strains can be compared with the two commonly used models presented above. Figures 4.5 - 4.11 present the total creep compliance of each mix compared with predicted creep compliance curves.

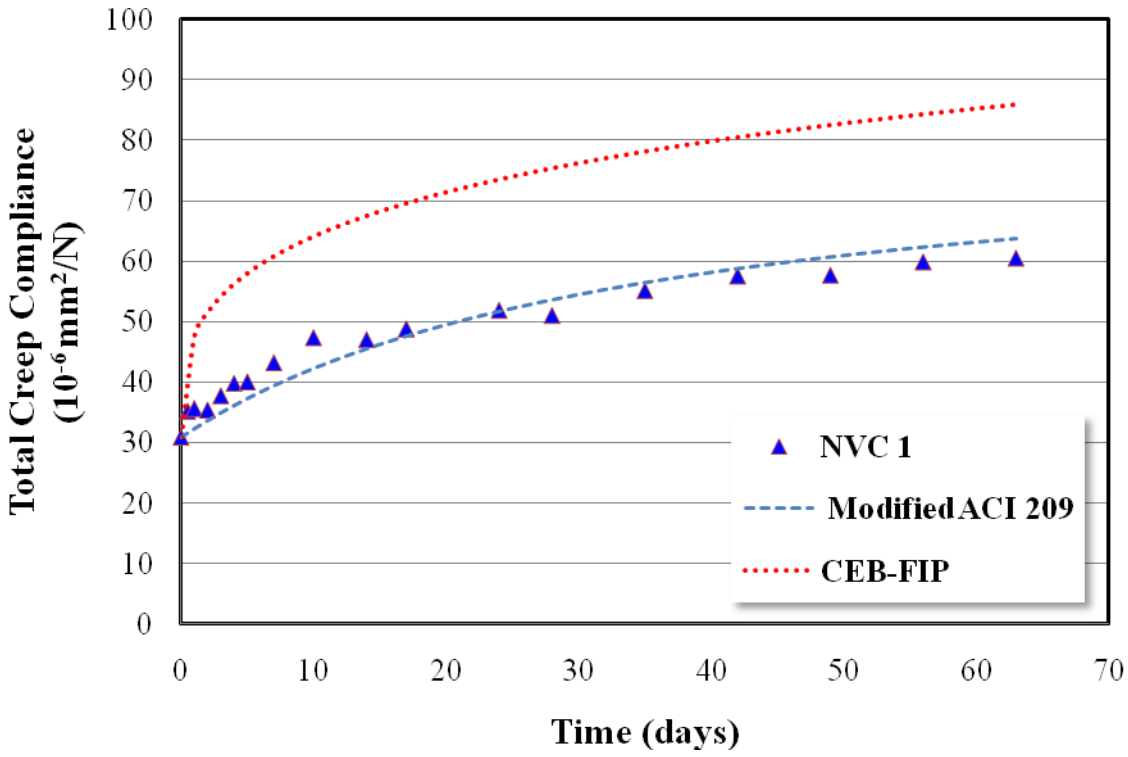

Figure 4.5 – Total Creep Compliance NVC 1

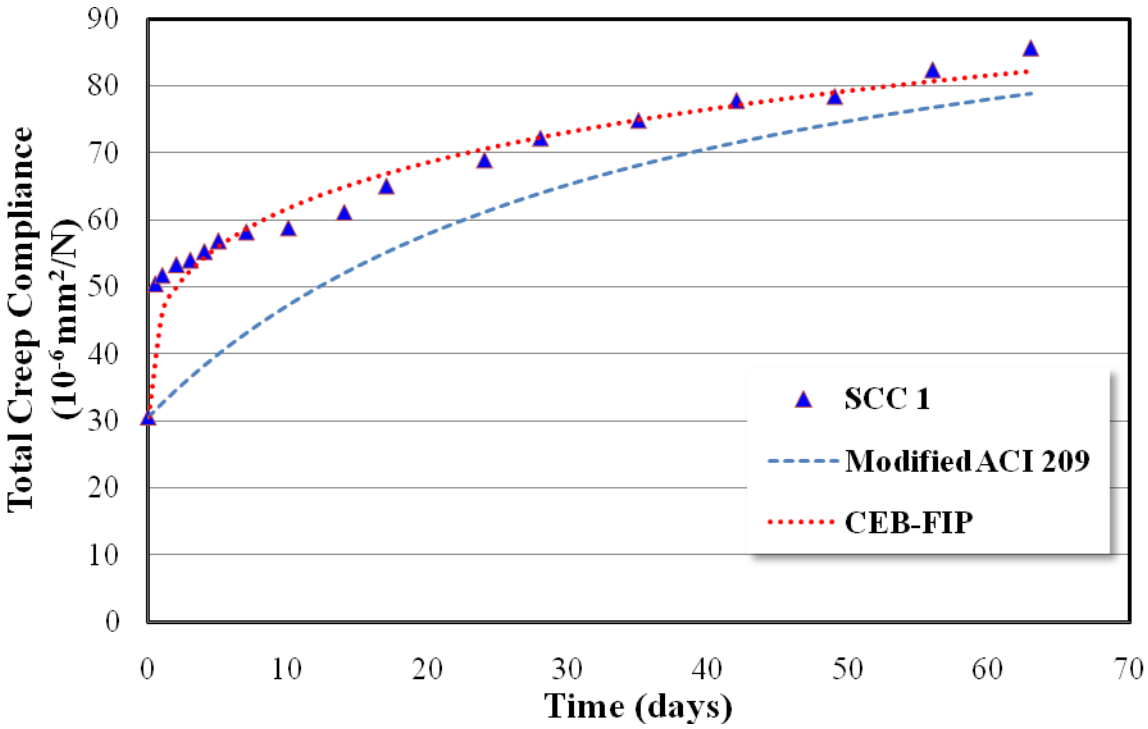

Figure 4.6 – Total Creep Compliance SCC1

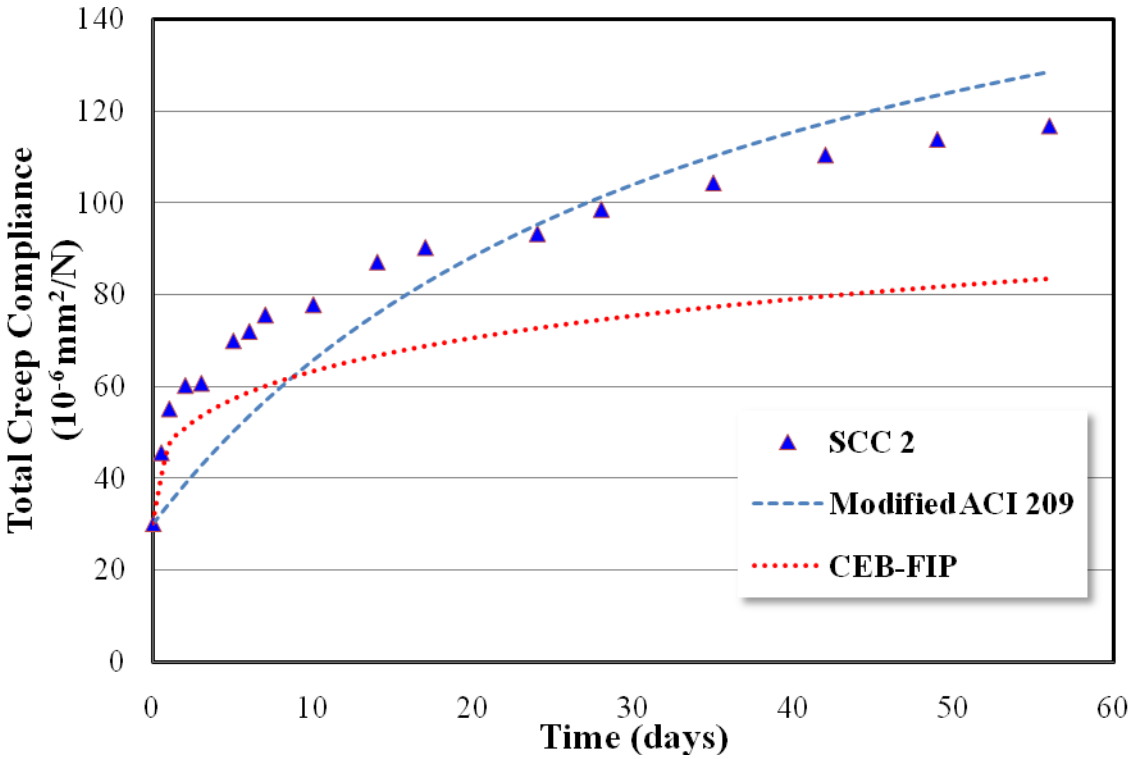

Figure 4.7 – Total Creep Compliance SCC2

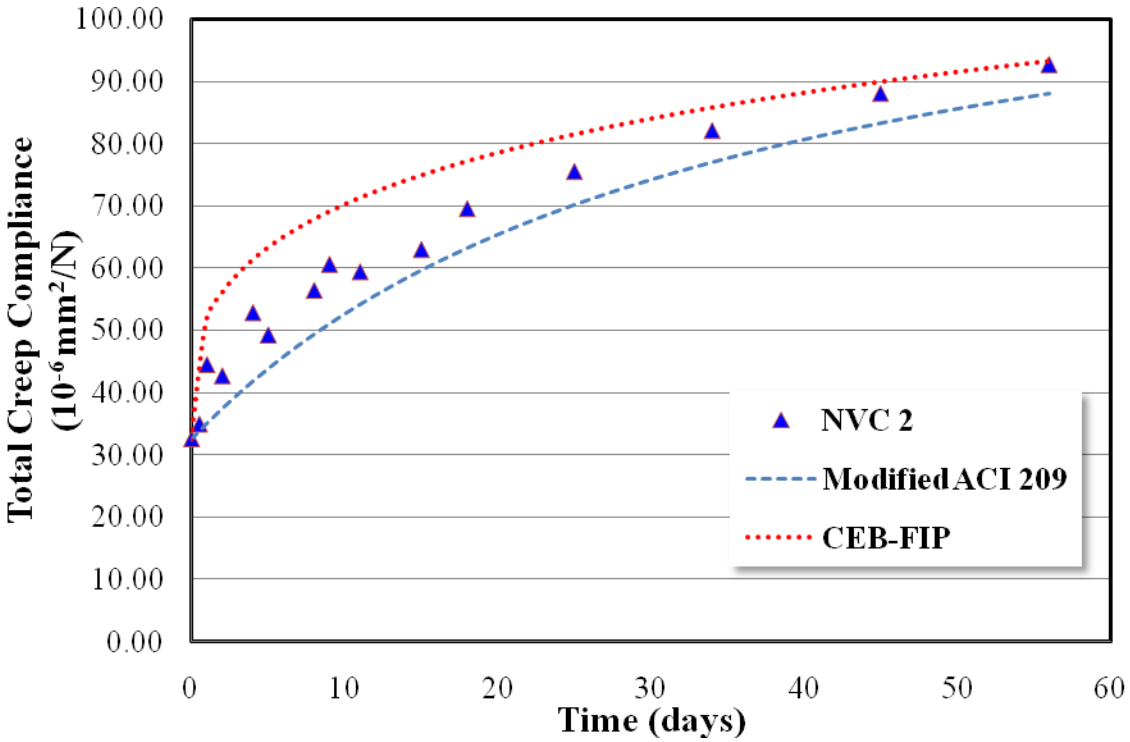

Figure 4.8 – Total Creep Compliance NVC 2

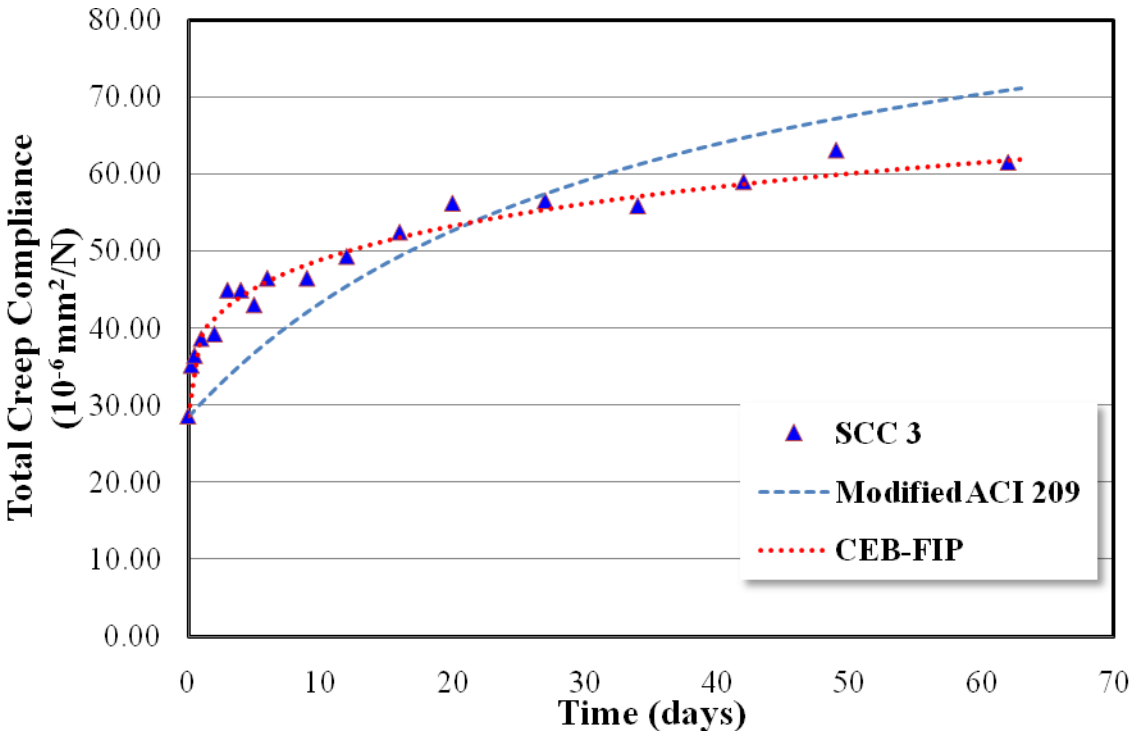

Figure 4.9 – Total Creep Compliance SCC3

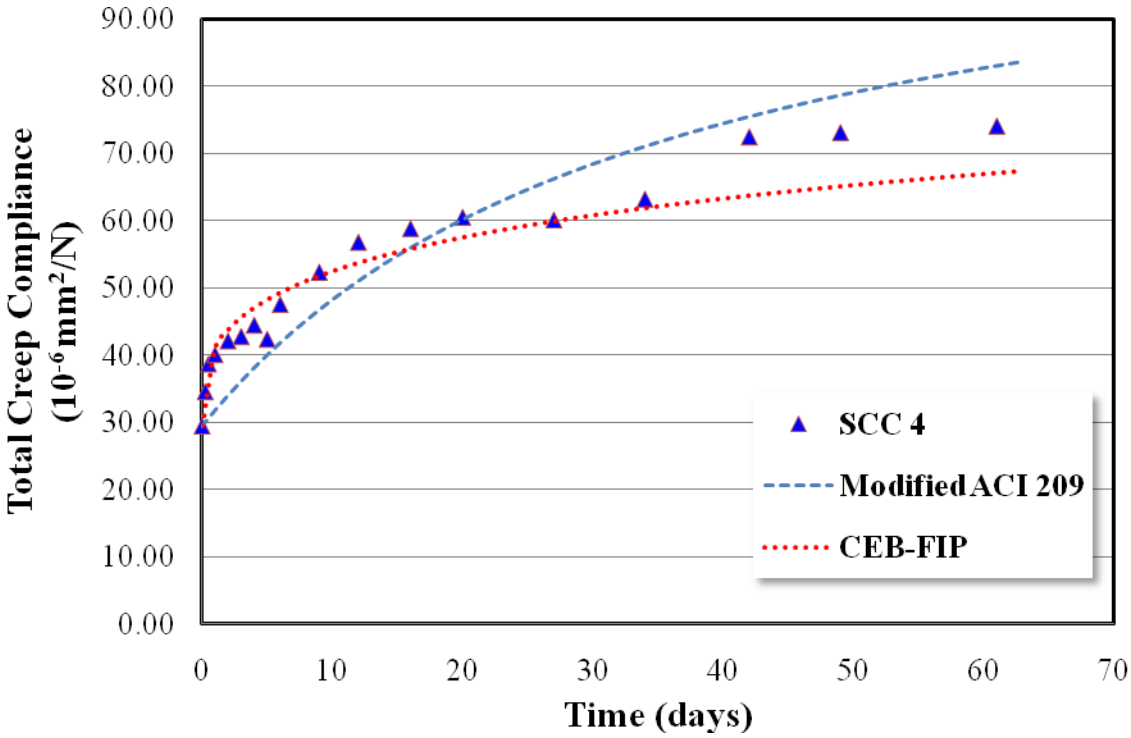

Figure 4.10 – Total Creep Compliance SCC4

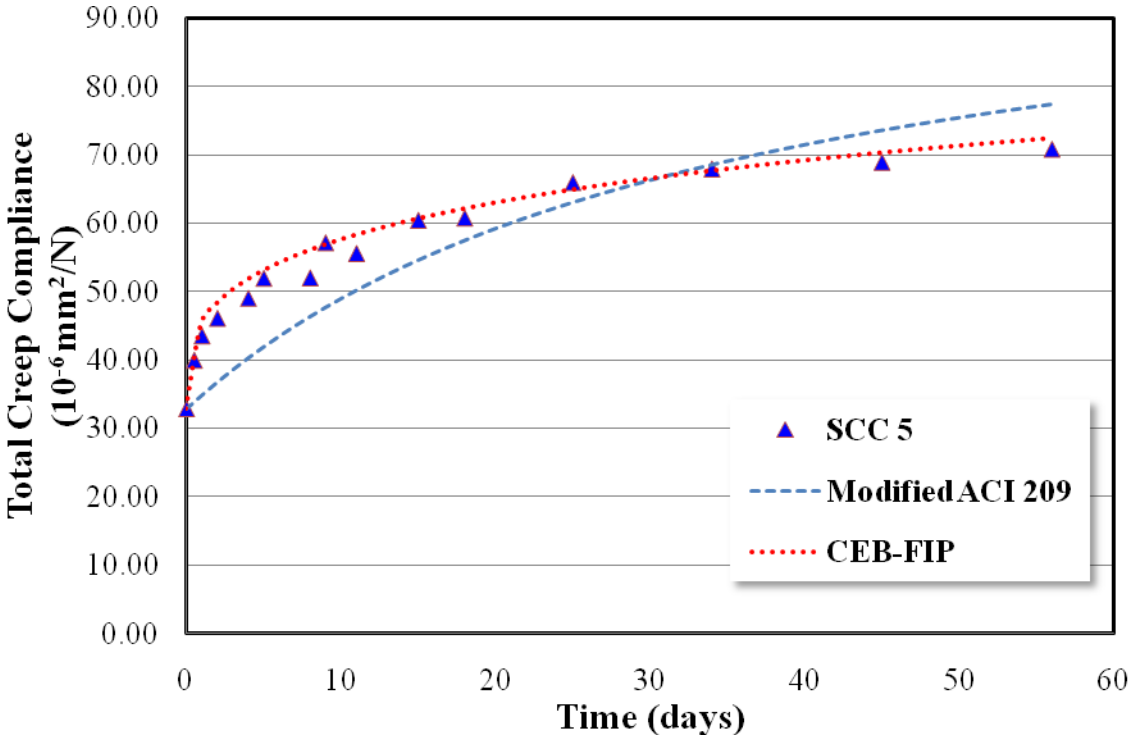

Figure 4.11 – Total Creep Compliance SCC5

It can be observed that the CEB-FIP model fits five of the seven mixes relatively accurately, with NVC1 and SCC2 being the two mixes that were not predicted well by the CEB-FIP code. The Modified ACI 209, predicted creep compliance of all the mixes accurately. These are observations consistent with Reinhardt's [7] work that showed the CEB-FIP model cannot predict SCC mixes with high volumes of fly ash when using the Placitas aggregate source. The Modified ACI model, however, seems like a reasonable prediction model for all the mixes produced.

Ultimate creep coefficients ($\phi(t, t_0)$) were also calculated at 56 days for all the mixes using Equation 3.9. The ultimate creep coefficients are compared with code predicted creep coefficients and are presented in Table 4.1 and Figure 4.12.

Table 4.1 – Calculate ultimate creep coefficients at 56 days

Aggregate Source	Mix #	Experimental $\phi(t, t_0)$	Modified ACI $\phi(t, t_0)$	CEB-FIP $\phi(t, t_0)$
Placitas	NVC1	0.96	1.02	1.73
	SCC1	1.42	1.51	1.64
	SCC2	2.89	3.28	1.78
Greigo and Sons	NVC2	1.85	1.71	1.87
	SCC3	1.21	1.43	1.13
	SCC4	1.50	1.76	1.26
	SCC5	1.15	1.35	1.2

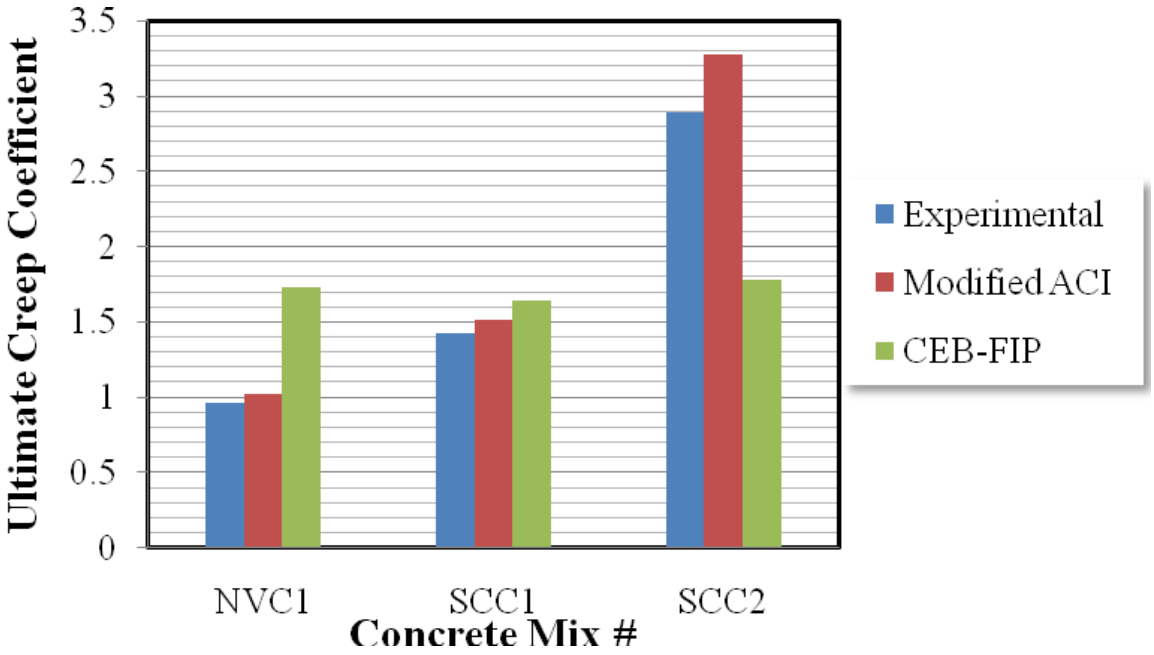

Figure 4.12 – Ultimate creep coefficients for Placitas aggregate source

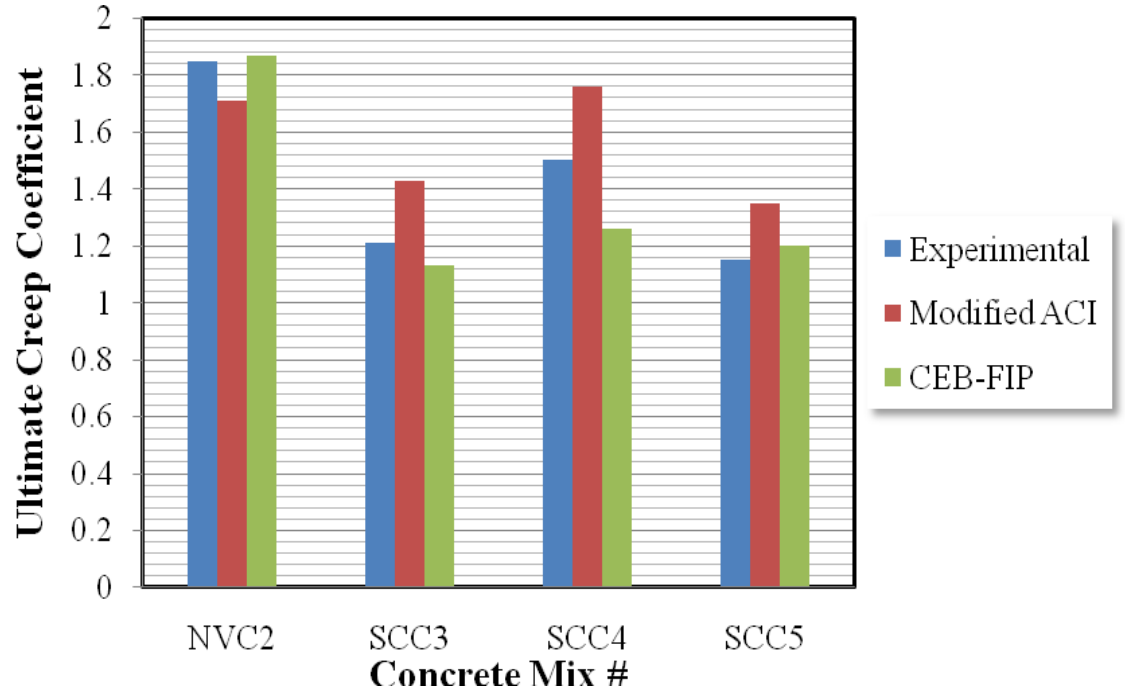

Figure 4.13 – Ultimate creep coefficients for Greigo and Sons aggregate source

It can be observed that the models predicted ultimate creep coefficients accurately with the exception of the CEB-FIP model for NVC1 and SCC2.

4.2 Fracture Toughness

The three high strength SCC mixes produced utilizing the Griego and Sons aggregate were reproduced to understand fracture toughness characteristics of SCC's with varying amounts of fly ash. All three SCC mixes had similar strengths making fracture toughness values a function of fly ash content within the SCC mix. Cement paste volumes were very similar across the mixes ranging from 34-36%. The first fracture toughness tests that were conducted were using the Notched Beam Level II test method outlined by ACI 446 [114]. To create the bilinear curve of interest, tensile strengths of concrete needed to be calculated using the splitting tension (Brazilian) test. The 28 and 42 day compression strengths, tensile strengths, modulus of elasticity, and Poisson's ratio were determined experimentally and presented in Table 4.2.

Table 4.2 – Summary of hardened properties for SCC3, SCC4, and SCC5

	SCC3 (20% F.A.)	SCC4 (30% F.A.)	SCC5 (40% F.A.)
28-day strength (MPa)	48.7 (±0.63)	50.1 (±2.13)	46.8 (±0.76)
42-day strength (MPa)	49.0 (±1.15)	57.3 (±0.432)	58.3 (±1.47)
Splitting Tension (MPa)	4.0 (±0.15)	4.71 (±0.12)	4.67 (±0.51)
42-day modulus (GPa)	36.2 (±1.28)	35.8 (±0.93)	35.8 (±0.95)
Poisson's ratio	0.2 (±.007)	0.2 (±0.007)	0.2 (±0)

The tensile strength test, outlined by ASTM [101], results cannot be directly obtained from the splitting tensile test, however, an equation can be used to calculate the tensile strength of the concrete. This relation can be observed in Equation 4.3.

$$f_t = \frac{2P}{\pi l d} \tag{4.3}$$

P is the ultimate load recorded at failure, l is the length of the cylinder, and d is the diameter of the cylinder.

Once the tensile strength is determined, the process to obtain the bilinear curve to obtain the fracture toughness of the different SCC mixes, outlined earlier, can be conducted. Figures 4.14, 4.15, and 4.16 are the corrected load versus loading point displacement curves for the different SCC mixes following the process described by ACI 446 [114].

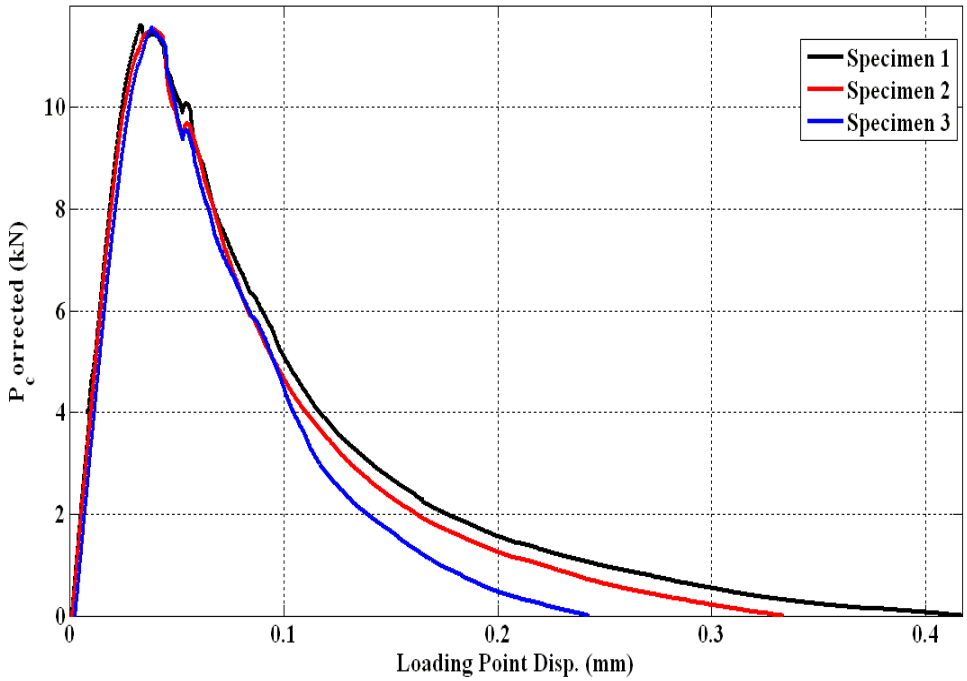

Figure 4.14 – Corrected load vs. displacement curve for SCC3

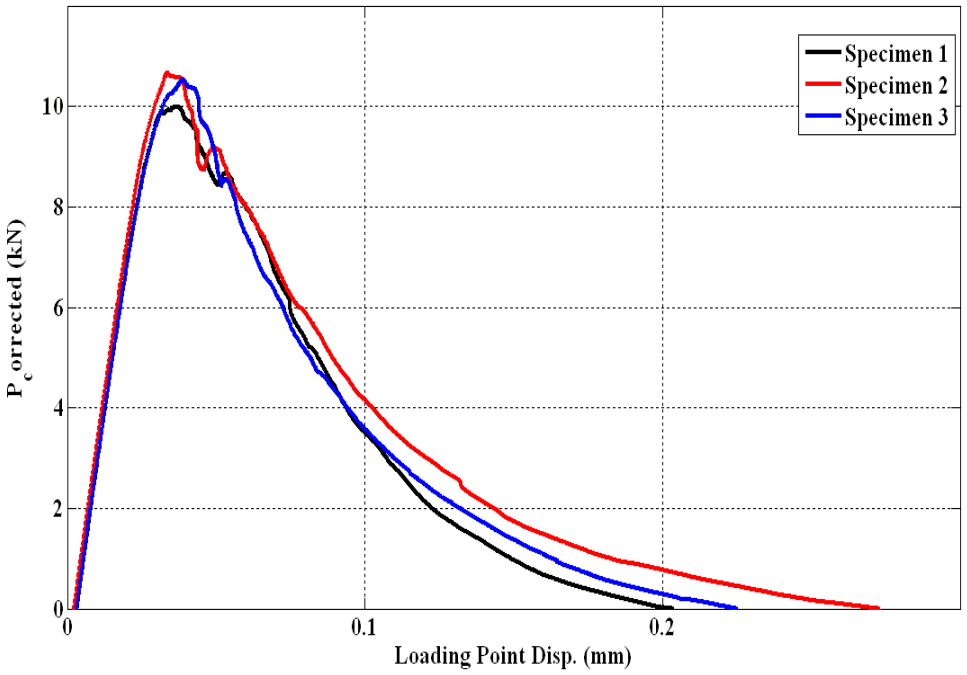

Figure 4.15 – Corrected load vs. displacement curve for SCC4

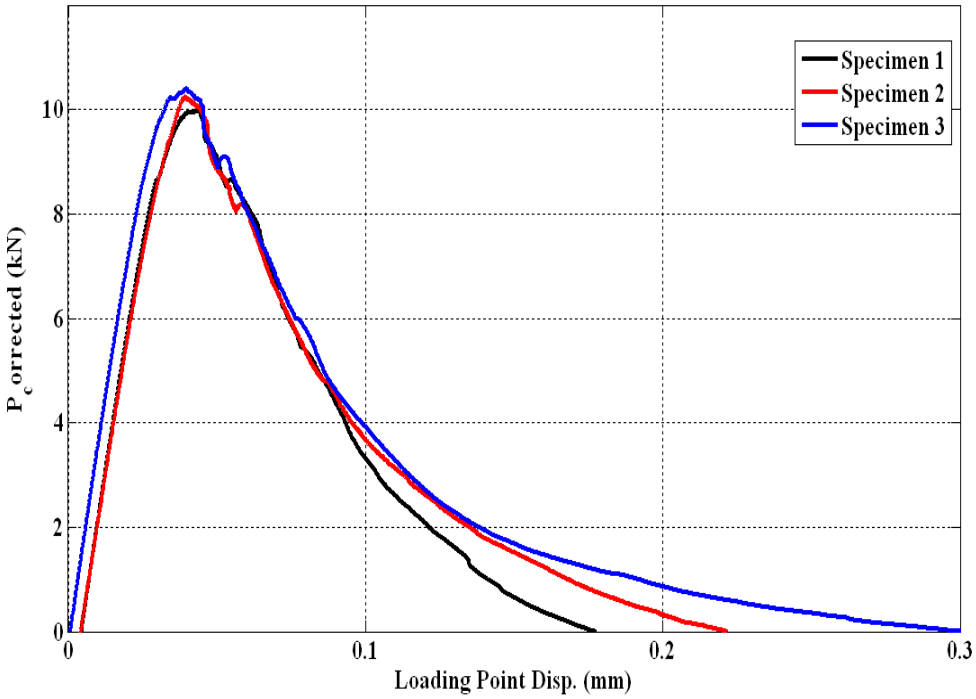

Figure 4.16 – Corrected load vs. displacement curve for SCC5

By using methods from ACI 446 [114], the method to create bilinear curves for each of the three different SCC mixes were conducted. From these curves, integration under the curve is performed to determine the fracture toughness values (G_F) for the three different mixes. The bilinear curves obtained for the three SCC mixes are presented in Figures 4.17, 4.18, and 4.19.

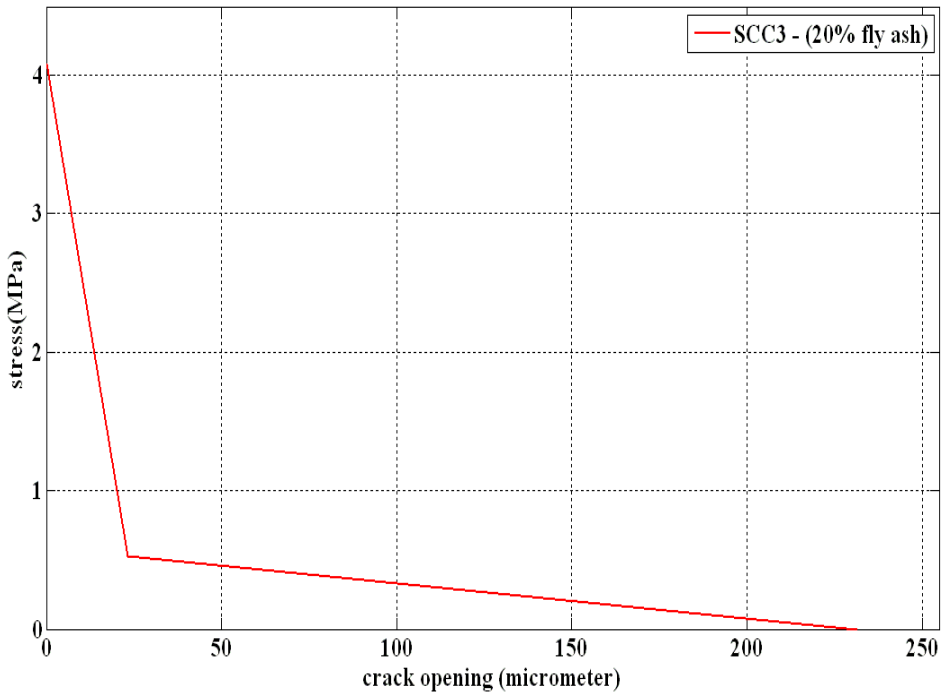

Figure 4.17 – Bilinear curve – SCC3

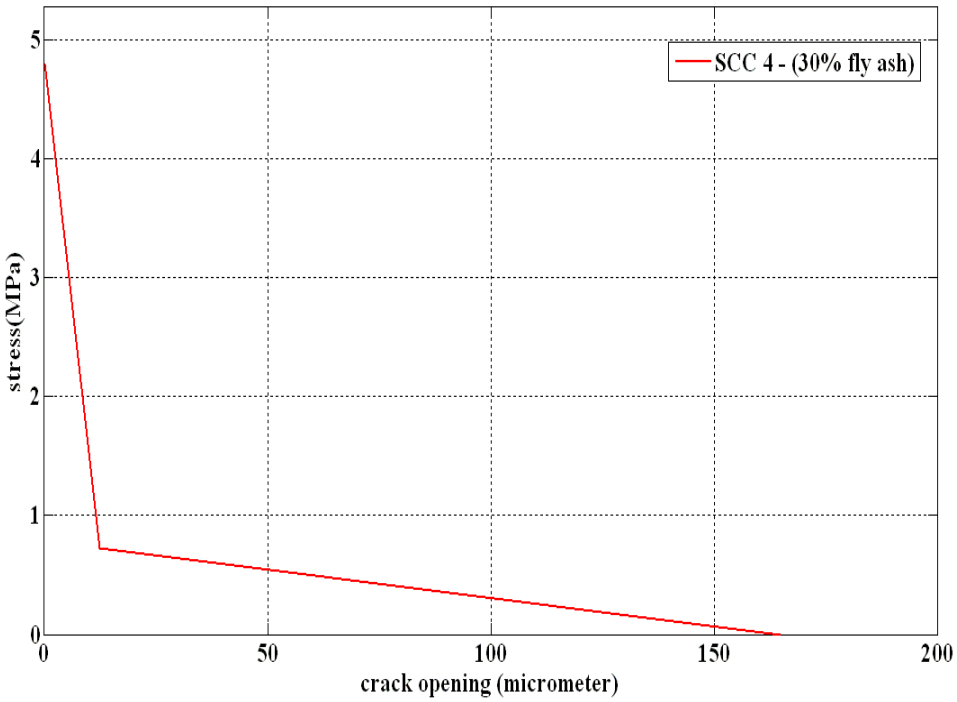

Figure 4.18 – Bilinear curve – SCC4

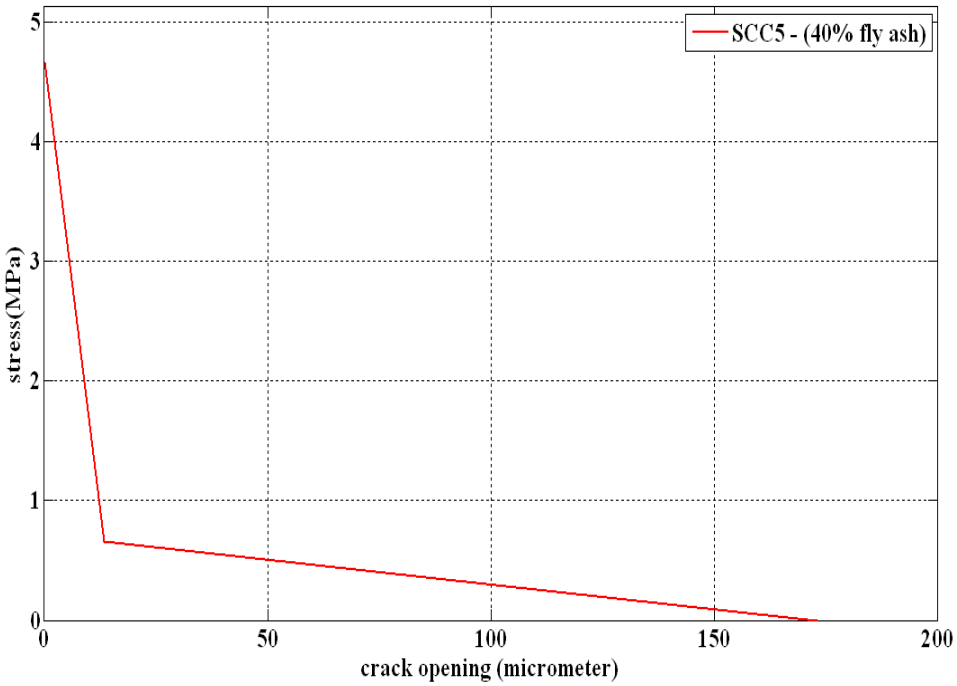

Figure 4.19 – Bilinear curve – SCC5

The fracture toughness values obtained by utilizing the Notched Beam Level II test can be observed in Table 4.3.

Table 4.3 – Fracture toughness calculations

	Specimen #	K_{IC} (Mpa $m^{.5}$)	G_F (N m/m^2)
SCC 20% Fly Ash	1	2.02	108.1
	2	2.11	118.4
	3	1.91	97.1
	Mean (std)	2.01 (±0.10)	107.9 (±10.7)
SCC 30% Fly Ash	1	1.83	89
	2	1.87	92.2
	3	1.80	85.9
	Mean (std)	1.83 (±0.04)	89.0 (±3.2)
SCC 40% Fly Ash	1	1.79	86.3
	2	1.80	86.6
	3	1.85	91.5
	Mean (std)	1.81 (±0.03)	88.1 (±2.9)

Using the statistical methods outlined in section 3.8, calculations can be made to determine if the different data sets are significantly different. When comparing K_{IC} and G_F, the values obtained from SCC3 are significantly different than the fracture toughness values obtained from SCC4 and SCC5 with 90% confidence. However, there is no significant difference between K_{IC} and G_F when comparing SCC4 and SCC5 at 90% confidence. The t-scores can be observed in Table 4.4 along with the critical t-score for a 90% confidence interval.

It seems there is a threshold for fine materials content beyond which the fracture toughness of SCC will no longer decrease. SCC4 and SCC5 are not significantly different at a 90% confidence level, however contain different amounts of fly ash.

Table 4.4 – Statistical significance t-scores

	K_{IC} t-scores	G_F t-scores	Critical t-score
SCC3-SCC4	2.9	2.9	2.132
SCC4-SCC5	0.7	0.4	2.132
SCC3-SCC5	3.3	3.1	2.132

The stiff tension fracture test (STFT) was also used to determine a stress versus crack opening displacement relationship directly to fracture toughness values by a direct integration. However, the stiff tension fracture test (STFT) setup was designed for normal strength concretes. With increased stiffness in the SCC mixes, a perfect softening curve was unattainable. There is a clear need to increase the stiffness of the steel bars in the test to enable smooth stress transfer. However, a method to try to estimate a bilinear curve from the data obtained experimentally was conducted to obtain fracture toughness values. The horizontal line AB is first drawn from 200 microns to the origin. Then a vertical line BC is drawn perpendicular to that line to the peak stress seen in the test. Next, the modified bilinear curve is constructed from the initial slope of the softening curve and the slope of the curve after the snap. The area between the lines ABCD can then be calculated using geometric equation. This area ABCD that is calculated is the modified fracture toughness. The area between the modified lines stress versus crack opening relation can be observed in Figure 4.20, and the method used to estimate a bilinear curve can also be observed in Figure 4.21.

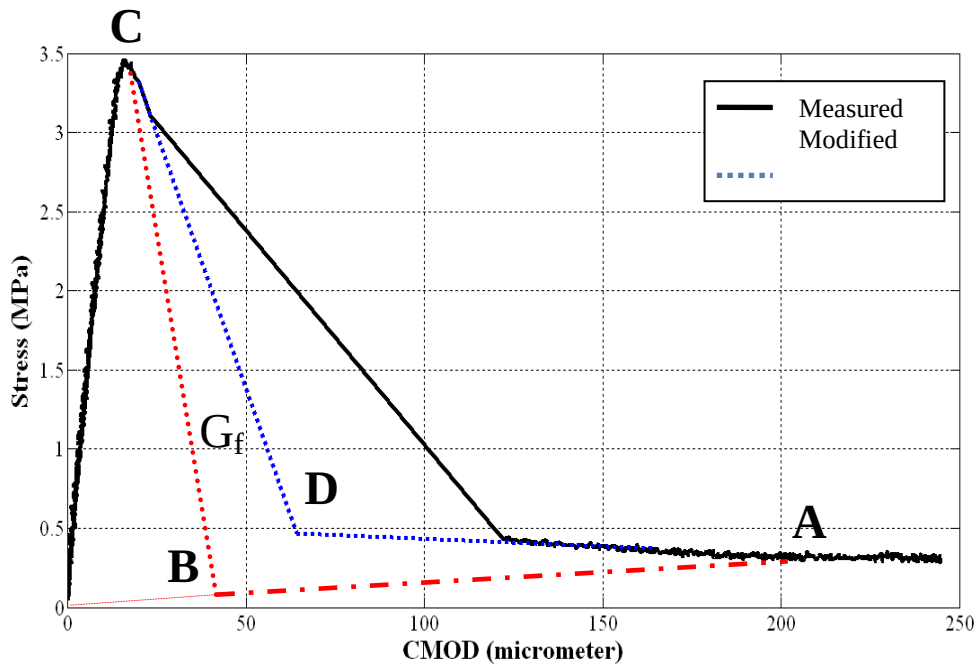

Figure 4.20 – SCC 3a results

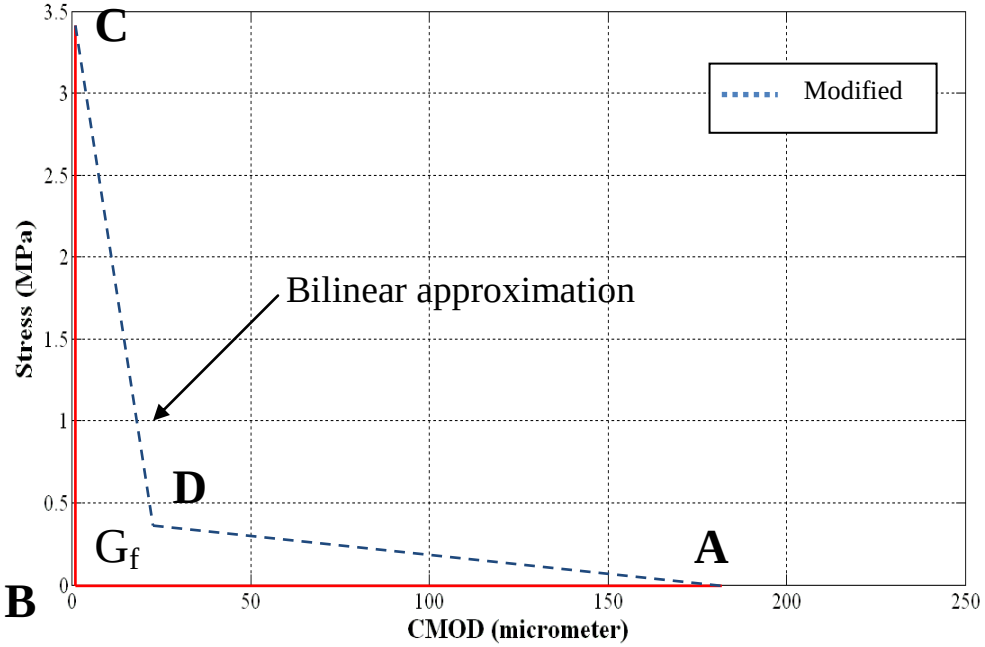

Figure 4.21 – Bilinear curve approximation

In Figures 4.22, 4.23, 4.24, 4.25, and 4.26, stress versus crack opening displacements for the different stiff tension test results for SCC3, SCC4, and SCC5. It

can be observed that the softening curves for the SCC's were not true softening curves due to the lack of stiffness in the testing setup, causing rapid crack propagation. The descending part was developing but a snap crack propagated and then had a steady growth. The fact that a small part of the original descending curve was provided in most tests; there was an idea of the original descending slope. This was used to correct the bilinear curve. The same analysis was conducted, as observed in Figure 4.18, however, fracture toughness values were significantly different in all the SCC mixes when compared to the results obtained from the Notched Beam Level II fracture test.

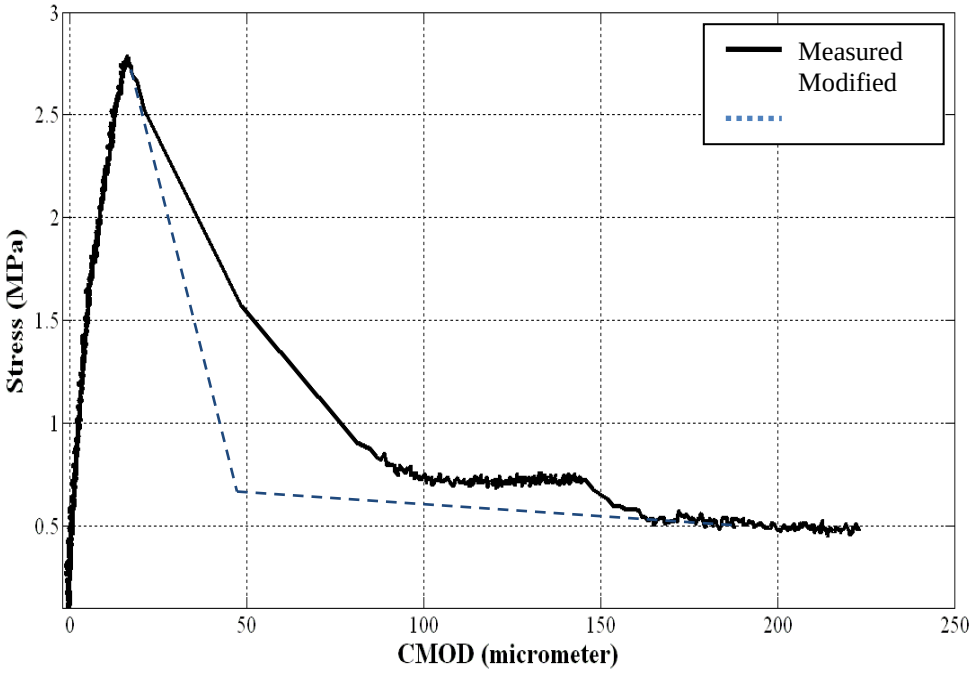

Figure 4.22 – SCC 3b results

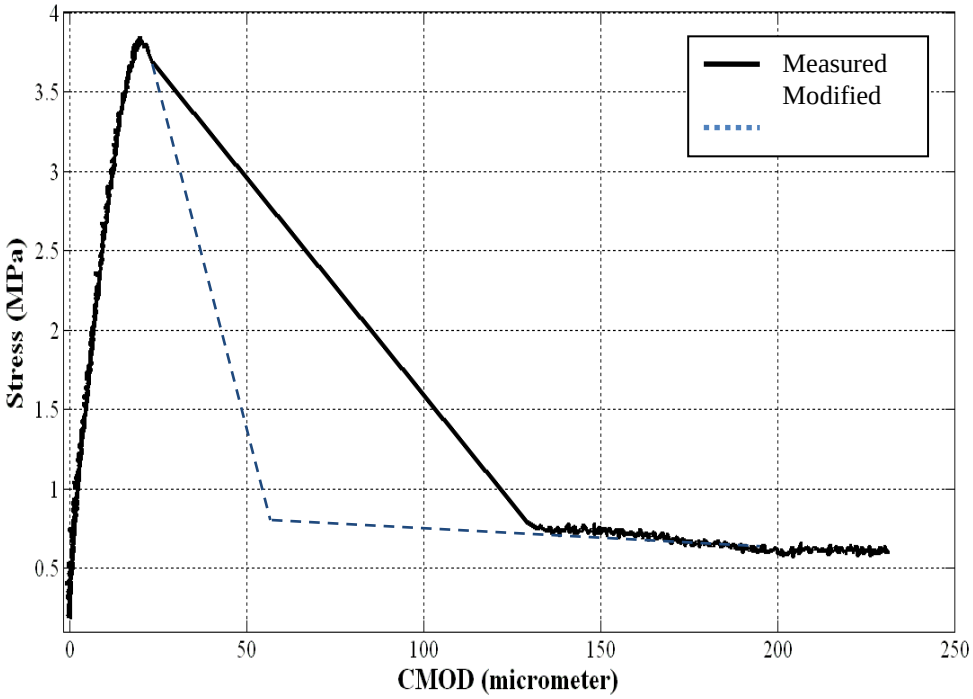

Figure 4.23 – SCC 4a results

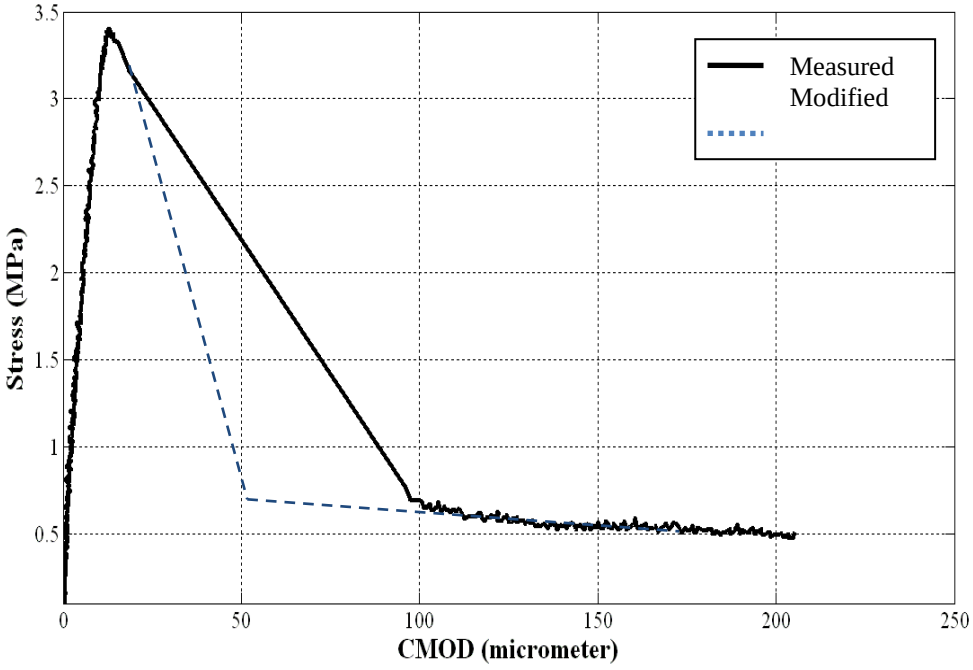

Figure 4.24 – SCC 4b results

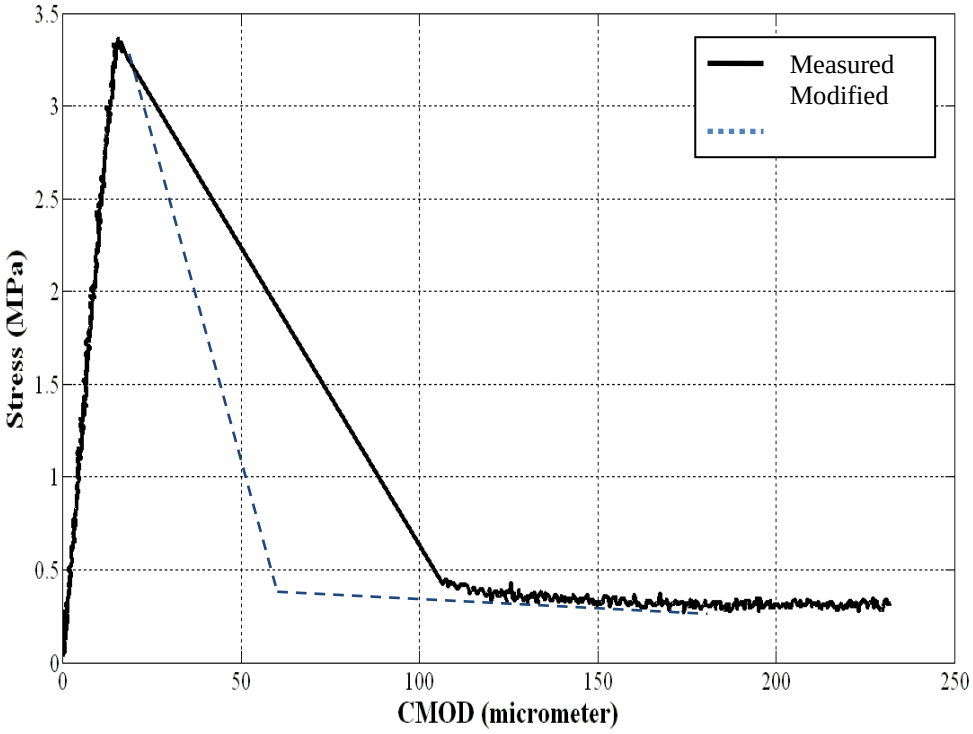

Figure 4.25 – SCC 5a results

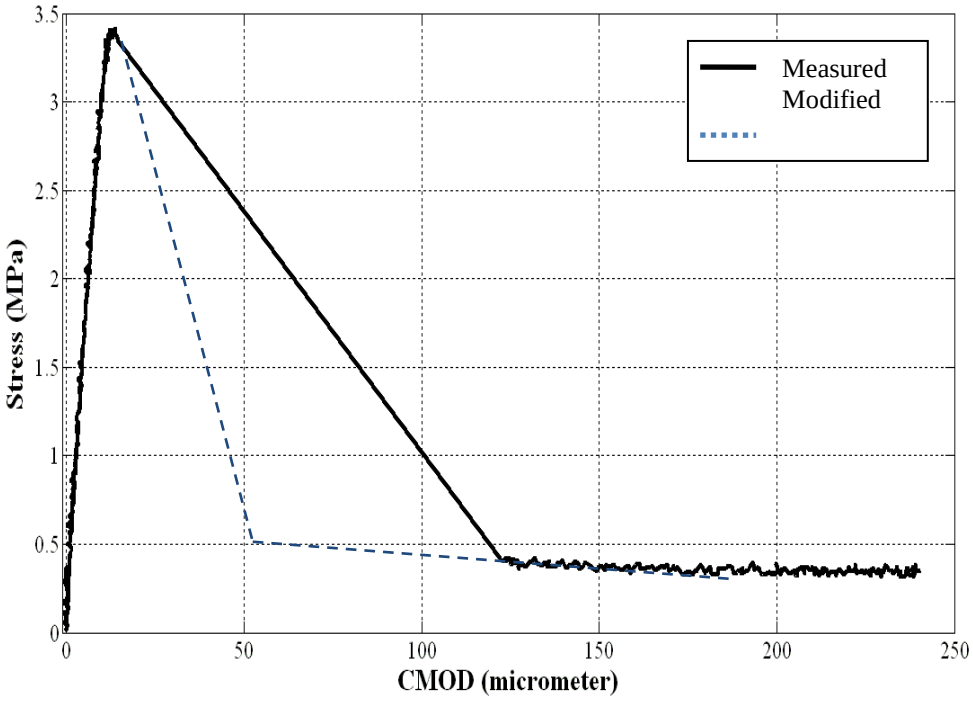

Figure 4.26 – SCC 5b results

By observing the figures above for the data obtained using the STFT, it can be seen that the softening curve never reaches zero stress. However, the test was concluded when a visible crack was observed throughout the entire concrete cylinder. A conclusion was drawn that the load rods where absorbing less load than calculated from the data acquisition program. A new calibration for the load rods needs to be conducted to obtain a softening curve that asymptotically approaches zero. Fracture toughness calculations were performed on each of the different mixes for the STFT and are presented in Table 4.5.

Table 4.5 – STFT results

	Specimen #	K_{IC} (Mpa $m^{.5}$)	G_F (N m/m^2)
SCC 20% Fly Ash	1	2.48	163
	2	2.32	143
	Mean (std)	2.40 (±0.11)	153 (±14.1)
SCC 30% Fly Ash	1	2.29	141
	2	2.28	139
	Mean (std)	2.29 (±0.01)	140 (±1.4)
SCC 40% Fly Ash	1	2.01	108
	2	2.16	125
	Mean (std)	2.09 (±0.11)	117 (±12.0)

It can be observed that the fracture toughness values (G_F) obtained by the STFT test is higher than the results obtained using the Notched Beam Level II test. This is due to the STFT test setup not having a high enough stiffness to obtain an accurate softening curve. The test results are therefore estimates; however, modifications to the STFT test setup to propagate the crack at a controlled rate to obtain a softening curve can be designed so the STFT can be utilized for higher strength concretes.

From the fracture toughness results obtained from the three different SCC mixes, it can be observed that SCC3 (20% fly ash) had the highest fracture toughness. SCC4 (30% fly ash) and SCC5 (40% fly ash) had similar fracture toughness values when compared to one-another. A relationship relating fracture toughness to amount of fly ash present in the concrete is hard to determine because SCC4 and SCC5 had essentially the same fracture toughness values when analyzing the Notched Beam Level II test results. The fracture toughness results obtained from the STFT exhibit a pattern that as the fly ash content is increased, the fracture toughness decreases. This is similar to that observed by the notched beam level II test results.

It is important to note that the three SCC mixes had slightly different volumes of cement paste. In earlier work conducted by Roziere [71], it was concluded that fracture toughness values of concrete are related to the cement paste volume. Roziere [71] showed a decrease in fracture toughness values when the cement paste volume in the mix was increased. The same pattern can be observed in the fracture toughness calculations of the three SCC mixes. SCC3 had the lowest cement paste volume equaling 34.8%. SCC4 and SCC5 had cement paste volumes of 35.6% and 36.5% respectively. And as the cement paste volume increased, fracture toughness values decreased. An increase in cement paste volume provides a medium for the crack to propagate easier because of decreased aggregate content serving as crack arresters. This cement paste volume increase also results in a stronger concrete. It can be observed that as the strength of the concrete increases, the fracture toughness decreases. This can be related to the relationship between strength and brittleness of concrete materials.

Using finite element methods outlined in section 3.9, experimental stress versus CMOD curves can be compared with the curves determined from the finite element model. The finite element model used thirty five displacement steps to control the crack growth and obtain an accurate softening curve. A plot of the concrete stress versus the CMOD can be created, which was determined by running a time history analysis of the displacements seen at the crack mouth opening. Results are presented in Figures 4.27, 4.28, and 4.29 for SCC3, SCC4, and SCC5 respectively.

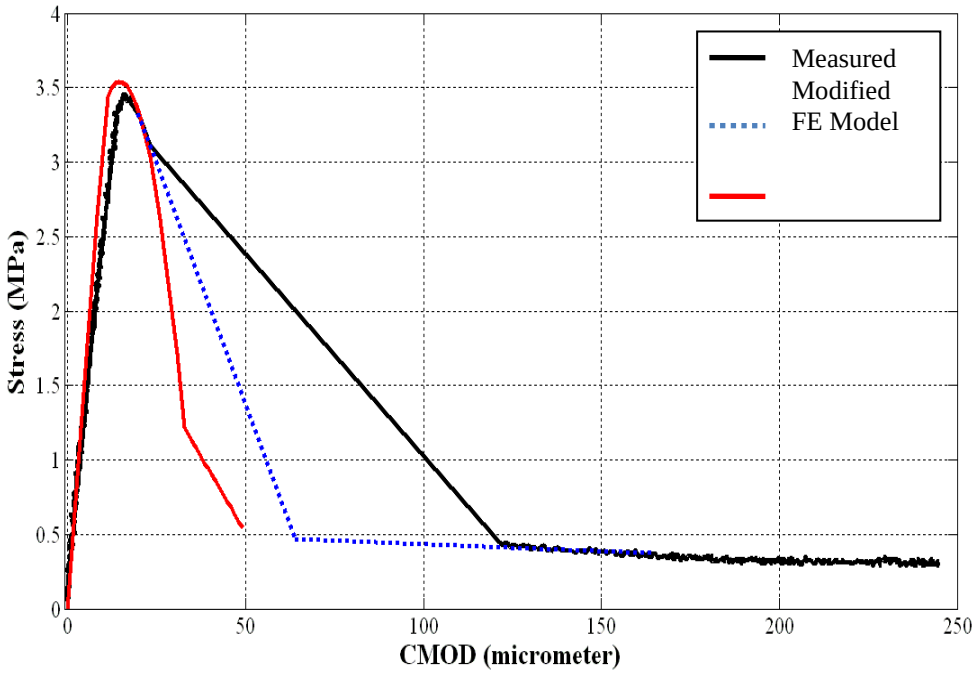

Figure 4.27 - Comparison of SCC3 experimental data, bilinear approximation, and model output

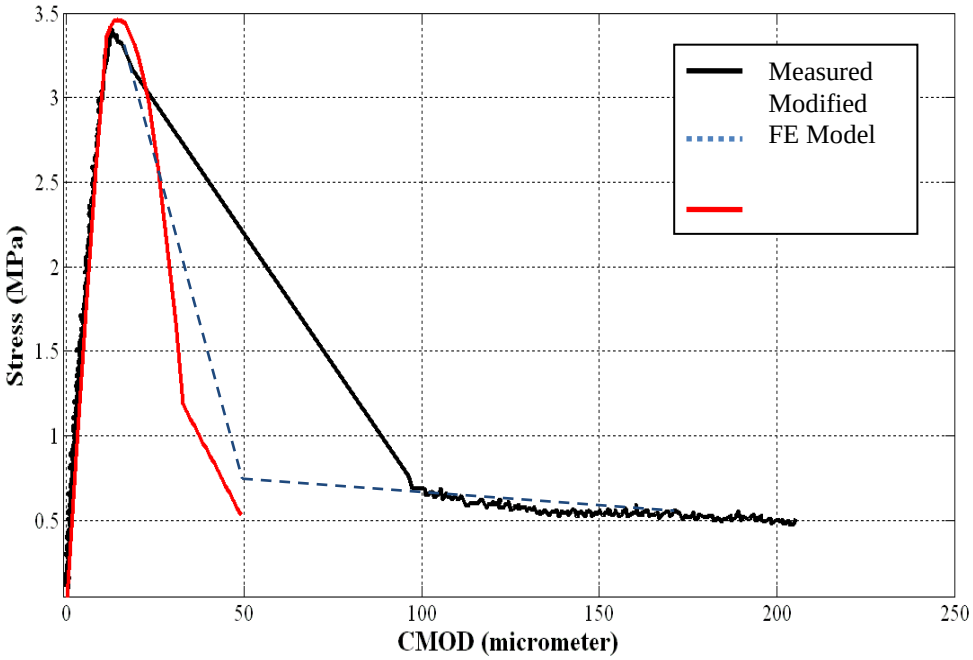

Figure 4.28 – Comparison of SCC4 experimental data, bilinear approximation, and model output

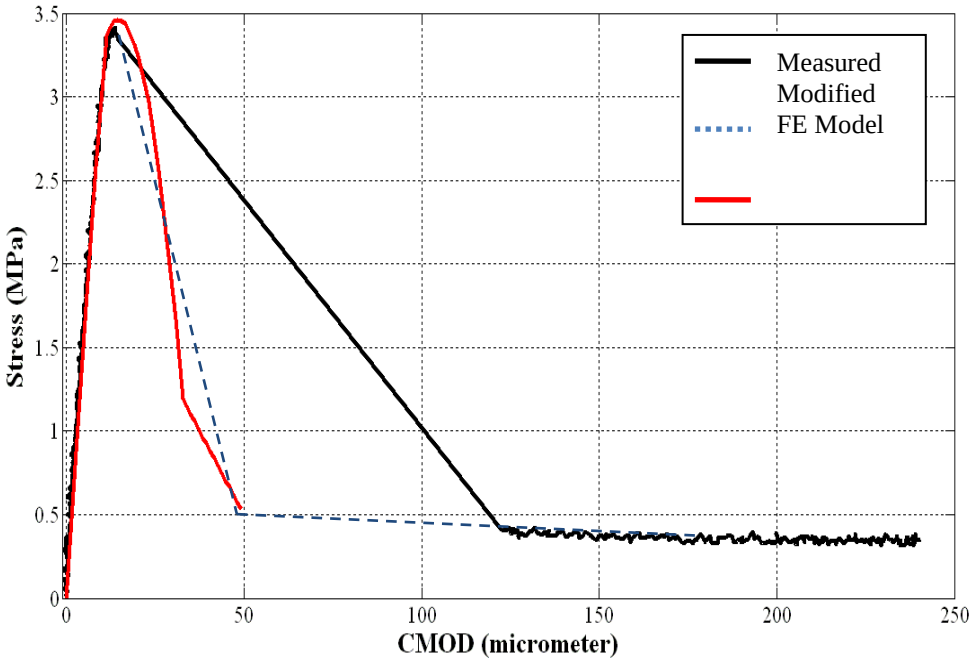

Figure 4.29 - Comparison of SCC5 experimental data, bilinear approximation, and model output

A displacement convergence criterion was used at a 0.5 tolerance level. Due to numerical simulation, error is inherent. Once the deformation between elements achieves a value within the tolerance assigned, due to compatibility, the model will converge. Convergence of this non-linear model was hard to obtain, hence the high tolerance level that was needed to achieve this convergence.

The FE model accurately models the initial slope of the softening curve, however, cannot model the entire softening curve. Unstable failure occurs in the FE model before it can predict the entire softening curve. This failure occurs because the model is no longer able to converge due to large differential displacements between the elements. The FE model used the fracture toughness values from the notched beam level II test, which were lower than the bilinear approximation used to analyze the STFT method, hence the steeper softening curve. These values were used due to more certainty in the notched beam level II test and because the values predicted by the CEB-FIP model agreed well with the values obtained by the ACI 446 method.

Plots of the relationships of fracture toughness (obtained by the Notched Beam Level II test method) versus cement paste volume (V_{cp}), fly ash percentage, and concrete strength (f_c) are presented in Figures 4.30, 4.31, and 4.32. Plots of the relationships for the STFT are shown in Figures 4.33, 4.34, and 4.35.

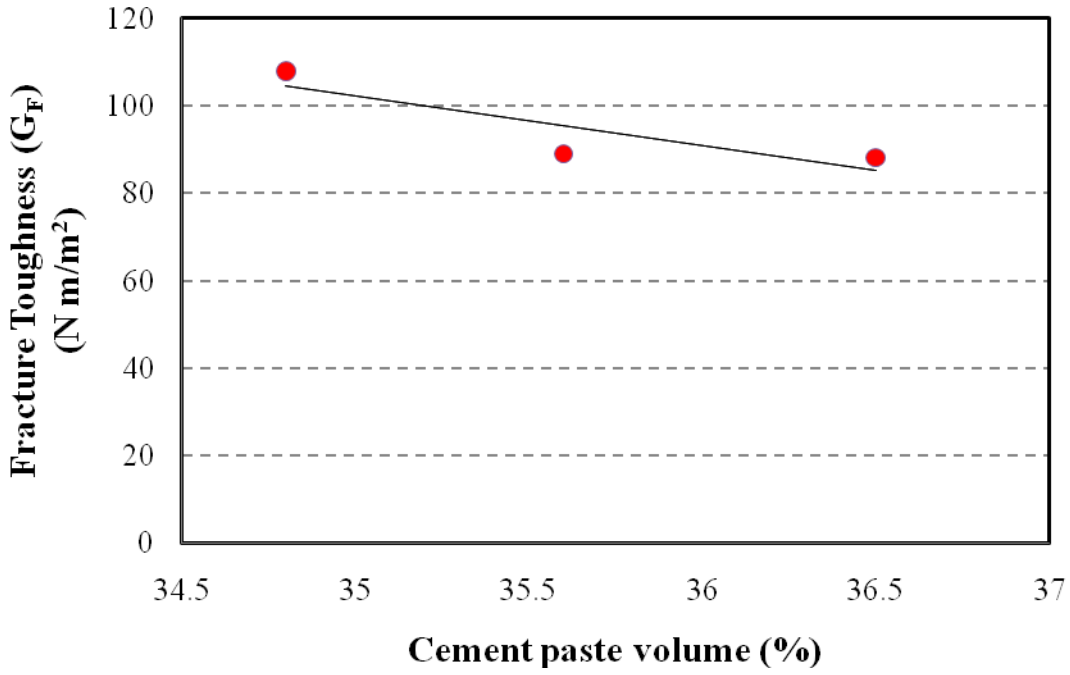

Figure 4.30 – Fracture toughness versus cement paste volume (ACI method)

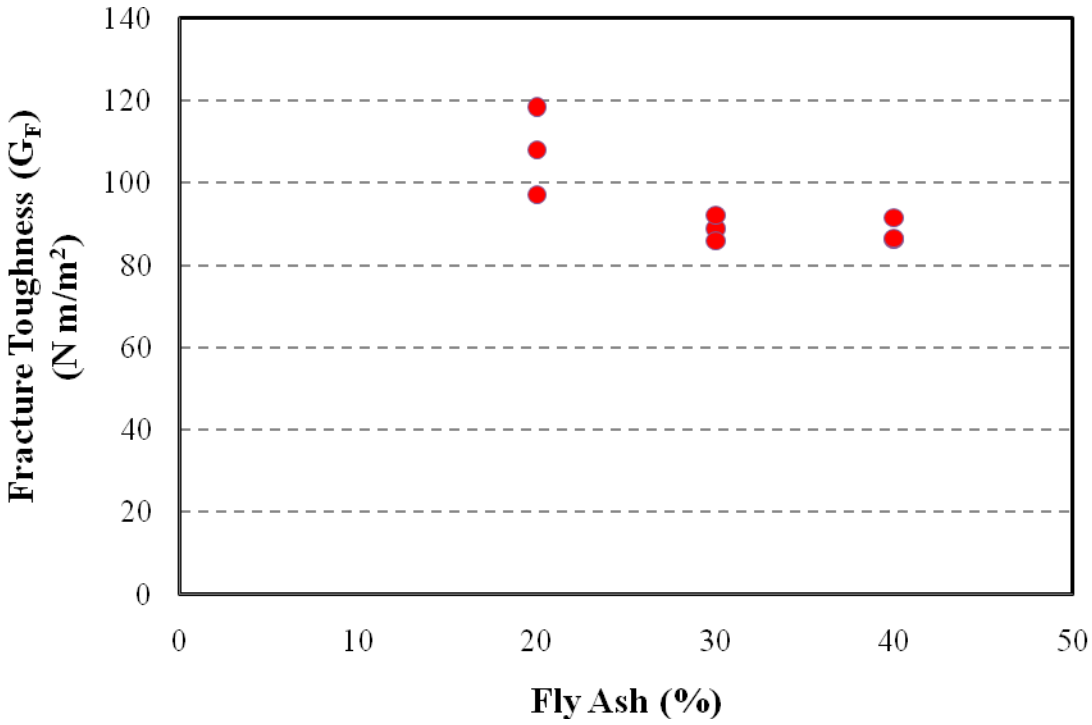

Figure 4.31 – Fracture toughness versus fly ash percentage (ACI method)

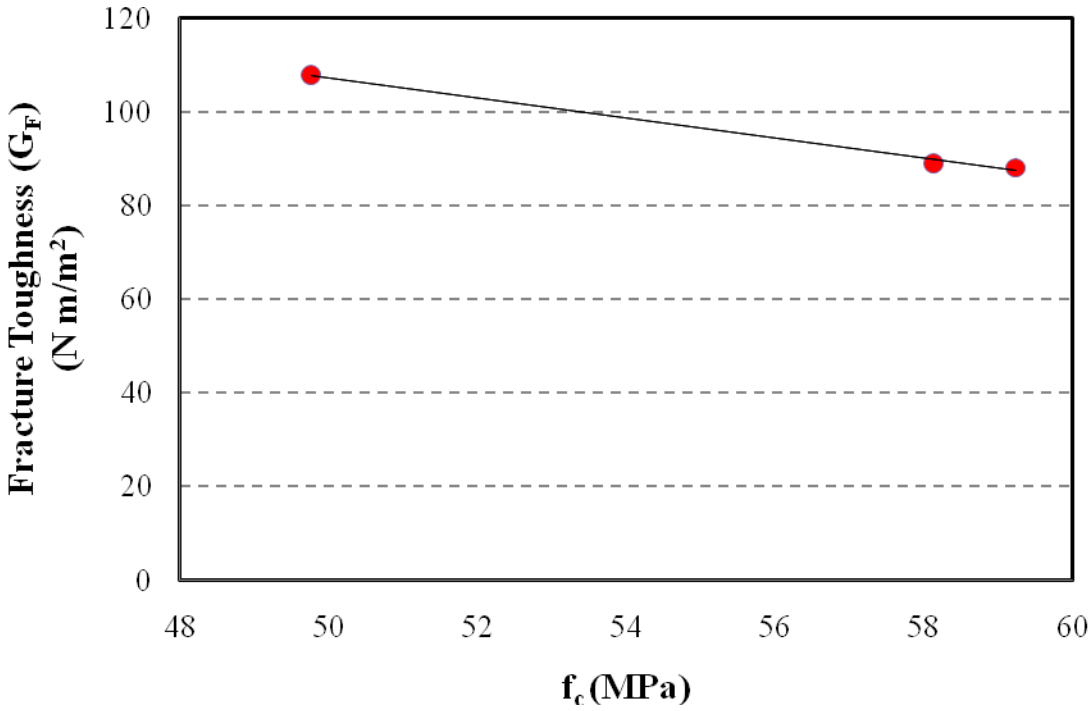

Figure 4.32 – Fracture toughness versus concrete strength (ACI method)

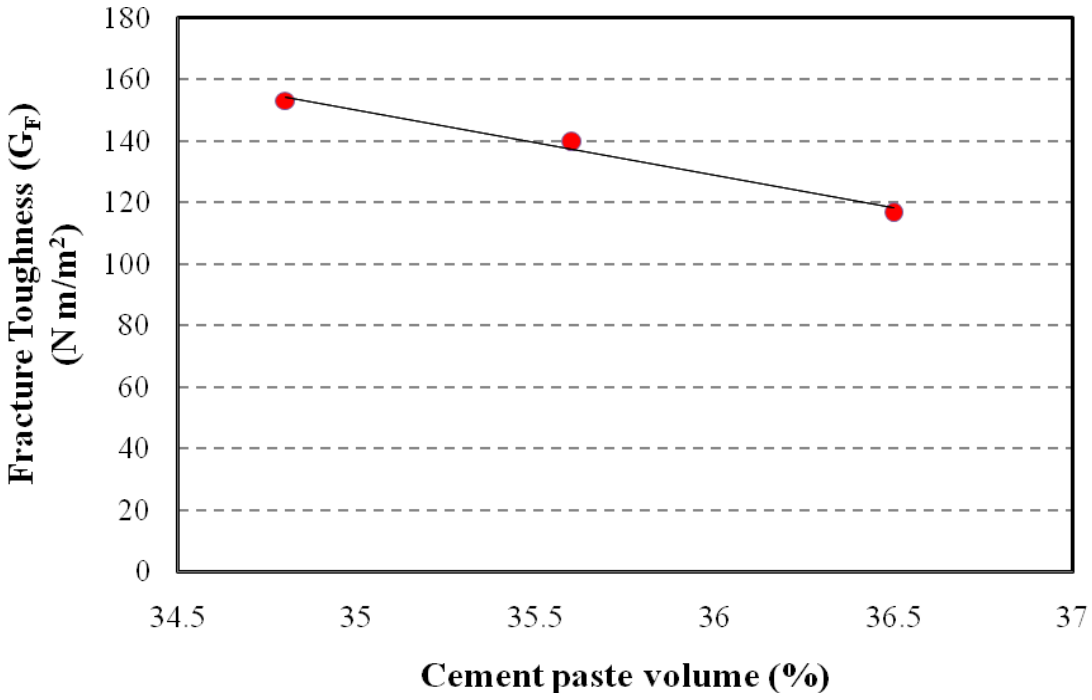

Figure 4.33 – Fracture toughness versus cement paste volume (STFT method)

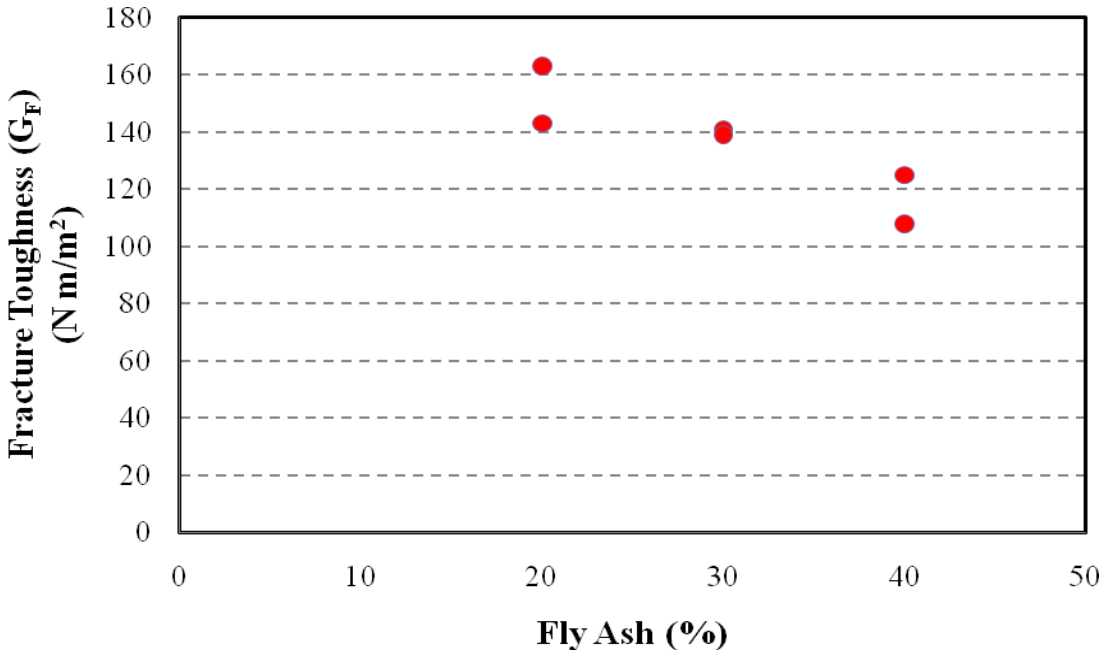

Figure 4.34 - Fracture toughness versus fly ash percentage (STFT method)

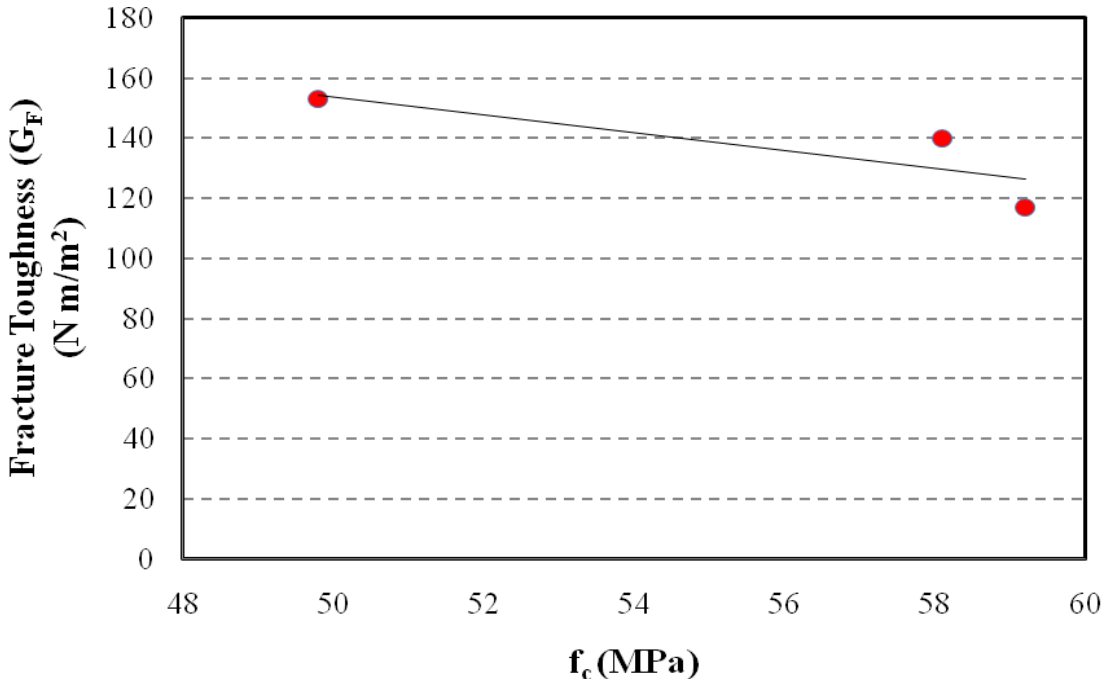

Figure 4.35 – Fracture toughness versus concrete strength (STFT method)

Many researchers believe that there is a direct correlation between a concrete's strength and its fracture toughness. High strength concretes become more brittle than

their normal strength counterparts due to the enhancements made at the ITZ causing decreased fracture toughness. Since fracture toughness is an important design parameter, design codes try to incorporate fracture toughness prediction models as a function of the concrete strength (f_c). The CEB-FIP MC-1990 [115] is one code that predicts these fracture toughness values based on conventional concretes. It is of interest to determine if these models can be utilized for SCC.

Using the CEB-FIP MC-1990 [115] code and using concrete strength values determined, a comparison can be determined to assess the prediction capabilities of this code when using SCC concretes. The actual fracture toughness determined from the notched beam level II test versus the CEB-FIP MC-1990 fracture toughness can be observed in Table 4.6.

Table 4.6 – Comparison of G_F values from experimental and CEB-FIP model

Type	SCC3	SCC4	SCC5	CEB-FIP	
f_c (Mpa)	49	57.2	58.3	49	57
G_F (Nm/m^2)	107.9	89.0	88.1	79.8	88.8

SCC4 and SCC5 fracture toughness values were predicted accurately, however, SCC3 was not predicted well using the CEB-FIP code. This difference can be attributed to the different aggregate grading as well as the increased cementitious filler content. A modification to the model might be necessary to accommodate all SCC concretes with varying amounts of fly ash.

The three SCC mixes exhibited different compressive strengths on the day the fracture tests were conducted. SCC3 showed the lowest strength (49MPa), while SCC4 and SCC5 exhibited similar strengths (57MPa and 58MPa). As the concrete strength increased, the stiffness also increased due to a denser cement paste matrix present within

the concrete. This change in cement paste microstructure exhibits characteristics more brittle in nature, which in turn, decreased the fracture toughness of the material. This characteristic might also explain the fracture toughness values observed from the Notched Beam Level II test. It is fair to suggest that the reduction of coarse aggregate content and the increase in the volume of fine materials and the cement paste all participated in producing SCC, enhancing the compressive strength and reducing the fracture toughness.

5. Conclusions

In this thesis, creep and fracture characteristics of self consolidating concrete (SCC) were examined and compared to normally vibrated concrete (NVC) mixes typically used in highway bridges in New Mexico. Analysis was performed to modify typical code models (ACI 209 [110] and CEB 1990 [115]) used to predict creep compliance of NVC to account for the special characteristics of SCC. Comparison of measured fracture toughness to that of CEB-FIP model is performed. The following pages summarize the major findings of this investigation.

The differences in aggregate grading and amounts of cementitious filler used are very different when comparing SCC to NVC. These differences at a microstructural level are hypothesized to alter the creep and fracture toughness characteristics. Due to the limited literature published on SCC in terms of fracture toughness and creep, it is of interest to accurately classify SCC and compare with code predictions to see if the behavior of SCC can be predicted as well as that of conventional concrete. The hypothesis of creep strains increasing and fracture toughness decreasing in SCCs with high volumes of fly ash was confirmed.

5.1 Creep

Compression creep tests were performed to understand basic and total creep compliance of SCC mixes incorporating local aggregate sources and fly ash. Once analyzed, creep compliance values were compared with NVC creep compliance values

and to design code predictions to determine if SCC's can be used in precast, pre-stressed bridge projects.

The SCC mixes produced using the Placitas aggregate source exhibited higher creep strains when compared to their NVC counterparts. The creep compliance was obviously a function of the fly ash content in the mix. It was observed that the CEB-FIP model was able to predict creep of all mixes except NVC1 and SCC2. On the other hand, the ACI model could not predict creep compliance of any SCC model. A modification to abandon the slump constant and use a new constant as a function of fly ash content is suggested. The Modified ACI model was able to predict the total creep compliance relatively well. SCC2 (40% fly ash) exhibited creep strains significantly higher than NVC1 and SCC1. This can be attributed to the high volume of fly ash present in the mix as well as the mixes slight instability in the plastic state. Minor bleeding was observed in SCC2, which may lead to increased microcracks forming in the cement paste matrix in the interfacial transition zone (ITZ) before load application.

Comparison of the SCC mixes and NVC mix incorporating the Griego and Sons aggregate source was also conducted. There was no significant difference in total creep strains among the SCCs and NVC mix. Creep of the SCC mixes was obviously a function of the fly ash content and the cement paste volume, however, didn't necessary show an increasing pattern with increasing fly ash and cement paste volumes. The ultimate creep coefficient of SCC was comparable to that predicted by the ACI and CEB-FIP codes for similar strength and curing conditions. It was also observed that the CEB-FIP model predicted all the Griego and Sons mixes relatively well and the modified ACI creep prediction model, also predicted total creep compliance well for all mixes.

To conclude, SCC mixes incorporating the Griego and Sons aggregate source can be used by the NMDOT for structural applications. Placitas SCC mixes exhibited higher creep strains than their NVC counterpart. A modification of ACI model is necessary to be used in designs of precast and prestressed bridge applications.

5.2 Fracture toughness

In this thesis, the fracture toughness of three different SCC mixes produced using Griego and Sons aggregate source with varying amounts of fly ash was examined. Tests using two different fracture toughness methods were conducted: the Notched Beam Level II test outlined by ACI 446 [114] and the stiff tension fracture test (STFT). All experiments were performed on concretes of 42 days of age.

It was observed in the Notched Beam Level II test that fracture toughness of SCC3 was the highest compared with SCC4 and SCC5. The increase of fly ash content resulted in reduced fracture toughness. This can be attributed to several factors. SCC3 contained the smallest amount of fly ash, cement paste volume, and compressive strength; all factors leading to high fracture toughness. The cement paste volume and compressive strengths of both SCC4 and SCC5 were very similar, which led to almost identical fracture toughness values. There is an obvious correlation between the increase in cement paste volume and fines volumes in the mix reducing its fracture toughness.

The CEB-FIP code to predict fracture toughness as a function of concrete strength agreed well with SCC4 and SCC5, however, did not accurately predict SCC3's fracture toughness. More SCC's with varying amounts of fly ash need to be tested and compared

with the predicted code values to determine if any revisions to the code need to be conducted to accurately predict SCC fracture toughness values.

In the STFT, similar trends were observed; however, the values obtained from the STFT test were not consistent with the Notched Beam Level II test. All the values determined by the STFT were significantly higher than the fracture toughness values from the same mixes that were produced by the 3-point bending test. This can be attributed to the need to change the stiffness of the steel bars when testing SCC's and relatively high strength concretes. Corrections in bilinear curves were necessary to account for the sudden crack growth of the notch in the STFT test. Finally, a similar trend to that described above was observed. Increasing fly ash content, cement paste volume, and strength resulted in decreasing fracture toughness. If a test setup was designed to provide the stiffness needed for high performance concretes, an accurate softening curve can be determined and a direct integration of this curve will produce more accurate fracture toughness values.

5.3 Future Work

5.3.1 Creep

Creep experiments with increased amount of samples and higher variance of fly ash percentages need to be conducted to obtain more confident creep strain values for SCC's as a function of fly ash. From these experiments, revisions to the ACI 209 code to predict creep strains can be designed to eliminate slump as an input variable.

5.3.2 Fracture Toughness

To further investigate fracture toughness of SCC's and their mechanisms to resist crack growth, NVC's need to be batched with similar strength and fly ash content for comparison. This will enable a better understanding of fracture toughness as a function of cementitious filler and different aggregate grading. From this understanding, better code prediction models can be produced for safer design.

The STFT method also needs to be revised to accommodate high strength concretes with increased stiffness. By increasing the stiffness of the load rods, a more accurate softening curve can be determined because of the stable crack propagation. Improvements in the STFT setup can produce fracture toughness values more easily by direct integration if an accurate softening curve can be produced.

References:

1. Ozawa, K., et al. *Developement of high-performance concrete based on durability design of concrete structures*. in *East Asia and Pacific Conference on Structural Engineering and Construction (EASEC-2)*. 1989.

2. Khayat, K.H. and D. Mitchell, *Self Consolidating Concrete for Precast, Prestressed Concrete Bridge Elements*, F.H.W.A. (FHWA), Editor. 2009, Transportation Research Board Washington, D.C.

3. Domone, P.L., *Self -compacting concrete: An analysis of 11 years of case studies* Cement & Concrete Composites, 2005. 28(2): p. 197-208.

4. Persson, B., *Self Consolidating Concrete, High Performance Concrete, and Normal Concrete, Affected by Creep at Different Age, Curing, Load Level, Strength, and Water-Cement Ratio with some Interrelated Properties.* American Concrete Institute Special Publication, 2005. 229: p. 63 - 91.

5. Persson, B., *Shrinkage and Creep of High-Performance Self-Compacting Concrete (HPSCC).* American Concrete Institute Special Publication, 2004. 220: p. 155-180.

6. Di Fabio, F., et al. *Long Term Behavior of SCC Precast Members* in *Third North American Conference on the Design and use of Self-Consolidating Concrete* 2008. Chicago, Illinois.

7. Reinhardt, A.K., I.A. Adam, and M.M.R. Taha. *Total and Basic Creep and Shrinkage of Self-Consolidating Concrete*. in *Third North American Conference on the Design and use of Self-Consolidating Concrete* 2008. Chicago, Illinois.

8. Bonen, D. and S.P. Shah, *Fresh and hardened properties of self-consolidating concrete.* Progress in Structural Engineering and Materials, 2005. 17(1): p. 14-26.

9. Brown, D.A., et al., *Evaluation of self-consolidating concrete for drilled shaft applications at lumber River Bridge project, South Carolina.* Transportation Research Record, 2007(2020): p. 67-75.

10. William F. Baker, D.S.K., Lawrence C Novak, *Burj Dubai: Engineering the World's Tallest Building.* The Structural Design of Tall and Special Buildings, 2007. 16: p. 361-375.

11. Heirman, G., et al., *Integration approach of the Couette inverse problem of powder type self-compacting concrete in a wide-gap concentric cylinder rheometer.* Journal of Non-Newtonian Fluid Mechanics, 2008. 150(2-3): p. 93-103.

12. Billberg, P. and K.H. Khayat. *Use of Viscosity-Modifying Admixtures to Enhance Robustness of SCC*. in *The Third North American Conference on the Design and Use of Self-Consolidating Concrete*. 2008. Chicago, Illinios.

13. Khayat, K.H., *Viscosity-enhancing admixtures for cement-based materials - An overview*. Cement & Concrete Composites, 1998. 20(2-3): p. 171-188.

14. Lachemi, M., et al., *Self-consolidating concrete incorporating new viscosity modifying admixtures.* Cement and Concrete Research, 2004. 34(6): p. 917-926.

15. Stirmer, N. and I.B. Pecur, *Mix design for self-compacting concrete.* Gradevinar, 2009. 61(4): p. 321-329.

16. Okamura, H. and M. Ouchi, *Self-compacting high performance concrete.* Progress in Structural Engineering and Materials, 1998. 1(4): p. 378-383.

17. Leemann, A. and F. Winnefeld, *The effect of viscosity modifying agents on mortar and concrete.* Cement & Concrete Composites, 2007. 29(5): p. 341-349.

18. Bouras, R., M. Chaouch, and S. Kaci, *Influence of Viscosity-Modifying Admixtures on the Thixotropic Behaviour of Cement Pastes.* Applied Rheology, 2008. 18(4): p. -.

19. Khayat, K.H., A. Ghezal, and M.S. Hadriche, *Factorial design models for proportioning self-consolidating concrete.* Materials and Structures, 1999. 32(223): p. 679-686.

20. Hwang, S.D., K.H. Khayat, and O. Bonneau, *Performance-based specifications of self-consolidating concrete used in structural applications.* Aci Materials Journal, 2006. 103(2): p. 121-129.

21. Lachemi, M., et al., *Influence of paste/mortar rheology on the flow characteristics of high-volume fly ash self-consolidating concrete.* Magazine of Concrete Research, 2007. 59(7): p. 517-528.

22. Patel, R., et al., *Development of statistical models for mixture design of high-volume fly ash self-consolidating concrete.* ACI Materials Journal, 2004. 101(4): p. 294-302.

23. ASTM, *ASTM C143 / C143M - 09 Standard Test Method for Slump of Hydraulic-Cement Concrete*. 2009, ASTM International: West Conshohocken, PA.

24. Concrete, T.E.G.f.S.C., *The European Guide lines for Self-Compacting Concrete*, BIBM, et al., Editors. 2004.

25. Khayat, K.H., J. Assaad, and J. Daczko, *Comparison of field-oriented test methods to assess dynamic stability of self-consolidating concrete.* Aci Materials Journal, 2004. 101(2): p. 168-176.

26. ASTM, *ASTM C1611 / C1611M - 09b Standard Test Method for Slump Flow of Self-Consolidating Concrete*. 2009, ASTM International West Conshohocken, PA.

27. Yang, E.H., et al., *Rheological Control in Production of Engineered Cementitious Composites.* ACI Materials Journal, 2009. 106(4): p. 357-366.

28. Shen, L., L. Struble, and D. Lange, *New method for measuring static segregation of self-consolidating concrete.* Journal of Testing and Evaluation, 2007. 35(3): p. 303-309.

29. Wu, Z.M., et al., *An experimental study on the workability of self-compacting lightweight concrete.* Construction and Building Materials, 2009. 23(5): p. 2087-2092.

30. Kwan, A.K.H. and I.Y.T. Ng, *Optimum superplasticiser dosage and aggregate proportions for SCC.* Magazine of Concrete Research, 2009. 61(4): p. 281-292.

31. Shen, L., L. Struble, and D. Lange, *Modeling Static Segregation of Self-Consolidating Concrete.* Aci Materials Journal, 2009. 106(4): p. 367-374.

32. Kasemchaisiri, R. and S. Tangtermsirikul, *Deformability prediction model for self-compacting concrete.* Magazine of Concrete Research, 2008. 60(2): p. 93-108.

33. Ng, I.Y.T., Wong, H.H.C., and Kwan, A.K.H. *Passing ability and segregation stability of self-consolidating concrete with different aggregate proportions.* Magazine of Concrete Research, 2006. 58(7): p. 447-457.

34. *The European Guide lines for Self-Compacting Concrete*. 2005.

35. Sahmaran, M., Yaman, I.O., and Tokyay, M. *Transport and mechanical properties of self consolidating concrete with high volume fly ash.* Cement & Concrete Composites, 2009. 31(2): p. 99-106.

36. Sonebi, M., *Applications of statistical models in proportioning medium-strength self-consolidating concrete.* Aci Materials Journal, 2004. 101(5): p. 339-346.

37. Nehdi, M. and J.D. Ladanchuk, *Fiber synergy in fiber-reinforced self-consolidating concrete.* Aci Materials Journal, 2004. 101(6): p. 508-517.

38. Sahmaran, M., O. Yaman, and M. Tokyay, *Development of high-volume low-lime and high-lime fly-ash-incorporated self-consolidating concrete.* Magazine of Concrete Research, 2007. 59(2): p. 97-106.

39. Sonebi, M., *Medium strength self-compacting concrete containing fly ash: Modelling using factorial experimental plans.* Cement and Concrete Research, 2004. 34(7): p. 1199-1208.

40. Sonebi, M. and P.J.M. Bartos, *Filling ability and plastic settlement of self-compacting concrete.* Materials and Structures, 2002. 35(252): p. 462-469.

41. Shen, L., L. Struble, and D. Lange, *Modeling Dynamic Segregation of Self-Consolidating Concrete.* Aci Materials Journal, 2009. 106(4): p. 375-380.

42. Sukumar, B., K. Nagamani, and R.S. Raghavan, *Evaluation of strength at early ages of self-compacting concrete with high volume fly ash.* Construction and Building Materials, 2008. 22(7): p. 1394-1401.

43. Gesoglu, M. and E. Ozbay, *Effects of mineral admixtures on fresh and hardened properties of self-compacting concretes: binary, ternary and quaternary systems.* Materials and Structures, 2007. 40(9): p. 923-937.

44. Sahmaran, M. and I.O. Yaman, *Hybrid fiber reinforced self-compacting concrete with a high-volume coarse fly ash.* Construction and Building Materials, 2007. 21(1): p. 150-156.

45. Prasad, B.K.R., H. Eskandari, and B.V.V. Reddy, *Prediction of compressive strength of SCC and HPC with high volume fly ash using ANN.* Construction and Building Materials, 2009. 23(1): p. 117-128.

46. Mindness, S., *Concrete*. 2002: Pearson Education Inc.

47. P. Dinakar, K.G.B., Manu Santhanam, *Durability Properties of High Volume Fly Ash Self Compacting Concretes.* Cement and Concrete Composties, 2008.

48. Reiner, M., *High-Volume Fly Ash Concrete: Analysis and Application.* Practice Periodical on Structural Design and Construction, 2006.

49. De Schutter, G. and R.T. Committee, *Final report of RILEM TC 205-DSC: durability of self-compacting concrete.* Materials and Structures, 2008. 41(2): p. 225-233.

50. Leemann, A., et al., *Influence of compaction on the interfacial transition zone and the permeability of concrete.* Cement and Concrete Research, 2006. 36(8): p. 1425-1433.

51. Coppola, L., T. Cerulli, and D. Salvioni, *Sustainable Developement and Durability of Self-Compacting Concretes.* ACI Special Issue, 2004. 221: p. 29-50.

52. Leemann, A. and C. Hoffmann, *Properties of self-compacting and conventional concrete - differences and similarities.* Magazine of Concrete Research, 2005. 57(6): p. 315-319.

53. Zhu, W., M. Sonebi, and P.J.M. Bartos, *Bond and interfacial properties of reinforcement in self-compacting concrete.* Materials and Structures, 2004. 37(271): p. 442-448.

54. Poppe, A.M. and G. De Schutter, *Cement hydration in the presence of high filler contents.* Cement and Concrete Research, 2005. 35(12): p. 2290-2299.

55. Assaad, J., K.H. Khayat, and H. Mesbah, *Assessment of thixotropy of flowable and self-consolidating concrete.* Aci Materials Journal, 2003. 100(2): p. 99-107.

56. El-Dieb, A.S., *Mechanical, durability and microstructural characteristics of ultra-high-strength self-compacting concrete incorporating steel fibers.* Materials & Design, 2009. 30(10): p. 4286-4292.

57. Domone, P.L., *A review of the hardened mechanical properties of self-compacting concrete.* Cement & Concrete Composites, 2007. 29(1): p. 1-12.

58. Golaszewski, J., *Influence of Viscosity Enhancing Agent on Rheology and Compressive Strength of Superplasticized Mortars.* Journal of Civil Engineering and Management, 2009. 15(2): p. 181-188.

59. Schindler, A.K., et al., *Properties of self-consolidating concrete for prestressed members.* Aci Materials Journal, 2007. 104(1): p. 53-61.

60. Neville, A.M., W.H. Dilger, and J.J. Brooks, *Creep of Plain and Structural Concrete*. 1983, New York, NY, USA: Longman Inc.

61. Bažant, Z.P., *Prediction of concrete creep effects using age-adjusted effective modulus method.* American Concrete Institute Journal, 1972. 69: p. 212-217.

62. Chiorino, M.A., *A Rational Approach to the Analysis of Creep Structural Effects.* J. Gardner and J Weiss eds., Shrinkage and Creep of Concrete ACI Special Issue, 2005. 227: p. 107-142.

63. Dilger, W.H. *Methods of Structural Creep Analysis*. in *Creep and Shrinkage in Concrete Structures*. 1982. New York and Chichester: Wiley.

64. Hanson, J.A., *Report No. SP-38 A ten-year study of creep properties of concrete*. 1953, Concrete Laboratory, US Department of Interior, Bureau of Reclamation: Denver

65. Ketton, J.R., *Study of creep in concrete Technical Reports R 333-I, R 333-II, R 333-III*. 1965, US Naval Civil Engineering Laboratory: Port Hueneme

66. Brooks, J.J. and A.M. Neville, *Estimating long-term creep and shrinkage from short-term tests.* Magazine of Concrete Research, 1975. 27(90): p. 3–12.

67. Gardner, N.J. and M.J. Lockman, *Design provisions for drying shrinkage and creep of normal-strength concrete.* ACI Materials Journal, 2001. 98(2): p. 159-167.

68. Kovler, K., *A new look at the problem of drying creep of concrete under tension.* Journal of Materials in Civil Engineering, 1999. 11(1): p. 84-87.

69. Mindess, S., J.F.Y., Darwin, *Concrete.* 2003.

70. Ogawa, A., K. Sakata, and S. Tanaka, *A Study on Reducing Shrinkage of Highly-Flowable Concrete Proceedings of the Second CANMET/ACL International Symposium on Advances in Concrete Technology.* American Concrete Institute Special Publication, 1995. 154: p. 55-72.

71. Yehia, S., et al. *Evaluation of Time Dependent Properties of a SCC Mix*. in *Third North American Conference on the Design and use of Self-Consolidating Concrete* 2008. Chicago, Illinois.

72. Roziere, E., et al., *Influence of paste volume on shrinkage cracking and fracture properties of self-compacting concrete.* Cement & Concrete Composites, 2007. 29(8): p. 626-636.

73. Rols, S., J. Ambroise, and J. Pera, *Effects of different viscosity agents on the properties of self-leveling concrete.* Cement and Concrete Research, 1999. 29(2): p. 261-266.

74. Turcry, P. and A. Loukili, *Evaluation of plastic shrinkage cracking of self-consolidating concrete.* Aci Materials Journal, 2006. 103(4): p. 272-279.

75. Bouzoubaa, N. and M. Lachemi, *Self-compacting concrete incorporating high volumes of class F fly ash - Preliminary results.* Cement and Concrete Research, 2001. 31(3): p. 413-420.

76. Lowke, D. and P. Schießl, *Effect of Powder Content and Viscosity Agents on Creep and Shrinkage of Self-Compacting Concrete*, in *Proc. of the Eighth*

International Conference on Creep, Shrinkage, and Durability of Concrete and Concrete Structures. 2008, CRC Press: Ise-Shima, Japan. p. 655-661.

77. Lowke, D., et al., *The potential durability of self-compacting concrete.* Beton- Und Stahlbetonbau, 2008. 103(5): p. 324-333.

78. Collepardi, M.E.A., *Strength, Shrinkage and Creep of SCC and Flowing Concrete*, in *Second North American Conference on the Design and Use of Self-Consolidating Concrete and the Fourth International RILEM Symposium on Self-Compacting Concrete*. 2005, Hanley-Wood: Addison, Illinois: Chicago, USA.

79. Mazzotti, C. and C. Ceccoli, *Creep and Shrinkage of Self Compacting Concrete: Experimental Behavior and Numerical Model*, in *Proc. of the Eighth International Conference on Creep, Shrinkage, and Durability of Concrete and Concrete Structures*. 2008: Ise-Shima, Japan. p. 667-673.

80. Maia, L.M., S. Nunes, and J.A. Figueiras, *Influence of Paste Content on Shrinkage and Creep of SCC*, in *Proc. of the Eighth International Conference on Creep, Shrinkage, and Durability of Concrete and Concrete Structures*. 2008, CRC Press: Ise-Shima, Japan. p. 675-680.

81. Reda Taha, M.M. , M.A.H., *Estimating the Error in Deflections of Reinforced Concrete Slabs, A Parametric Study Usint the Theory of Error Propagation.* American Concrete Institute, 2003(ACI Special Publication): p. 65-92.

82. S.P. Shah, S.E.S., C. Ouyang, *Fracture Mechanics of Concrete: Applications to Concrete, Rock, and other Quasi-Brittle Materials*. 1995, New York, New York: John Wiley & Sons, Inc.

83. Reda Taha, M.M., N.G. Shrive, *Evaluation of Flexural Fracture Toughness for Quasi-Brittle Structural Materials Using a Simple Test Method.* NRC Canada, 2002. 29: p. 567-575.

84. Griffith, A.A., *The Phenomena of Rupture and Flow in Solids.* Philosopical transactions of Royal Society of London, 1921. A221: p. 163-197.

85. Richart, F.E., Brandtzeaeg, P.L., Brown, P.L., *A Study of the Failure of Concrete Under Combined Compressive Stresses.* Engineering Experiment Station, 1923. Bulletin No. 185.

86. Kaplan, M.F., *Crack Propagation and Fracture of Concrete.* American Concrete Institute, 1961. 58: p. 591-610.

87. Glucklich, J., *Fracture of Plain Concrete.* ASCE Journal of the Engineering Mechanics Division, 1963. 89: p. 127-138.

88. Patterson,W.A., H.C.C., *Fracture Toughness of Glass Reinforced Cement.* Journal of Composites, 1975. 6: p. 102-104.

89. Lamkin, M.S., V.I. Paschenko, , *Determination of the Critical Stress Intensity Factor of Concrete.* Izvestiya VNIIG imeni B.E. Vedeneeva, 1972. 99(234-239).

90. Velazco, G., K.Visalvanich, P.S. Shah, , *Fracture Behaviour and Analysis of Fiber Reinforced Concrete Beams.* Cement and Concrete Research, 1980. 10: p. 41-51.

91. Rice, J.R., *A Path Independent Integral and the Approximate Analysis of Strain Concentration by Notches and Cracks.* Journal of Applied Mechanics, 1968. 35(379-386).

92. Mobasher, B., C.Y., Li, A. Arino, *Experimental R-curves for Assesment of Toughening in Fiber Reinforced Cementitious Composites.* American Concrete Institute, 1995: p. 93-114.

93. Hillerborg, A.M., M. Peterson, P.E., *Analysis of Crack Formation and Crack Growth in Concrete by Means of Fracture Mechanics and Finite Elements.* Cement and Concrete Research, 1976. 6: p. 773-782.

94. Visalvanich, K., A.E. Naaman, *Fracture Model for Fiber Reinforced Concrete.* ACI Journal, 1983. 83: p. 128-138.

95. Wecharatana, M., S.P. Shah, *A Model For Predicting Fracture Resistance of Fiber Reinforced Concrete.* Cement and Concrete Research, 1983. 13: p. 819-829.

96. Bazant, Z.P., B.H. Oh, *Crack Band Theory for Fracture of Concrete.* Materials and Structures, 1983. 16: p. 155-177.

97. Jenq, Y.S., S.P. Shah, *A Two Parameter Fracture model for Concrete.* ASCE Journal of the Engineering Mechanics Division, 1985. 111: p. 1227-1241.

98. Lenke, L.R., W. Gerstle, *Tension Test of Stress Versus Crack Opening Displacement Using Cylindrical Specimens.*

99. Zhao, X.L. and J.A. Packer, *Tests and design of concrete-filled elliptical hollow section stub columns.* Thin-Walled Structures, 2009. 47(6-7): p. 617-628.

100. Fava, C., et al., *Fracture Behaviour of Self-Compacting Concrete*, in *Proceedings of 3rd International RILEM Symposium on Self-Compacting Concrete* 2003, RILEM Publications: Reykjavik, Iceland. p. 628-636.

101. ASTM, *ASTM C128 - 07a Standard Test Method for Density, Relative Density (Specific Gravity), and Absorption of Fine Aggregate*. 2007, ASTM International: West Conshohocken, PA.

102. ASTM, *ASTM C496 / C496M - 04e1 Standard Test Method for Splitting Tensile Strength of Cylindrical Concrete Specimens*
West Conshohocken, PA, 2009. ASTM International.

103. ASTM, *ASTM C136 Sieve Analysis for Fine and Coarse Aggregate.* West Conshohocken, PA, ASTM International, 2009.

104. ASTM, *ASTM C192 / C192M - 07 Standard Practice for Making and Curing Concrete Test Specimens in the Laboratory*. 2007, ASTM International: West Conshohocken, PA.

105. ASTM, *ASTM C29 / C29M - 07 Standard Test Method for Bulk Density ("Unit Weight") and Voids in Aggregate*. 2007, ASTM International West Conshohocken, PA.

106. ASTM, *ASTM C231 - Air Content By Pressure Method.* West Conshohocken, PA, ASTM International, 2009.

107. ASTM, *ASTM C39 / C39M - 05e2 Standard Test Method for Compressive Strength of Cylindrical Concrete Specimens*. 2005, ASTM International West Conshohocken, PA.

108. ASTM, *ASTM C469 - Static Modulus of Elasticity and Poissan's Ratio of Concrete in Compression.* ASTM International. West Conshohocken, PA., 2009.

109. ASTM and *ASTM C293 - Standard Test Method for Flexural Strength of Concrete.* ASTM International. West Conshohocken, PA., 2009.

110. ACI, *Guide for Modeling and Calculating Shrinkage and Creep in Hardened Concrete*. 2008, American Concrete Institute.

111. Kim, Y.H., D. Trejo, M.B. Hueste, J.J. Kim, *Experimental Study on Creep and Durability of High-Early Strength Self-Consolidating Concrete for Precast Elements.* ACI Materials Journam, 2011. 108: p. 128-138.

112. Leemann, A., P. Lura, R. Loser, *Shrinkage and creep of SCC - The influence of paste volume and binder content.* Construction and Building Materials, 2010. 25: p. 2283-2289.

113. Wang, Y.F., Y.S. Ma, L. Zhou, *Creep of FRP-wrapped concrete columns with or without fly ash under axial load.* Construction and Building Materials, 2010. 25: p. 697-704.

114. ACI 446, Report 5, 2009, *Fracture Toughness Testing of Concrete*

115. CEP-FIP Model Code 90, 1993, *Model Code for Concrete Structures*, Comité Euro-International du Béton (CEB) - Fédération Internationale de la Précontrainte (FIP), Thomas Telford Ltd.,UK.